SIZE CONTROLLED GERMANIUM NANOCRYSTALS IN DIELECTRICS: STRUCTURAL AND OPTICAL ANALYSIS AND STRESS EVOLUTION

A DISSERTATION SUBMITTED TO

THE GRADUATE SCHOOL OF ENGINEERING AND SCIENCE

OF BILKENT UNIVERSITY

IN PARTIAL FULFILLMENT OF THE REQUIREMENTS FOR

THE DEGREE OF

DOCTOR OF PHILOSOPHY

IN

PHYSICS

By

Rahim Bahariqushchi

August 2017

Size controlled Germanium nanocrystals in dielectrics: Structural and optical analysis and stress evolution
By Rahim Bahariqushchi
August 2017

We certify that we have read this dissertation and that in our opinion it is fully adequate, in scope and in quality, as a dissertation for the degree of Doctor of Philosophy.

Oğuz Gülseren (Advisor)

Atilla Aydınlı(Co-Advisor)

Raşit Turan

Ceyhun Bulutay

Sinan Balcı

Serap Aksu Ramazanoğlu

Approved for the Graduate School of Engineering and Science:

Ezhan Karaşan
Director of the Graduate School

ABSTRACT

SIZE CONTROLLED GERMANIUM NANOCRYSTALS IN DIELECTRICS: STRUCTURAL AND OPTICAL ANALYSIS AND STRESS EVOLUTION

Rahim Bahariqushchi
Ph.D. in Physics
Advisor: Oğuz Gülseren
August 2017

Group IV semiconductor nanocrystals, namely silicon and germanium have attracted much interest in the past two decades due to their broad applications in photovoltaic, memory, optoelectronic, medical imaging and photodetection devices. Generally, there are two major features of semiconducor nanocrystals: First, spatial confinement of charge carriers which leads to the significant changes in optical and electronic properties of materials as a function of size. This effect gives the possibility to use the size and shape of the nanocrystals to tune the energy of electronic energy states. Second feature of nanocrystals, is the increased of surface area to volume ratio of the nanocrystal with reducing size. This leads to an enhanced role of the effects related to surface and interface of the nanocrystal. Furthermore, stress on the nanocrystals can lead modification of the band structure as well as influencing the crystallization of the nanomaterials. Recent works show that measurement and control of the stress can open the way for strain engineering of the electronic band structure, thereby opening the way for new physics and applications. In this thesis, we first carry out a study on the synthesis of germanium embedded in silicon nitride and oxide matrices. Influence of the annealing method as well as germanium concentration on the formation of nanocrystals is discussed. It was found that Ge concentration and annealing play important roles in the formation of the Ge nanocrystals. With crystallographic data obtained from high resolution transmission electron microscopy, quantitative analysis of stress state of germanium nanocrystals have been done by analyzing Raman peak shift of embedded nanocrystals taking into account the phonon confinement effect. Finally, using stressors as buffer layers, superlattices of Ge nanosheets were studied to understand the effects of the stressors on the stress state of Ge nanocrystals. We demonstrate that it is possible to tune the stress on the Ge nanocrystals from compressive to tensile. Finally we showed a three dimensional Ge quantum solid that can be used in optoelectronic applications.

Keywords: Germanium nanocrystals , dielectric matrices, Quantum confinement effect, Phonon confinement model, Phonon Raman spectroscopy, High resolution transmission electron microscopy , Strain engineering, Photoluminescence spectroscopy,Superlattices.

ÖZET

DİELEKTRİK MATRİSLERDE GERMANİUM NANOKRİSTALLER: YAPISAL VE OPTİK ANALİZ VE ZOR EVRİMİ

Rahim Bahariqushchi
Fizik, Doktora
Tez Danışmanı: Oğuz Gülseren
Ağustos 2017

Grup IV yarıiletken nanokristaller, yani silisyum ve germanyum, fotovoltaik, bellek uygulamaları, optoelektronik, tıbbi görüntüleme ve ultra hassas tespit cihazları gibi bir çok alanda ilgi çeken bir konu olmuştur. yarıiletken nanokristallerin iki önemli özelliği vardır: kuantum hapsolma etkisinden dolayı malzemenin boyutları küçüldüküe optik özelliklerinde büyük değişiklikler oluşur. Bu etki nanokristallerin boyut ve şekillerini ayarlayarak elektronik enerji seviyelerinin kontrol edilebilmesini sağlar. Ikinci özellik ise azalan boyutla birlikte "uzey/hacim" oraninin artması ve buna bağlı olarak yüzeyle alakalı etkilerin rolunun artmasıdır. Yarıletken nanokristaller superörgüler gibi karmaşık nanoyapıların da geliştirilmesini mümkün kılar. Bu tezde silicon nitrür matrisine gömülü germanyum nanokristallerin "uretilmesi "uzerine bir çalışma yürütülmüştür. Tavlama yöntemleri ile germanyum derisiminin nanokristallerin olusumuna etkisi tartişılmıştır. Germanyum derisiminin ve tavlama yönteminin nanokristal oluşumunda önemli rol oynadığı görülmüştur. Sonrasında, germanyum nanokristaller silicon nitrür matriste sentezlenerek kristalleri çevreleyen matrisin etkisi incelenmiştir. Germanyumun stres durumunun nicel analizi fonon hapsolma etkileri göz önünde bulundurularak Raman pikinin kaymasının incelenmesi ile gerçekleştirilmiştir. Yüksek çözunurluklu gecirimli electron mikroskopu kullanılarak nanokristallerin ortalama boyutu belirlenmiş ve fonon hapsolma modeline uygulanarak analiz edilmiştir. Daha sonra süperörgü örneklerinde tavlama yöntemi, çevreleyen matris ve stress yaratıcı katman degiştirilerek nanokristallerin stress durumu ayarlanmıştır.

Anahtar sözcükler: Germanyum nanokristalleri, Dielektrik matrisler, Kuantum kustama, Fonon kusatılması , Fonon Raman spektroskopisi, Yüksek ç ö zünürlüklü transmisyon elektron mikroskopisi, stres mühendisliği, fotolüminesans spektroskopisi, süperörgüler.

Acknowledgement

I would like to express my special thanks to my advisor Prof. Oğuz Gülseren, who has been a tremendous mentor for me. I would especially like to express my sincere gratitude to my co-advisor Prof. Atilla Aydınlı for his continuous support of me during Ph.D study and related research, for his patience, motivation, and immense knowledge. His guidance helped me throughout research and writing of this thesis. My sincere thanks also goes to Prof. Emre Gür, who provided me with an opportunity to work in his laboratory at Atatürk University. Thanks are also due to Prof. Salvatore Mirabella and his team for performing the RBS measurements of our samples and Dr. Meltem Sezen of Sabancı University who kindly prepared some our TEM samples with FIB and Prof. Eren Kalay, and his students who did the preliminary TEM work. I am grateful to the operator of the HRTEM in UNAM Mustafa Güler for help with the HRTEM measurements. I also would like to thank professor Sinan Balcı for fruitful discussions and all of supports gave me during my Ph.D carrier. I would also like to thank my committee members, Prof. Raşit Turan, Prof. Ceyhun Bulutay, Prof. Sinan Balci and Prof. Serap Aksu for serving as my committee. Also I thank my friends in the UNAM, ARL, and Bilkent University. In particular, I am grateful to Akbar Alipour, Muhammad yahyavi, Sinan Gundogdu, Ramez Kian, Sabuhi Badalov, Seval Saritas, Ertugrul Karademir, Ahmet Emre Kasapoglu from Ataturk University. All of you were there to support me when I required your patience. I would also like to thank all of my friends who supported me in writing and encouraged me to strive towards my goal. Last but not the least, I would like to thank my family for supporting me spiritually throughout the writing of this thesis and my life in general.

Contents

List of Figures

List of Tables

Chapter 1

Introduction

Semiconductor nanocrystals (NCs) have different electrical and optical properties than their bulk counterparts due to the confinement of charge carriers and vibronic modes, the so called quantum confinement effect QCE which alters the band structures of materials and also increasing of surface to volume ratio with size reduction which leads to increase in surface related effects [1] [6]. Due to this high surface to volume ratio in nanoscale regime, a larger number of atoms are located in the surface of nanoclusters which in turn leads to completely different thermodynamic properties compare to bulk material [6]. Quantum confinement effect takes place when a structure becomes as small as exciton Bohr radius in one or more dimensions [7]. In this thesis, we consider nanocrystals that can be considered quantum dots (QDs) that are confined in all three dimensions. Strong size-dependent properties for particle sizes below 10 nanometers have been shown theoretically and experimentally by several studies [8]. This size-dependent behavior of NCs electronic structure, allows for tailoring the optical and electronic properties of materials which in turn leads to many potential applications such as nanocrystal solar cells [9],quantum dot (QD) photodetectors [10] light emitting devices [11] and non-volatile memorial (NVM) devices [12], biological imaging [13]. However, most of research on nanocrystal structures have been done on group $II-VI$ and $III-V$ semiconductors, such as $CdSe$ and CdS. Despite the importance of group IV semiconductors Si and Ge in semiconductor technology, less attention had been paid to this group due to indirect nature of their band structure and poor optical efficiency of these materials. However since observation of photoluminescence (PL) [14] from porous silicon in the 1990s, interests in Group IV nanocrystals such as silicon (Si) and germanium (Ge) have increased. Quantum confinement of carriers enables indirect bandgap semiconductors to become more efficient light emitters [15]. However a main challenge still remains in determining whether the origin of PL is defects located in matrix and nanocrystal-matrix interface or quantum confinement effect. There is lack of agreement in experiment reports on the origin of luminescence and in any study the origin of luminescence should be investigated with care. Even though it is now widely accepted that both defects located on NC-matrix interface and quantum confinement of charge carriers have important roles to play in the photoluminescence it is difficult to distinguish two luminescence mechanism. It is reported [16–19] that photoluminescence intensity from defects located at NCs, interface strongly depends on NCs size. For example in the work of [16] it is argued that luminescence in a $Si/SiO2$ superlattice structure originates from transitions between defect states at surface. Origin of the defects is due to dangling bonds on the surface of th $NC's$ $i.e$ large bond mismatch between NCs and embedding matrix. There are several other reports relating the origin of PL to surface defects [17,18] Other reports for example [20,21] relate the PL origin to quantum confinement. Zacharias et al. [22] have argued based on measurements in a high magnetic fields, that defects are the main source of photoluminescence from Si nanocrystals. They also, show that it is possible to control the origin of photoluminescence in a simple way: First they remove the defects by hydrogen passivation, which leads to almost pure photoluminescence from quantum-confined states, then they reinduced the defect states by illuminating ultraviolet radiation, making them the main origin of the light. Charge transport behavior of Si nanocrystals embedded in a silicon oxide matrix also investigated [23] taking into account three different mechanism namely tunneling, hopping and percolation and show that in low and high density regime, different mechanisms dominate the transport process. Pavesi et al. [23] discussed the importance of surface chemistry in developing functional Si nanocrystals since in very small regime, surface chemistry becomes crucial in controlling properties of nanocrystals. Zacharias et al. [24]

proposed a superlattice method for controlling size and density of nanocrystals. These multilayer structures, control size of nanocrystals at least in growth direction by hindering Ge atoms during diffusion in annealing process, it also provides possibility to control density of nanocrystals simultaneously, these highly packed nanostructures have potential applications in photovoltaic and charge transport applications. Theoretically, Ge has some advantages over Si. Ge has larger excitonic Bohr radius (24.3nm) compared to that of Si (4.9nm) [25] due to its smaller electron and hole effective masses and larger dielectric constant. Therefore, quantum confinement effect can be seen even in larger Ge QDs and it would be easier to tune electrical and optical properties of Ge by controlling the size of QDs. In Ge with small energy difference between direct and indirect band gaps, radiative recombination occurs more rapidly compared to Si. Ge also has melting point of 938 C which is lower than that of Si (1414C), suggesting that Ge QDs can be fabricated at lower temperatures which reduces costs of manufacturing. Germanium nanocrystals embedded in a wide band gap matrix like SiO_2, Si_3N_4 and Al_2O_3 are in particular importance because of blue luminescence of Ge in such matrices reported by several groups [26–29]. However, the origin of this photoluminescence is not clear and has been attributed to $matrix - Ge$ interface states [30], matrix defects [31], as well as quantum confinement effects [4]. Recently, nanocrystalline silicon and nanocrystalline germanium quantum dot flash memories have been incorporated in the full complementary MOS (CMOS) compatible technologies based on discrete isolated charge storage modules. Tiwari et al. proposed an NC-Si memory device that can be programmed at fast speeds (hundreds of nanoseconds) using low voltages for direct tunneling and electron storage in NC-Si [32] King et al. also demonstrated a $NC - Ge$ memory device with high programming speed and high retention time [33, 34] in comparison to conventional flash memories. Moreover, Ge absorbs light more efficiently [1] than Si. As shown in Fig (1.1), the absorption coefficient of crystalline Ge is more than one order of magnitude larger than Si. This is related to the smaller band gap and the nearly-direct band-gap with respect to Si. The capability to absorb light also in near infra red region range where bulk Si is optically blind, combined with its high carrier mobility [35] proposed Ge as a good candidate for the fabrication of infrared photodetectors, high-speed optical modulators as well as high efficiency multi-junction solar cells [36–38]. For the above mentioned reasons, Ge is principally more suitable than Si for light absorption. However, its usage in the bulk form have been limited because of its high production costs. The usage of Ge in nanostructure form can solve the scarcity problem of this element, giving also the possibility to exploit the quantum confinement effect in these systems. Since, Ge has an exciton Bohr radius much larger than that of Si it is potentially possible to tune the absorption edge of Ge NCs from the infrared up to visible range without shrinking the NCs size too much. Such a possibility, together with the larger absorption capability and the quasi-direct bandgap, make Ge NCs very attractive for the application in a large variety of devices, from energy-tunable light harvesters (e.g. multi-junction solar cells and photodetectors) to efficient optoelectronic devices. These include: optical modulators, efficient photodetectors and solar cells. Due to its high absorption coefficient in the near infra red region and the advantage of ease integration with Si, photodetectors based on bulk Ge has been already largely utilized for light detection in the telecommunication wavelength range of 1300-1600 nm, but the cost and the device speed issues remain. In recent years, various configurations of thin film Ge-based photodetectors (p-i-n, waveguide coupled or avalanche gain detector design) have been developed and demonstrated high values of performance (0.5 - 1 A/W at 1550 nm) [38]. However, further miniaturization of the components design and optimization of the performance at low or zero bias is essential to achieve high energy efficiency and reduced costs for a large-scale electronic-photonic integration. In this scenario, the discrete levels produced in Ge NCs by quantum confinement can guarantee promising applications for light detection in narrow spectral infra red and compatibility with CMOS technology as well as reduce production costs. NC-Ge, though posing several fabrication challenges such as lower evaporation temperature and difference in surface energy with respect to the oxide, is a perfect candidate as Ge can readily incorporated into mature silicon technologies. In addition, diffusion of Ge is not significant at temperatures below 500C. As such, the device will not be adversely affected by subsequent low temperature processing steps. Last but not least, Ge nanocrystals can be more easily differentiated from Si in a Si_2O matrix. On the other hand embedding of ge NCs in dielectric matrices leads to large compressive or tensile stress which can alter the band gap

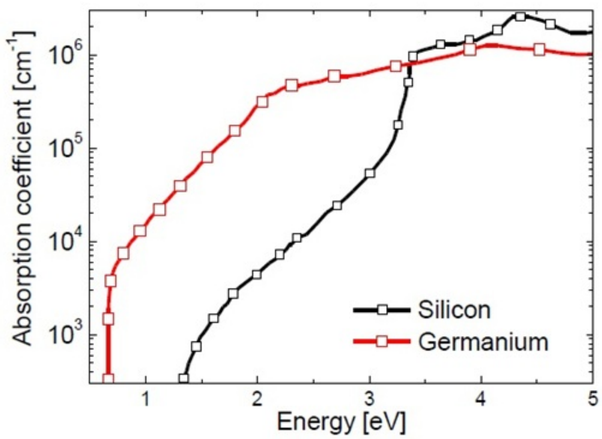

Figure 1.1: Absorption coefficient for crystalline silicon and germanium. From ref. [1].

structure of nanostructures. A significant development that shows the interest in Ge and role of stress in its application is a demonstration of a near-infrared germanium laser reported recently [39]. One of the critical points to obtain lasing with such a indirect band gap material is to decrease the energy separation between the L and zone center valley and therefore increasing the population of the zone center conduction band minimum and lead to efficient recombination of carriers. It has been shown that applying tensile stress can lead to decrease in separation of this energy. Several approaches have been proposed to obtain a tensile strain to germanium [40–44]. The most direct strategy is to use the difference of thermal expansion coefficients between germanium and silicon that can lead to a tensile strain for germanium nanocrystals [45]. using buffer layers with different lattice parameters like $InGaAs$ alloys [46] or $Ge-Sn$ buffer layers [47]is also a good choice as it can lead to large tensile strain. Silicon nitride layers are particularly interesting as their deposition is fully compatible with complementary metal oxide semiconductor (CMOS) processing on a silicon substrate. Nitride layers as stressors is broadly used in the microelectronic applications [48]. For photonics application, optical gain has been recently evidenced in germanium photonic wires strained by a $Si3N4$ layer indicating the potential of this approach. Therefore it is important to study the stress state of NCs in dielectric matrix. It is possible to tune the band gap of NCs by varying the stress of NCs. In this thesis we first review the growth mechanism of Ge NCs inside a dielectric matrix. We grow Ge NCs in two different matrices namely $SiO2$ and $Si3N4$. We study structural and optical properties of Ge embedded in these matrices via employing methods like Raman spectroscopy, High resolution transmission electron microscopy ($HRTEM$), photoluminescence (PL) spectroscopy. Effect of Ge content, surrounding matrix as well as annealing method on stress state and heir PL properties have been studied. We also prepared Ge embedded in ultrathin films using multilayer structures to control simultaneously size and density of Ge NCs. This method also allows for controlling stress of NCs from compressive to tensile stress which is desirable in optoelectronic applications. Armed with these results on the control of stress, we envision new possibilities in engineering of three dimensional quantum solids. The organization of this thesis is as follow: In the second chapter of the thesis, theoretical background of the work is described, with first an overview on semiconductors. Direct and indirect band gap semiconductors and emission processes in these two type of materials is reviewed with indirect band gap semiconductors having low optical efficiency due to low probability of radiative recombination of electrons and holes between conducting and valence band. This low recombination rate is a result of momentum conservation rule which hinder electron transition between two points in the Brilouin zone with different momentum. Indirect to quasi-direct transition of band structure in nanocrystals is presented considering Heisenberg uncertainty relationship and momentum conservation relaxation due to confinement of charge carriers. This includes quantum confinement of excitons and confinement of phonons which are going to be used in analyzing optical and structural properties of samples in the following chapters. In the third chapter characterization techniques used for analysis of the materials will be introduced briefly, this includes techniques for compositional analysis such as Rutherford backscattering spectroscopy (RBS) and $X - ray$ photoelectron spectroscopy (XPS). These methods are very important as the precise determination of elemental composition is essential in final form of $nanocrystal's$ size , shape and size distribution. In the fourth chapter, stress on Ge NCs is studied, Firstly, stress on Ge NCs embedded in silicon nitride matrix is estimated using combination of Raman spectroscopy and transmission electron microscopy data. Raman shift of nanocrystal compared to that of bulk crystal is related to nanocrystal size and size distribution. Total Raman shift is assumed to be a combination of a red shift due to confinement of phonons and a stress induced shift blue shift (for compressive stress) or red shift (for tensile stress). by comparing experimental results of Raman shift with shift predicted by phonon confinement models, stress on NCs is extracted. This stress is found to be independent of size of NCs in the dielectric matrices including silcon dioxide and silicon nitride. This stress is also estimated via relaxation of Ge NCs from matrix via HF etching of matrix and measuring Raman shift of released Ge NCs, these results are in agreement with those obtained via applying phonon confinement model. In other section of chapter four, stress of Ge NCs is tuned via different methods namely processing method, matrix and buffer layer in superlattice structures. Samples are annealed in two different approaches, i.e. conventional furnace annealing and rapid thermal processing and results are compared. Then Ge NCs embedded in silicon oxide matrix are synthesized and analyzed via Raman spectroscopy and TEM microscopy. It is found that stress of Ge NCs depends on the surrounding matrix. Then two sets of superlattice multilayer structures are fabricated: $SiGeN/SiO2$ and $SiGeN/Si3N4$. Stoichiometric $SiO2$ and $Si3N4$ are used as thin stressors buffer layers which control size and density of NCs by limiting Ge atoms from diffusion during annealing. The effect of choosing the buffer layers on stress state of the samples is investigated and found that $SiO2$ leads to compressive stress while $Si3N4$ buffer layer can result in tensile stress. Therefore we managed to tune stress state of Ge NCs from compressive to tensile stress. A correlation between stress and crystallization threshold also was observed. It is found that while compressive stress enhances the crystallization process, tensile stress suppresses crystallization. In chapter five, optical characterization of single layer and multilayer samples are performed using a HeCd laser operating at 325 nm as the exciting source. Photoluminescence results are discussed an origin of the emission is related to defects located at the interface of Ge nanocrystal and matrix. Furthermore enhancement of photoluminescence intensity is observed in superlattices compare to single layer samples. This enhancement is also discussed. In chapter six, conclusions are presented and future work is proposed.

.

Chapter 2

Theoretical background

In this chapter the theoretical background for this thesis is presented. Description of nanocrystals, their formation and properties are outlined. The concept of quantum confinement of carriers (QCE) is discussed and its role in determination of electronic and optical properties is described. Finally critical in determination of stress, an overview on phonon confinement effect will be presented.

2.1 Semiconducting Nanocrystals: Si and Ge

We concentrate on group IV elements, as Si and Ge are very similar to each other in many respects and Ge nanocrystals are the subject of this thesis.

2.1.1 Direct vs indirect band gap semiconductors

Si is the dominant element in semiconductor industry due to its abundance in nature and non-toxicity properties. Furthermore its electrical conductivity can be controlled dynamically or permanently and its oxide ($SiO2$) is one of the best insulators. However Si, has weak optical efficiency [2]. Weak photoluminescence of Si is due to indirect energy band gap of silicon; that is minimum energy of the conducting band and maximum energy of valence band do not correspond to the same momentum. Fig. (2.1) illustrates energy band diagram of Si and GaAs which is a direct band gap material. In a semiconductor, electrons occupy the

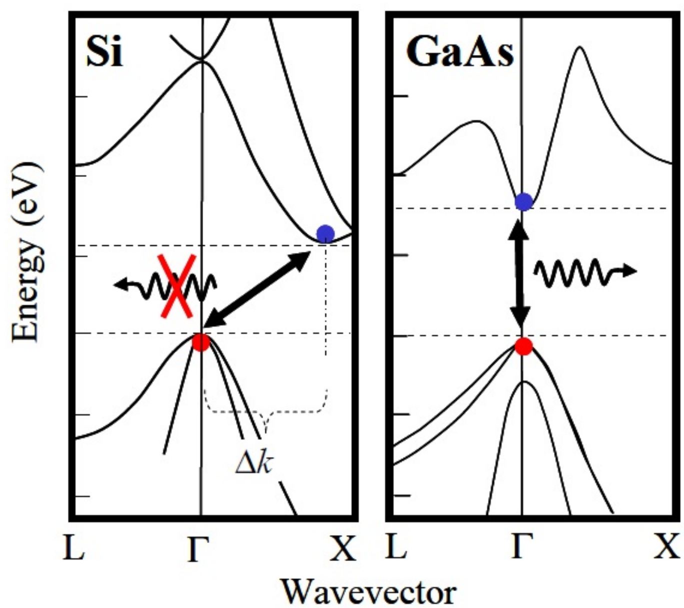

Figure 2.1: Energy-band diagrams for Si and GaAs. In bulk Si, conduction electrons and valence holes occupy the band's minima and maxima with different momentum. Photon emission without assistance of phonon is not allowed for silicon. (Ref [2]).

lowest energy states of the conduction band and holes occupy the highest states of the valence band. Recombination of an electron and a hole leads to emission of a photon, that is conduction electrons transit to the valence band and release their energy in the form of a photon. Photons with energy equal to the bandgap of the semiconductor are emitted. Besides energy, momentum conservation is also required in photon emission process. However, photon momentum is negligible compared to electron's and hole's momentum by a factor of 1000. In a direct bandgap material, the electrons are in the the conduction band minima and can recombine with holes at the valence band maxima since they are of the same momentum at the center of the Brillouin zone and therefore radiative recombination is possible without breaking momentum conservation rule. In a indirect bandgap material like silicon and germanium, there is large difference between momentum of electrons in the conduction band minima and holes in the valence band maxima and therefore a direct recombination of electron and holes (without phonon assist) is not possible due to momentum conservation rule. Photon emission process is possible only with assistance of another entity such as a phonon. However this is a process with low probability and as a result, silicon is a poor light emitter semiconductor. Eventhough in many cases, this property of Si is a disadvantage it is a desirable property in electronic applications [2]. This is because in Si due to indirect nature of energy diagram, radiative recombination is slow (on the order of a few miliseconds) [2]. Minority carriers lifetimes are long enough that they can diffuse for distances up to few hundreds of micrometers. In a direct semiconductor on the other hand, the lifetime is on the order of a few nanoseconds which limits diffusion of minority carriers in these materials. However when Si nanocrystals are considered, situation becomes different. At the nanometer scale, Heisenberg uncertainty principles plays important role, that is due to spatial confinement of electron and holes in a nanoscale region, there is relaxation in the momentum of carriers which increases with decreasing nanocrystal's size. It is therefore expected that probability of radiative recombination and therefore optical efficiency increases and allows the possibility to use Si nanocrystals as active photonic element [49, 50]. This phenomena was first reported in 1990 by Canham [14] when he observed an efficient light emission from porous Si under excitation with a UV source. Intensity of that photoluminescence was comparable with direct band gap semiconductors, moreover a blue-shift of photoluminescence peak was observed with decreasing the size of nanocrystals. These two points suggests that the origin of emission can be quantum confinement of charge carriers in nanostructures.

2.1.2 Photoluminescence in Si and Ge nanocrystals

Despite the enormous number of reports on photoluminescence from Si and Ge which confirm existence of quantum confinement in the nanocrystals, there are considerable number of other works that are not in agreement with quantum confinement models. That is blue shift upon size reduction predicted by the the confinement models is not observed in the nanocrystals. This is more challenging in Ge nanocrystals as there is only one report [4] on Ge nanocrystals embedded in dielectric matrices. The main reason of this disagreement is the role of surface states in emission of light which makes observation of PL from quantum confinement effect very difficult. Control of surface chemistry that is critical since it governs the way dangling bonds are satisfied. Furthermore since the ratio of surface to volume increases as the size decrease, the effect become more important in smaller nanocrystals and smaller nanocrystals exhibit higher defect related emission. Fig.(2.2) illustrates ratio of surface to volume as a function of nanocrystal's size in "0","1" and "2"D structures. In the case of spherical silicon or germanium nanocrystals the effect of NC's size on surface states is as follows. From Fig.(2.2) surface to volume ratio (STV) for spherical geometries is:

$$STV = 3(\frac{d}{R}) \tag{2.1}$$

Where "d" is considered as surface thickness that is region in which the atoms can be considered as surface atoms. We estimate this thickness to be around 1 to 3 monolayers thick and since lattice constant for Si and Ge are 5.4 A and 5.6 A respectively we can take "d" to be 1"nm". Therefore, for spherical Si and Ge NCs surface to volume atom ratio (STV) can be written as:

$$STV = (\frac{d}{R}) \tag{2.2}$$

Where "R" is radius of NC. For NCs with radius of 3.0 ,6.0 and 10.0 nm for example, (STV) is approximately: 0.7, 0.5 and 0.3. It means that for Si or Ge NCs with radius 3nm, around 70 percent of atoms are located at the surface of nanocrystal while for NCs with radius 10 nm only 30 percent of atoms are at the surface. It can be concluded that surface related phenomena are more important as the size of the nanocrystals decreases, therefore, at the nanometer scale, besides quantum mechanical effects which arise from the Heisenberg uncertainty principle, surface related effects should also be considered carefully as an emission source.

In the next section we review the theory of quantum confinement effect (QCE) in more details and discuss its effect on modifying the band gap and photoluminescence of nanocrystals.

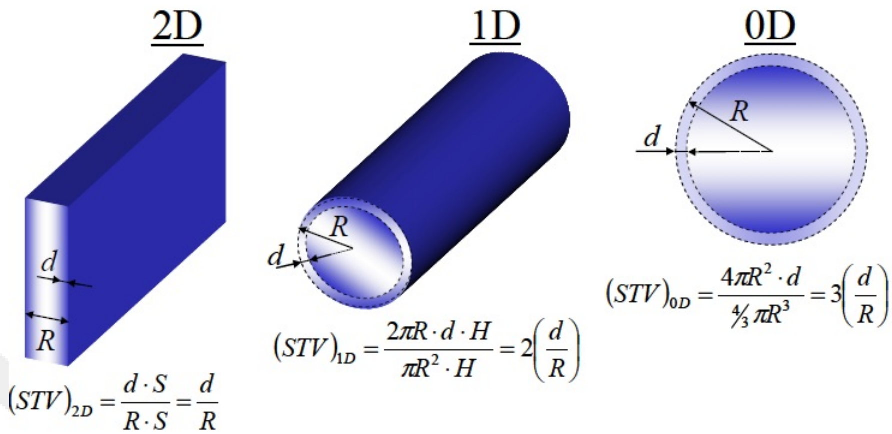

Figure 2.2: Surface to volume ratio for 2D, 1D and 0D geometries. Here "R" represents the thickness of slab, radius of cylinder and sphere respectively. "d" is the thickness of surfaces in all geometries. (Ref. [2])

2.2 Spatial confinement of charge carriers in nanocrystals

The most interesting feature in nanotechnology is the spatial confinement of charge carriers in one, two or three dimensions. This spatial enclosure gives rise to shift in the energy of charge carriers compare to bulk material. The basic principle of quantum confinement effect is shown in Fig.(2.3). When the size of a nanocrystal is comparable with wavelength of charge carriers in the conduction band (CB) or the valence band (VB), the nanocrystal can be considered as a potential well with finite dimensions and up to first approximation with infinitely high potential barriers. Generally there are three classes of nanostructures: quantum dots (QD) which is a system in which charge carriers are confined in all three dimensions and therefore there is zero degree of freedom. When the system is confined in two dimensions it is called a quantum or nano-wire (NW). Finally quantum well (QW) is a structure confined in one dimension. Figure (2.2) schematically also shows these three classes of nanostructures. This classification is base on the size of nanostructures compare to Bohr radius (a_B):

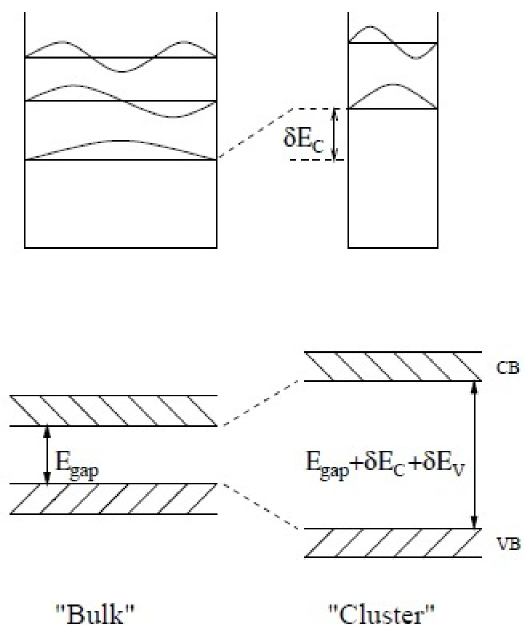

Figure 2.3: Schematic of the quantum confinement effect. Widening the band gap of nanocrystals compared to bulk counterpart as predicted by quantum confinement.

$$a_B = \frac{4\pi\epsilon\hbar^2}{m_* e^2} \tag{2.3}$$

Where "m" is the effective mass of electron or hole or exciton, "e" is the electric charge carrier and ϵ is the dielectric constant. Because of different effective mass and dielectric constants, silicon and germanium have different Bohr radius. Si has a Bohr radius of 4.5 nm and Ge Bohr radius is 24 nm. [25]. Bohr radius determines the approximate sizes below which quantum confinement effect becomes significant [51]. Generally there are three regimes of confinement in nanostructures [51]: Weak confinement is the regime in which the dimensions of the nanostructure is much larger than bulk Bohr exciton radius and the energy is dominated by Coulomb energy. But still the exciton feels the bounds of nanostructure. Intermediate confinement is defined as the regime in which the dimensions of the nanostructure is much smaller than electron Bohr radius but still larger than hole and exciton Bohr radius. Therefore only electrons are efficiently confined. This is the case for the most nanostructure. Strong confinement is defined as the regime in which the dimensions of nanostructure is much smaller than both electron and hole's Bohr exciton radius. In this regime both electrons and holes are efficiently confined and in this regime it is generally believed that Coulomb term is too small and therefor can be treated as a perturbation term [51]. However some recent theoretical calculations for Si nanostructures show that even for strong confinement regime, Coulomb interaction is the most important in determining optical properties of nanostructures. [52]. A more useful definition of strong confinement is the regime in which the band structure of nanostructure is changed by the reducing size of nanostructures. In this thesis our focus will be on this strong confinement regime. Here we briefly discuss the physics behind quantum confinement: In a bulk crystal, the charge carriers can be described as Bloch waves, propagating freely in the whole crystal's periodic field. When become confined inside a nanostructure, carriers can not be described as freely propagating Bloch waves anymore as they are confined in one or more dimensions. For nanocrystals embedded in a wide band gap material, like SiO_2, Si_3N_4 or Al_2O_3, quantum confinement effect occurs via use of a confinement potential due to differences of band gap between nanocrystal and surrounding matrix. Strength of confinement is determined via the misalignment of valence band (VB) and conduction band (CB) at the nanocrystal-matrix interface. Confinement potential function is usually considered as Gaussian, Poschl-Teller or in the simplest form as a function representing a parabolic well. In a quantum dot (QD), with finite dimensions. charge carriers, to a first approximation, are confined with infinite potential barriers. Therefore Bloch waves are reflected at the potential barriers For a charge carrier with effective mass m^* confined inside a cubic nanostructure with infinite barriers, energy level is shifted compared to bulk crystal by the amount ΔE_{ni}:

$$\Delta E_{ni} = \frac{\hbar^2 pi^2 n_i^2}{2m^* D_i^2} \tag{2.4}$$

Where n_i is principle quantum number, D_i is nanostrusture's diameter, E_{ni} is the energy of the considered state with $i = x, y, z$. This shift in ground state energy in the nanostructure is defined as quantum confinement or confinement energy. Due to the positive shift in energy the ground state of a nanocrystal increases, hence, overall band gap increases compared to bulk crystal. Quantum confinement can also be understood in terms of Heisenberg uncertainty principle where:

$$\Delta P \Delta X \approx \hbar \tag{2.5}$$

Therefore increasing spatial resolution, leads to increasing uncertainty in momentum of the carriers on the order of:

$$\frac{\hbar}{L} \tag{2.6}$$

or uncertainty in energy of the order of:

$$\frac{\hbar^2}{2mL^2} \tag{2.7}$$

Thus band gap engineering is possible by modifying the dimensions of the nanostructurs. Band gap engineering can alternatively be done in another way. Due to the fact that bulk germanium is an indirect gap material, in an optical absorption or emission process, a phonon is required to maintain momentum conservation. However in a nanocrystal, optical transition is possible without phonon assistance due to relaxation of the momentum conservation rule or via the process of Brilouin zone-folding makes the material quasi-direct [53]. Eventhough origins of these two processes are principally different, they lead to nearly same effects. Relaxation of the momentum conservation rule due to Heisenberg uncertainty principle leads to uncertainty in momentum of charge carriers in nanocrystals. When confinement dimensions is reduced width or the uncertainty in the momentum of the carriers increased. For Ge with a hole at the $\Gamma - point(K = 0)$ in the valence band and electron at $L - point$ in the minimum point of conduction band, decreasing spatial dimensions, leads to increasing in momentum width and therefore enhancement of coupling in the transition matrix elements between electrons and holes and therefore increasing in transition probability. To summarize due to relaxation of the momentum conservation rule, transition between valence band and conduction band between different locations in Brilouin zone can become possible without assistance of phonons and this possibility increases with reducing dimensions of nanostructures. Breaking of momentum conservation rule strongly depends on size and shape of nanostructures [54]. In silicon nanocrystals for sizes below 2.5 nm, momentum conservation rule is strongly broken and phonon-free transitions drastically increases. For germanium this momentum conservation rule break happens at larger nanocrystals due to larger Bohr radius for germanium compared to Si [55]. Photoluminescence measurements show that for small enough nanostructures, optical transitions without phonon assist is dominant which confirms the results of [54]. For experimentally investigating quantum confinement effect, it is therefore crucial to determine the average size of the nanocrystals inside matrix. Direct observation is possible via high resolution transmission electron microscopy (HRTEM). An issue about this method is the available contrast between the nanocrystal and the matrix. In the case the contrast is poor, size uncertainty can be on the order of 1 nm [56]. There are also indirect methods for determining nanocrystals size including X-ray diffraction (XRD) [57] and X-Ray photo electron spectroscopy (XPS) [58]. In the case of germanium nanocrystals it is difficult to observe quantum confinement in embedded nanocrystals. Despite the larger Bohr radius compared to silicon which essentially should lead to easier observation of the effect, there are very few reports [4] on optical tunability of germanium nanocrystals embedded in dielectric matrices. Actually to our knowledge there is only one report on literature with photoluminescence shift in agreement with quantum confinement [4]. This difficulty in observing quantum confinement in germanium arises most likely from ill-defined chemistry in nanocrystal-matrix composition, sub-oxide states and defects. However, there are promising reports of progress in this area [59].

2.2.1 Band gap engineering of Si and Ge nanocrystals via quantum confinement of charge carriers

In this section band gap engineering of Si and Ge nanocrystals by means of size variation will be discussed as predicted by quantum confinement. Experimental reports in the literature are compared with those predicted by quantum confinement models. There are several models which describe the effects of quantum confinement on band structure of Si and Ge nanocrystals. Among them perturbative effective mass theory is widely used for all nanostructures that is quantum dots (QDs), Quantum well(QW) and quantum wires (Q-wire). Effective mass approximation (EMA) model predicts the band gap of Si and Ge as a function of size, using QCE discussed in the previous section and after some calculations [51] gives:

$$E_{gap}(D) = E_{gap}(bulk) + \frac{A}{D^2} \tag{2.8}$$

where $E_{gap}(Bulk)$ represents the band gap of bulk crystal and "D" is the diameter of QDs, thickness of Q-wire and QW. "A" is a parameter that determines confinement regime for Si and Ge in 1D, 2D and 3D. However in Ge nanocrystals observation of QCE is more challenging due to tendency to form defects at the nanocrystal's surface and ill defined chemistry at the interface. For the electronic structure of large-scale atomistic systems, Wang and Zunger have developed the "LCBB" method which is particularly convenient for embedded NCs containing several thousand atoms [60], Bulutay [3] have used semi empirical pseudopotentials (EPM) for Si and Ge which developed specially for strained Si/Ge superlattices, which reproduces a large variety of measured physical data such as bulk band structures, deformation potentials, electron-phonon matrix elements, and heterostructure valence band offsets [61]. The resultant bulk band structures for Si and Ge and their host wide band-gap matrices are shown in Fig.(2.4) [3] With the use of such a lattice-matched matrix providing the perfect termination of

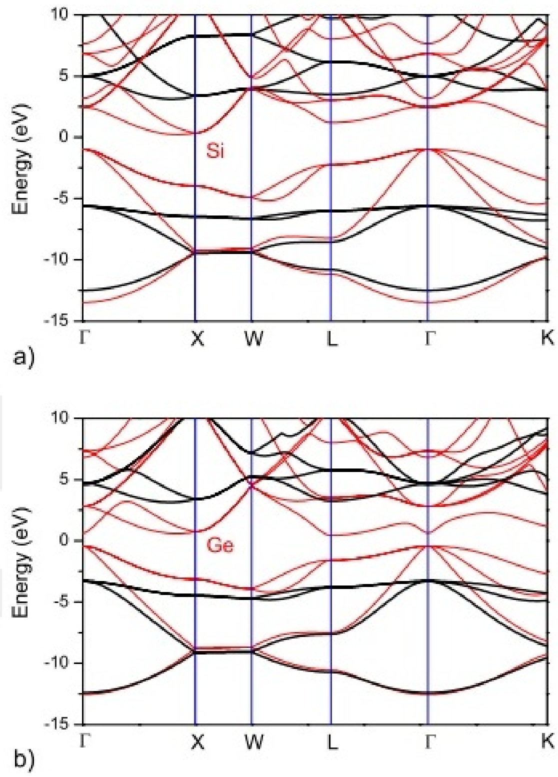

Figure 2.4: EPM band structures for bulk (a). Si and (b). Ge together with their wide band-gap matrices (thick lines), which for the former reproduces the band lineup of the Si/SiO2 interface. (Ref. [3])

the surface bonds of the NC core atoms leads to band gap variation with size as represented in Fig.(2.5) In these plots, the evolution of the effective band gaps toward their bulk values marked by dashed lines is clearly seen as the diameter increases. To verify quantum size effect in Si and Ge NCs, the effective optical gap have been studied with a number of theoretical [21, 62–65] and experimental [4, 66, 67] within the last two decades. Figure (2.6) contains a compilation of some representative results. For Si NCs, it can be observed that there is a good agreement among the experimental and theoretical data. On the other hand, for Ge NCs, there is a large disagreement among the experimental data reported by several groups. First report on observation of quantum confinement was by Takeoka et al. [4]. In that work, Ge QDs were prepared by co-sputtering followed

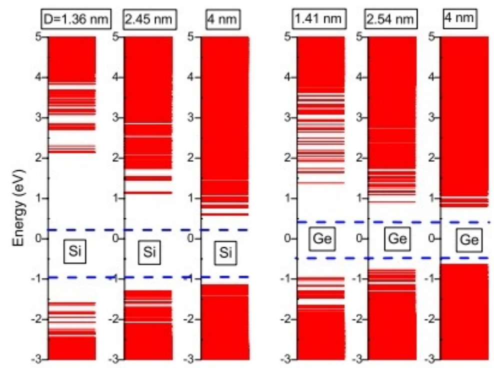

Figure 2.5: The variation of NC states with respect to diameter for Si and Ge NCs. The bulk band edges are marked with a dashed line for comparison. (Ref. [3])

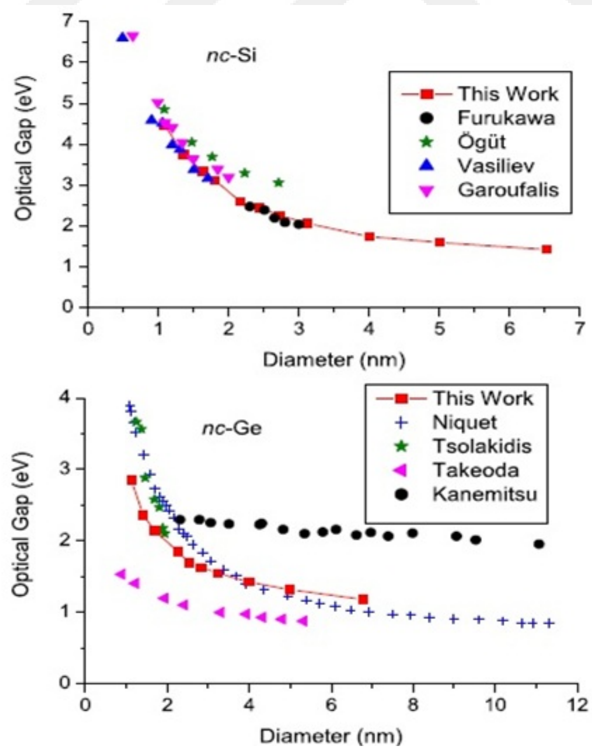

Figure 2.6: Optical gap for Si and Ge. Theoretical predictions and experimental reports. Si NCs shows more agreement between theoretical and experimental results. In Ge NCs however there is not an agreement between theoretical and experimental results. This is probably due to high ratio of surface effect located at the surface of Ge NCs. (Ref. [3])

by thermal annealing. PL measurement was at room temperature and a red luminescence with blue shift with size decreasing in agreement with QC was observed. Fig.(2.7) shows PL spectra of Takeokas experiment. However observation of this red luminescence and blue shift was not repeated by other groups later. As can be seen from Fig.(2.6), there is not agreement on experimental reports on PL from Ge nanocrystals. Si nanocrystals show better agreement with predictions of quantum confinement models, for Ge this agreement is not observed probably due to ill-defined chemistry of Ge nanocrystals surfaces which leads to high density of surface defects, as a result emission from these defects becomes prominent in Ge nanocrystals and makes observation of quantum confinement effect very challenging.

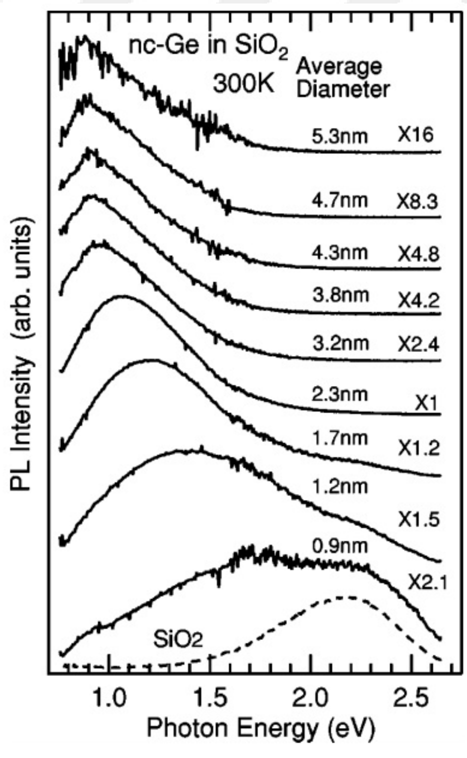

Figure 2.7: Photoluminescence from Ge QDs prepared by co-sputtering by Takeoka et al. at 1998. This is the only report on PL emission of embedded Ge NCs in agreement with QCE. (Ref. [4])

2.3 Phonon confinement in low dimensional solids

Besides size tuning of NCs for band gap engineering, stress engineering gives an extra degree of freedom for modifying band gap of NCs. It is well understood that stress in NCs can change microelectric structure of materials and therefore optical properties. For example Yuan et al. [68] show that stress tuning in Si NC can lead to transformation in the microstructureof the naocrystals from cubic to hexagonal which in turn lowers band gap of NC. Therefore stress analysis of NCs play an important role in determining the NC band gap. A tool for studying stress induced processes in nanocrystals is Raman spectroscopy. Raman study can give stress state of nanocrystal by analyzing shift of the scattered photon due to strained nanocrystal. Since phonons in a nanostructure are confined, Raman spectra of nanostructures would be different from bulk crystal counterpart. This situation is similar to confinement of charge carriers in nanocrystals which leads to a different electronic structures with bulk crystal. Quantum confinement of charge carriers leads freely propagating Bloch waves in infinite lattice structure to be confined in a nanoscale region and therefore an upshift in energy states of electrons and also relaxation of k-conservation rule occurs. In the same way, phonon confinement effect, leads the freely propagating phonons to be confined in a finite region of crystal space and results in an uncertainty in momentum of phonons. This leads to a shifted Raman spectra for nanocrystals compared to bulk crystal. Several models have been proposed to explain optical phonon confinement in nanocrystals. Some of these methods are Gaussian Confinement Model (GCM), Continuum theory and Microscopic Lattice Dynamical Calculations [33]. Most commonly used model is the Gaussian Confinement Model proposed by Richter et al [35] and generalized by Campbell and Fauchet [36]. This model is based on the contributions of the phonons out of the center at Brilouin zone. To describe this model, consider a spherical nanoparticle of diameter of "D" and phonon wave function $\Psi(q_0, r)$. This wave function must be multiplied by envelope function W(r) which decays close to zone center, due to the existence of the phonon wave function within the particle. Plane-like wave function can not propagate beyond the crystal surface. Envelope function is commonly chosen as a Gaussian function as;

$$W(r, L) = \exp(-\alpha \frac{r^2}{L^2}) \tag{2.9}$$

where α is related with how rapidly wave function decays. One-photon Raman scattering weight function C(q) which is used to define the contribution of the phonons away from zone edge and which is simply Fourier transform of the envelope function is:

$$C(q_0, q) = \frac{1}{(2\pi)^3} \int d^3q \Psi(q_0, r) \exp(-iq_0 r) \tag{2.10}$$

Using these functions, first order Raman Spectrum is obtained by integration as:

$$I(\omega, l) = \int d^3q \frac{lC(q, l)I^2}{[\omega - \omega(q)]^2 + (\frac{\gamma_0}{2})^2} \tag{2.11}$$

where $\omega(q)$ is phonon dispersion relationship and γ_0 is the natural line width of the optical phonon for bulk materials. Figure(2.8) represents phonon dispersion graph for optical and acoustical phonons in first Brilouin zone. For a nanocrystal with dimension "L", Heisenberg uncertainty can be written as Eq.(2.5) in which "P" represent the momentum of phonons. For a nanocrystal with length "L", Heisenberg uncertainty gives an uncertainty to momentum which is on the order of $\hbar L$. Therefore momentum conservation rule is broken in nanostructures and phonons with q≠0 involve in Raman scattering process. The smaller the dimensions of NCs the higher the uncertainty in momentum of phonons. it is obvious from Fig.(2.8) that phonons with $q = 0$ have maximum frequency and phonons with q≠0 have lower frequency. Therefore phonon scattering in nanocrystals occurs with lower frequency shift compared to bulk crystal. That is for freestanding nanocrystals there would be a red shift in the Raman spectra compared to bulk crystals. Also since a variety of phonons with varied values of q≠0 involved in Raman scattering, there would be a broadening of Raman spectra compared to bulk crystal. However in experimental Raman spectra of Ge NCs embedded in matrices there is generally a blue shift compared to bulk crystal. This is generally due to strong compressive stress exerted by the surrounding matrix on the nanocrystal. Since compressive stress leads phonons to oscillate faster and therefore with higher frequency and tensile stress leads phonons to oscillate with lower

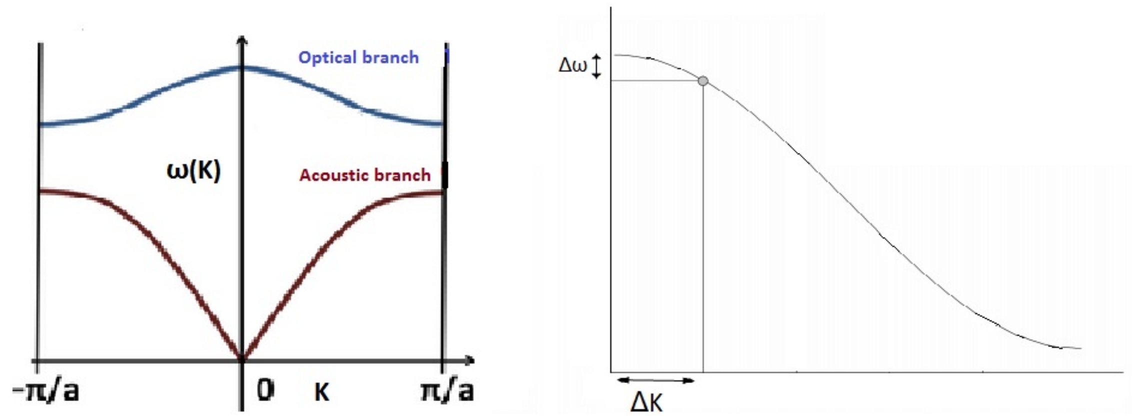

Figure 2.8: Principle of phonon confinement effect in nanocrystals. Heisenberg uncertainty principle leads to a relaxation of q=0 for phonon momentum and phonons with nonzero momentum can involve in Raman scattering, this phonons have lower frequency and therefore a red shift in Raman peak is predicted via phonon confinement. (Ref. [5])

frequency. As a result, compressive stress leads to a blue shift and tensile stress results in a red shift when compared with free standing nanocrystals. Therefore in an experimental Raman spectra of NCs, the observed Raman shift compared to bulk crystal is combination of shifts due to phonon confinement effect which is always redshifted in the case of longitudinal optical phonons and stress induced shift which is blue shifted for compressive stress and red shifted for tensile stress. Since shift due to phonon confinement effect is size dependent, by measuring nanocrystals via methods like HRTEM and applying phonon confinement effects it is possible to extract stress state of nanocrystals. This stress is important in optical properties of nanocrystals. Paillard et al. [69] have used phonon confinement model for measuring stress of Ge nacocrystals embedded in silicon oxide matrix. They considered Raman peak shift as a combination of stress induced and phonon confinement induced shift. Having obtained size of nanocrystals from TEM micrographs, they extract stress state of nanocrystals by applying phonon confinement model. In experimental discussion part of this work we discuss this approach in more details as we will show there, stress depends on the surrounding matrix, processing approach and stressor caps.

Chapter 3

Experimental

In this chapter, details of synthesis of Ge NCs as well as analyzing techniques used for the project is discussed. First, the processes used in the films growth and post growth annealing are presented. This, includes Plasma Enhanced Chemical Vapor Deposition (PECVD), Conventional furnace annealing (CFA) and rapid thermal processing (RTP). Various techniques used for structural and optical characterization of nanocrystals are presented. These are: Rutherford backscattering Spectroscopy (RBS), X-Ray Photo electron spectroscopy (XPS), for compositional analysis of materials and Raman spectroscopy which is used to examine crystallinity and stress state of the nanocrystals and photoluminescence (PL) spectroscopy for optical characterization of the NCs.

3.1 Sample preparation

Samples are grown on silicon and quartz substrates. p-type, two sided polished silicon wafers are used. The wafers are of [1 0 0] orientation with resistivity of 10-20 ohm-cm. Contamination of samples were removed by standard acetone-isopropanol- water cleaning to ensure high quality of thin film growing. The native oxide which usually are left on substrate was removed by immersing the wafers in a diluted hydrofluoric acid for a duration of around 10 to 20 seconds. Then the samples are immersed in distilled water before the wafers are blown dry with nitrogen.

3.2 Thin film deposition of Ge rich dielectrics

There are many methods for the deposition of thin films.E-beam and thermal evaporation,d.c and magnetron sputtering are among the most common methods. Plasma Enhanced Chemical Vapor Deposition (PECVD) method is a widely used technique in fabrication of semiconductor devices [70]. It is very common in deposition of oxides and nitrides. Fig (3-1) shows schematic of a PECVD system.

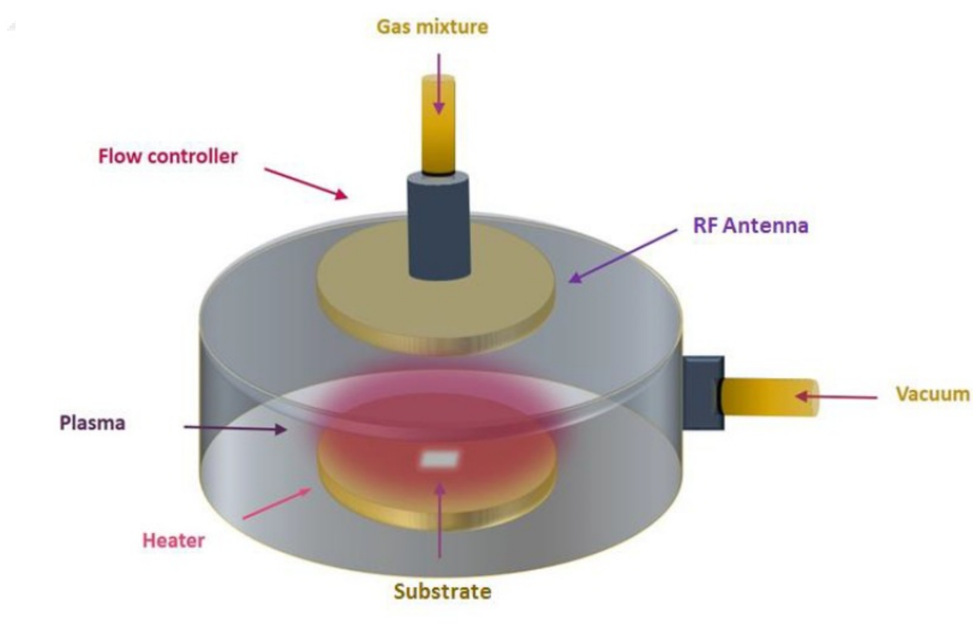

Figure 3.1: Schematic of a PECVD system used for to growth the samples.

In a PECVD system, an RF field is applied to a low-pressure gas and generates a plasma; RF field gives enough kinetic energy to electrons inside the reactor to collide with molecules of process gases. Reactant gases dissociate and ionize and high energy ions and radicals are adsorbed to the substrate surface and due to high kinetic energy, are able to migrate easily along the substrate surface. Therefore in film growth via PECVD, films are conformal. Finally processing species like ions and electrons, rearranged and react with other adsorbed species on the substrate and film is grown [71]. Typically PECVD is a low temperature processing method (generally below 400C), This is due to the fact that reactant gases gain enough energy from RF-induced plasma and therefore have energy for diffusion on the substrate surface and the required reactions for deposition. An issue about PECVD process is the various parameters involved in film growing including substrate temperature, RF power, gas pressure, gases flow rates. It is important to have reliable control over all these parameters. Especially controlling temperature is very important. PECVD method has some advantages over other methods like co-sputtering including good adhesion to substrate, good coverage of substrate and low temperature processing. in this work we used an Oxford Plasma (model PLASMALab 8510C) system. In this system, RF generator can produce an RF with frequency of 13.56 MHz and maximum power of 300 Watt.The reactor is equipped with 6 gas lines including $NH34$, $N2O$, $GeH4$, $SiH4$ diluted in He, $SiH4$ diluted in $N2$, $NH3$ and $CO2$. $SiH4$ and $N2O$ gases are used for deposition of $SiO2$ while $SiH4$ and $NH3$ are used for growing $Si3N4$ films. $GeH4$ gives Ge to the $SiO2$ and $Si3N4$ matrices.

3.2.1 Conventional urnace annealing (CFA) for the formation of Ge NCs.

Furnace annealing is widely used in synthesis of embedded nanocrystals. This method provides required energy for diffusion and formation of germanium nanocrystals. This step in the whole process of crystallization is very important as controlling parameters of annealing like ambient gas, gases flow rate, temperature and annealing duration can affect the crystallization process. Its advantage over rapid thermal processing (RTP) is the possibility for annealing in larger duration which allows to study the time dependent processes. Fig(3.2) shows schematically a CFA system. Samples are loaded onto a quartz carrier

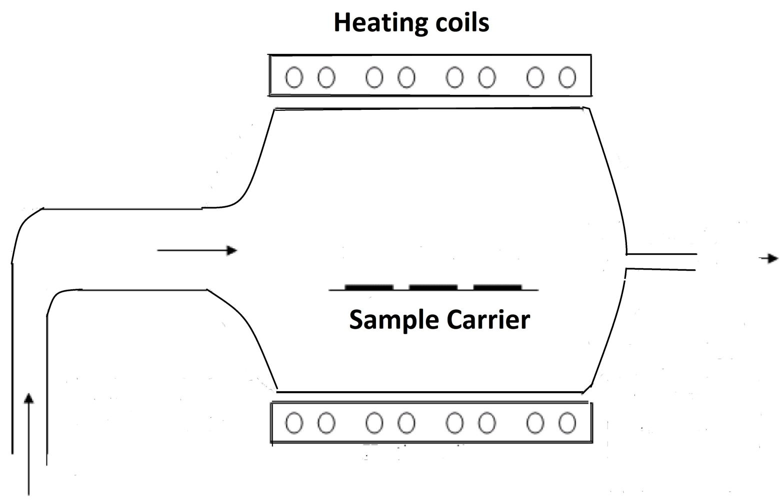

Figure 3.2: Conventional furnace annealing system used for Ge NCs formation.

resting in the quartz furnace tube at the loading port. The loading port is closed and the quartz tube is purged with pure $N2$ or Ar. Then the quartz carrier is moved inside to the central part of the furnace where the temperature is uniform and stable. The temperature can rise up to 1400 C in our system. External zone of the furnace is designed such that to protect furnace from losing out the energy and therefore central part of furnace has a uniform temperature [72]. Samples are loaded and unloaded inside furnace very slowly to avoid the effect of the large thermal gradient across the wafers. this minimize any thermal shock or thermal stress which can affect quality of nanocrystals.

3.3 Rapid Thermal Processing (RTP) for the formation of Ge NCs.

Rapid Thermal Processing (RTP) is an alternative to furnace annealing in synthesis of ge NCs, having some advantages over it. RTP is cleaner than furnace annealing, because RTP chamber has cold chamber walls and therefore does not introduce contamination or impurities. In furnace system, due to hot chamber wall, the system tends to have contaminations from walls. Second advantage of RTP over furnace annealing is that the short processing time in RTP is compatible with IC device fabrication process which needs lowest diffusion of dopants in the films. Fig.(3.3) illustrates schematic of a RTP system. RTP reaction chamber is typically made of a quartz cover with incoherent light sources, located at the top and bottom of the chamber. These halogen lamps serve as heat sources for the synthesis of Ge nanocrystals in the matrix. The samples are located on a wafer holder and a pyrometer directly below it measures the substrate temperature and sends the data to an integrated closed-loop temperature control system, which controls the process temperature.

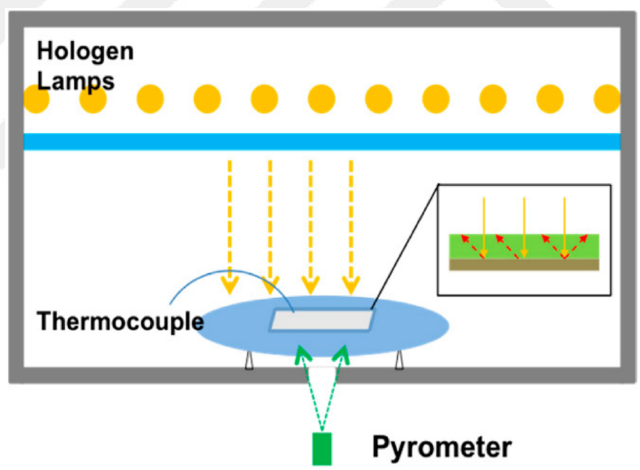

Figure 3.3: **Schematic of a RTP system**

3.4 Compositional analysis :Rutherford backscattering spectroscopy (RBS)

Rutherford Backscattering Spectroscopy (RBS) is a widely used method for near surface layer analysis of solids. This method originated from classical nuclear physics experiments in the first half of the twentieth century. In 1960s it was developed for those days growing semiconductor field. A beam of collimated $He+$

at an energy ranges between 0.5-4 MeV is made incident normally on a target and the energy of backscattered particles is recorded with a solid state detector. Due to the very large free space between atoms in RBS process, most of the $He+$ ions are trapped into the target and do not scattered.Therefore very few percent on incident ions are scattered [73,74] The basic process is represented in Fig.(3.4) A collimated beam of known ions with mass "m" collide to target particles with

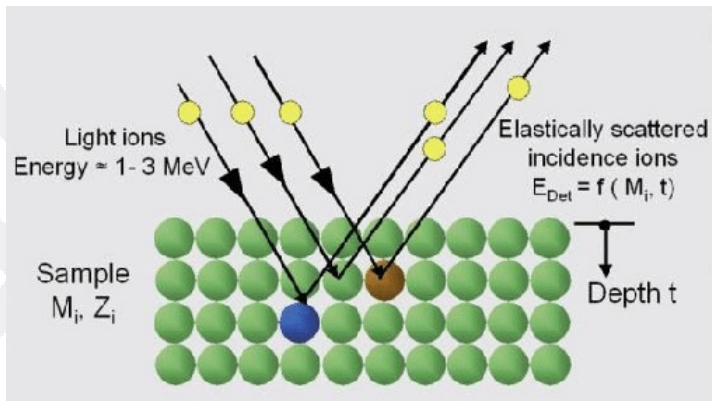

Figure 3.4: **Schematic of a RBS process.Elastically scattered ions gives information on composition of target material.**

mass "M" and scattered with different energy at scattering angle of "θ", energy of "E". Scattering angle is detected and using momentum and energy conversation laws, mass of the target particles obtained. Also since the probability of scattering of ions in any certain angle is known through Rutherford cross section, it is possible to obtain quantitative information on targeted particles. RBS provides possibility to quantitatively determine composition of materials on depth profile of elements. RBS method is also a nondestructive tool (unlike XPS and SIMS) and reference sample is not required. It has also a good depth resolution on the order of a few nanometers and very high sensitivity for heavy elements on the order of parts per million (ppm). Figure(3.5) shows schematically a typical RBS system. A RBS system consist of a particle accelerator that delivers ions in the Mev range. In the system represented at Fig.(3.5) the machine provides negative ions, then the ions are accelerated toward positive potentials and are transported in a vacuum system at high voltage terminal, there are electrons and the particle charge became positive. Then the particles are repelled by high positive voltage and their energy increases further. Then the beam is analyzed and sent to the target chamber. The detector is normally mounted in a backscattered angle from

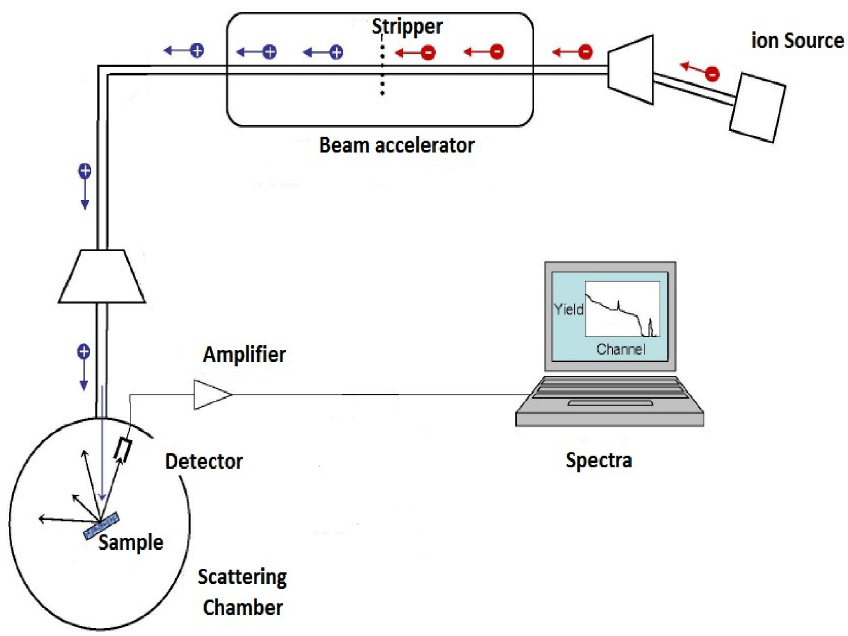

Figure 3.5: **Schematic of a RBS system**

the incident beam. When the incident particles collide the target matrix, some of them experience Rutherford scattering and deflect from their path and backscattered into the detector. In this work RBS measurement were done by Professor Salvatore Mirabella at Catania University-Italy. Measurement were carried out with a 3.5 MeV HVEE Singletron accelerator, using a 2.0 MeV $He+$ beam in random configuration and with a backscattered angle of 165. RBS spectra have been simulated using SIMNRA software [75] to determine the Si, Ge, and N content and the stoichiometry of each film.

3.5 Compositional analysis: X-ray Photo electron spectroscopy(XPS)

X-ray photoelectron spectroscopy (XPS) is a strong and very sensitive technique in analyzing elemental composition and chemical state of materials. It is a surface spectroscopy method which collects information from a depth of around 3 to 10 nm from the surface. XPS is based on photoelectron effect. Fig.(3.6) represents the principle of an XPS experiment. Target sample is irradiated by X-ray beam, then energy of beam is transfered to the material's electrons. kinetic energy of ejected electrons is measured. this energy depends on characteristic binding energy of irradiated material. each element has a characteristic binding energy for its core electrons. The binding energy also depends on the chemical environment of the element, that is the chemical bonding with neighboring atoms,therefore measuring the energy of ejected electrons gives information about the chemical elements and its bonding with other elements [76] Kinetic energy of photoelectrons is determined by:

$$E_k = h\nu - (E_B + \phi) \tag{3.1}$$

Where E_k is kinetic energy of photoelectrons,$h\nu$ is energy of X-ray radiation, E_B is electron binding energy and ϕ is the spectrometer work function. XPS measurments of this work is done by Professor Emre Gur and Ahmet Emre Kasapoglu in Ataturk University.

3.6 Structural analysis: Raman spectroscopy

Raman spectroscopy is a widely used method in analysis of semiconductor layers, heterostructures and interfaces [77]. It is a nondestructive method for analyzing of regions around some nanometers below the surface as well as deeper parts up to micrometers that is a buried interface. Invention of laser in 1960 and also development of very sensitive detector systems in 1980's made Raman spectroscopy a very useful tool. Raman spectroscopy can give a great value of information about

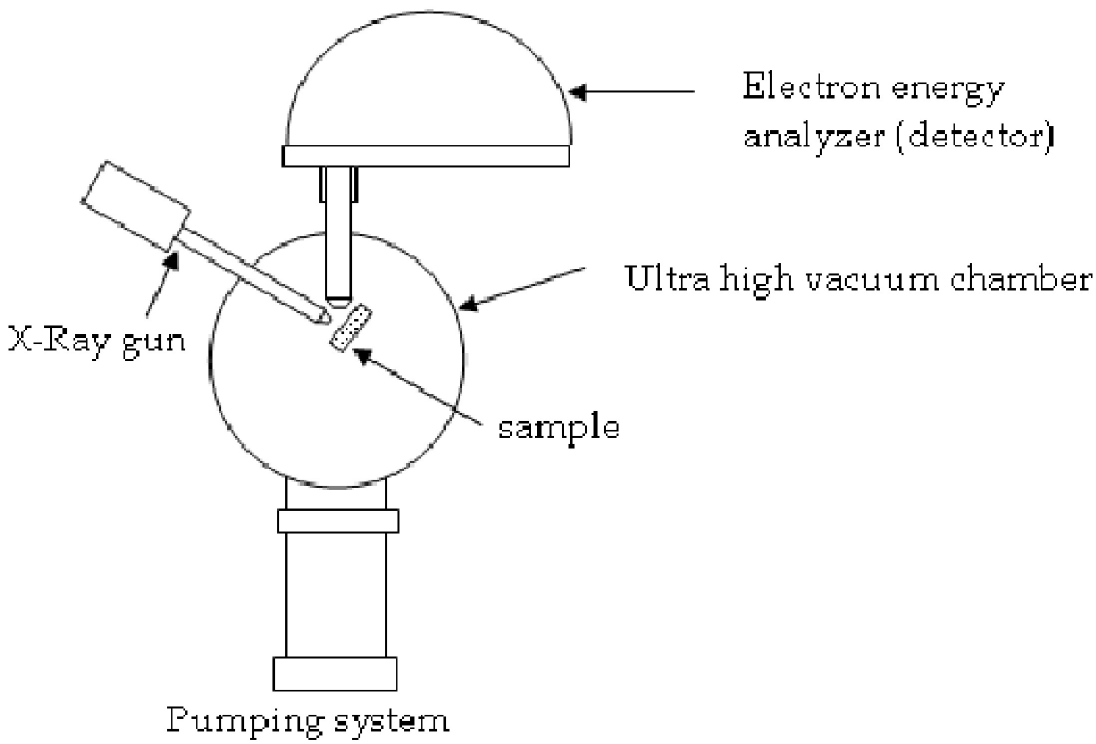

Figure 3.6: **Schematic of a XPS system.**

material. This information is extracted from phonon density of state of materials and include amorphous or crystallinity of material via analyzing of phonon line shape, quality of crystal via Raman spectra width, content of material via signal intensity, stress state of nanocrystals via blue or red shift compared to bulk crystal. Raman spectroscopy is inelastic scattering of light, that is a process in which energy of incident photon is transferred to the sample and result in a scattered photon with different energy [78]. The amount of this energy corresponds to the eigenenergies of elementary excitations such as phonons, plasmons, polaritons, coupled plasma-phonon mode, single electron or hole. In a Raman process, eigenfrequencies of the elementary excitons is determined via analysis of Raman peak shift in scattered light, since shift in the frequency of the incident light corresponds to that eigenfrequencies. Energy conservation yields:

$$\hbar\omega_s = \hbar\omega_i \pm \hbar\Omega_j \tag{3.2}$$

where "ω_s" is scattered light frequency, "ω_i" is incident light frequency, "ω_j" is frequency of the elementary excitations. " $-$ " sign stand for "Stokes" process in which an elementary exciton is generated and " $+$ " sign corresponds o "anti-Stokes" process where an elementary exciton is annihilated. Fig.(3.7) shows diagram of Rayleigh, Stoke and Anti-Stoke scattering. In this work we

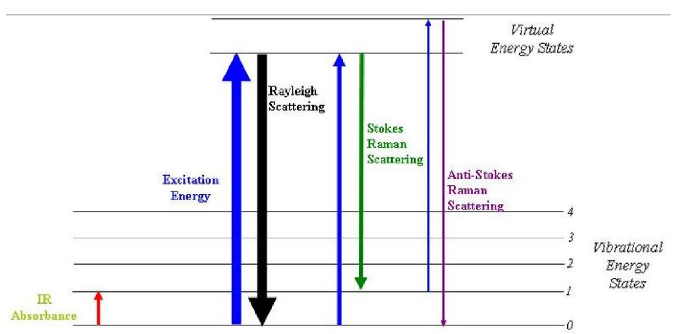

Figure 3.7: **Schematic of a Raman scattering process**.

have used a 514.5nm of Ar ion laser as exciton source, a double monochromator and CCD camera cooled with liquid nitrogen. Fig3.8 shows schematic of Raman spectroscopy set up. First order phonon Raman scattering in solids typically observes TO and LO modes of the solid close to the the gamma point on the phonon dispersion curves of the solid, Fig.(3.9). Observation of acoustic phonons are typically done with Brillouin scattering. Due to inversion symmetry of crystal Ge, LO and TO phonons are degenerate in bulk Ge. Bulk crystalline germanium

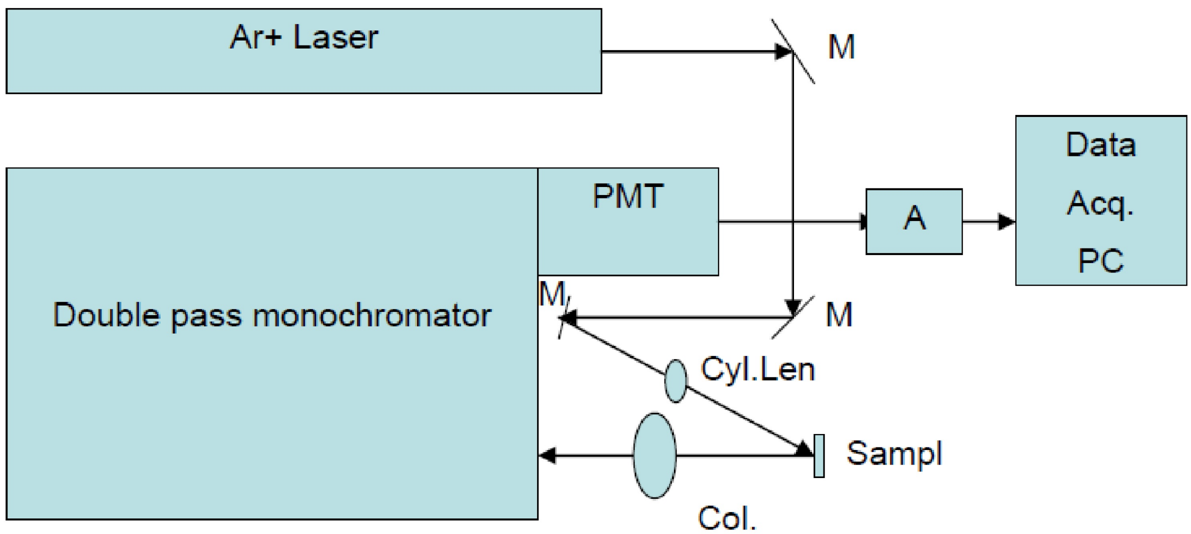

Figure 3.8: **Experimental set up for Raman spectroscopy**

has a characteristic Raman peak at around 300.7cm-1 [69].

However due to factors like stress and phonon confinement there would be a red or blue shift compared to bulk germanium. In his work this shift is analyzed to get stress state of Ge nanocrystals embedded in different dielectircs. Fig.(3.10) shows a typical Raman spectra of samples containing Ge nanocrystals from two samples containing Ge nanocrystals. Both samples show a shift compared to bulk germanium. Different shift and line shapes of two samples provide information about nanocrystals embedded in two samples including NCs average size and size distribution, stress state etc.

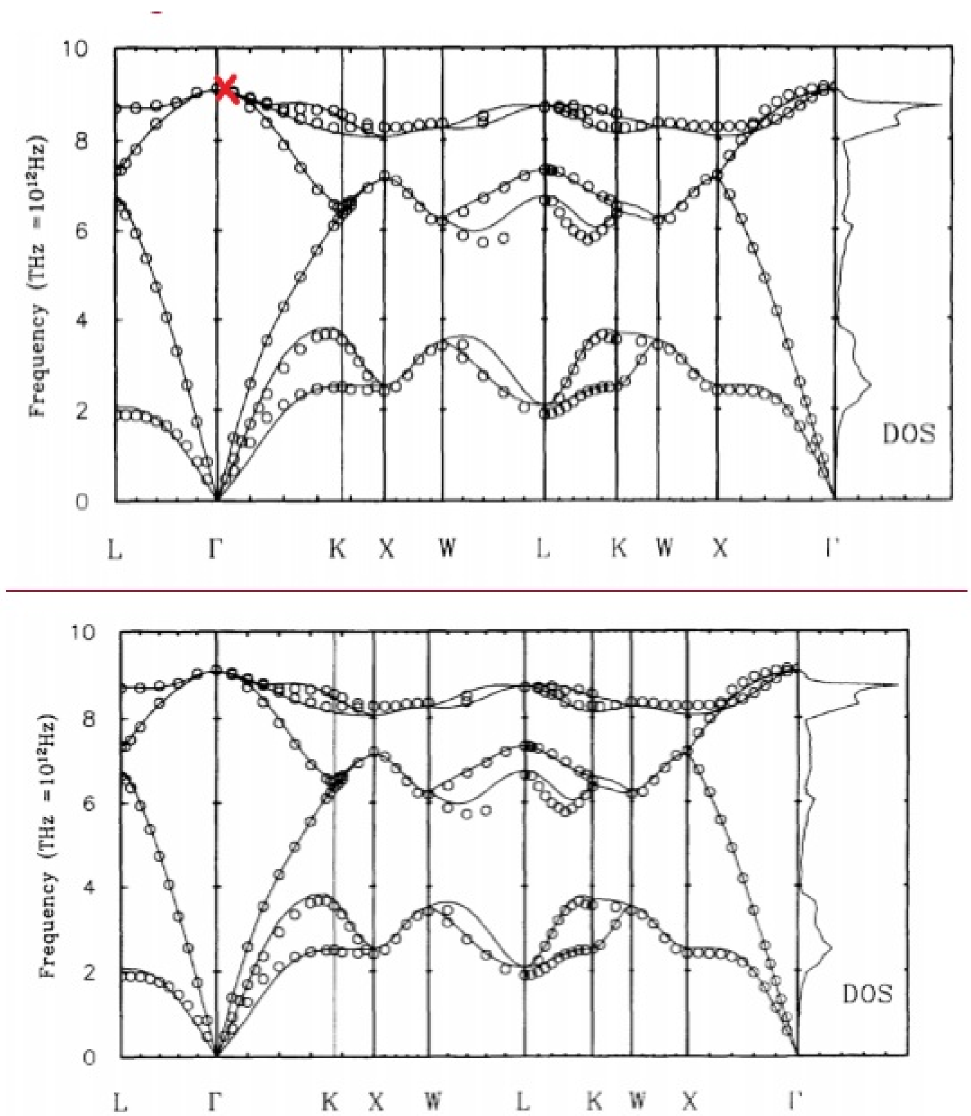

Figure 3.9: **Phonon dispersion of silicon and germanium from first-principle calculations. From [79]**

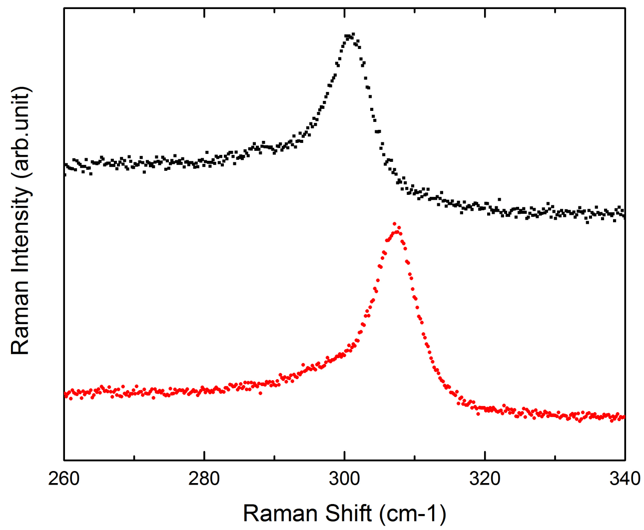

Figure 3.10: **Typical Raman spectra for two samples containing Ge nanocrystals with different size distribution. Different Raman shift of two samples give information about nanocrystals average size, stress state, etc.**

3.7 Structural analysis:High resolution transmission electron microscopy (TEM)

Transmission electron microscopy (TEM) technique is the most direct approach for the observation of nanostructures. In the current work, this method is employed to investigate the formation of the nanocrystals and to get information about their size and size distribution. Figure(3.11) shows The schematic setup of a TEM system. In a TEM system, electrons are accelerated by the same method as that in the scanning electron microscope (SEM), but they pass through the specimen. The specimen must be very thin and flat (around 0.1 micron or less). Similar to a slide projector, more electrons can pass through the less dense regions, and fewer electrons pass through the regions that are denser. The diffracted electron beams are brought to focus in the back focal plane of the objective lens, which is the plane of the diffraction pattern. When the microscope is operated in the diffraction mode, the diffraction lens is focused on the back focal plane and

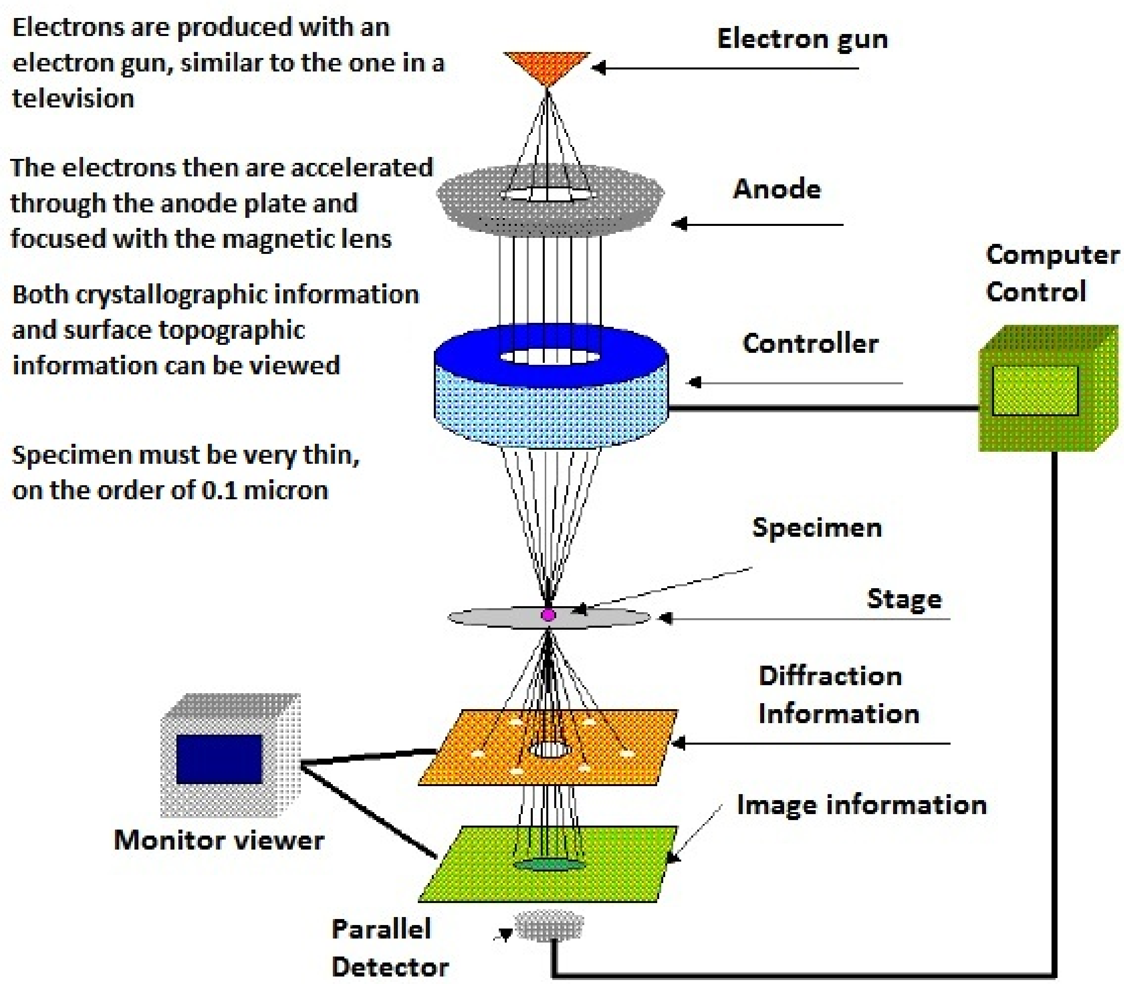

Figure 3.11: **Schematic setup of a TEM system [80]**

the subsequent lenses project a magnified diffraction pattern on the fluorescent screen allowing the user to observe the diffraction pattern. The objective lens also produces an inverted image of the specimen in the first image plane. If the diffraction lens is focused on this plane, the microscope is in the imaging mode and produces magnified image on the florescent screen for observation The TEM technique has great advantages. It can image individual atoms and their relative positions, and also gives compositional information over an area of interest. There are, however, drawbacks to this technique as well. Prior to the imaging, tedious sample preparation steps from polishing, dimpling and ion milling have to be conducted, because the sample has to be very flat and thin for observation, as mentioned above. Furthermore, TEM is a destructive characterization technique as the sample would be destroyed after sample preparation and imaging. In TEM, the bright field and the dark field imaging methods are generally used. In bright field imaging, the objective aperture is placed such that only the center electron beam can pass through and the diffracted beam is screened off. As such, only the center beam forms the image and the background of the image is bright, as shown in Figure 3.12 (a). However in dark field imaging, the objective aperture is placed

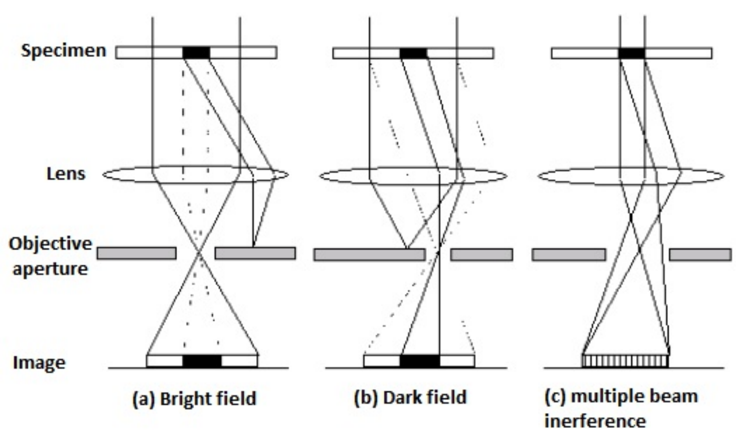

Figure 3.12: **Different imaging techniques used in TEM.(a) Bright field (b) Dark field and (c) multiple beam interference imaging** [80]

such that the center beam is blocked off. Thus only the diffracted beam forms the image, as shown in Figure 3.12 (b). In addition, in high-resolution transmission electron microscopy (HRTEM), multiple beam interference imaging is used, as shown in Figure(3.12) (c) [80]. In the analysis of TEM images, two types of contrast must be considered, which are illustrated in Figure.(3.13) The first type

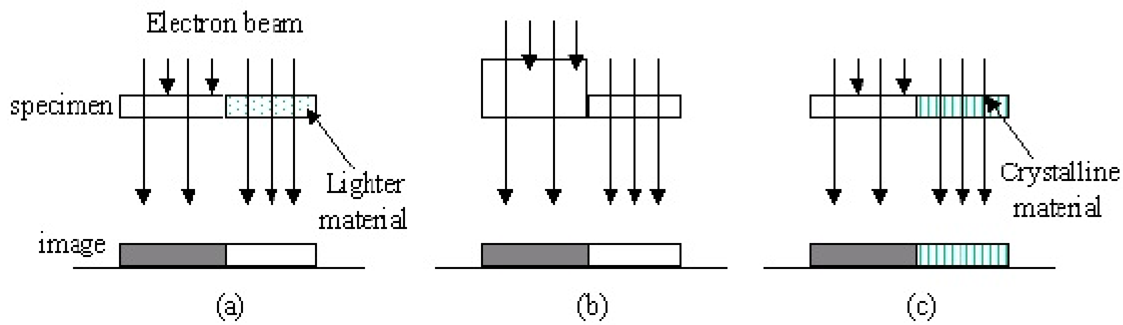

Figure 3.13: **Different contrast modes used in a TEM. (a) Scattering mass contrast image. (b) Scattering thickness contrast image and (c) Lattice fringe image due to phase contrast** [80]

is termed as the scattering contrast. This is the result of mass difference or thickness difference in the sample. With different materials, the absorption may be different due to the difference in densities. This leads to the formation of a mass contrast image. Then in thicker regions, fewer electrons would be transmitted, therefore resulting in a thickness contrast image. The second type of contrast is termed as the phase contrast. This is formed by interference of two or more electron beams. In this sense, fringe patterns would be produced if crystalline materials were imaged. The TEM images, in this work, were obtained using a TECNAI f30 field emission transmission electron microscope operating at 300 kV. Samples were prepared by first hand-grinding the samples down to about 30 m thick, followed by focused ion beam in order to achieve a thickness of0.1μm at the region that was to be imaged.

Chapter 4

Stress measurement and stress evolution: Ge nanocrystals embedded in dielectrics

This chapter is based on publications “Correlation of TEM data with confined phonons to determine strain and size of Ge nanocrystals in embedded $SixNy$ matrix. Superlattices and Microstructures. ”Bahariqushchi, R., Gundogdu, S., Aydinli, A. (2017). and “Stress evolution of germanium nanocrystals embedded in dielectric matrices ”Rahim Bahariqushchi, Atilla Aydinli, et al. *under submission*.

4.1 Introduction

Since observation of visible photoluminescence [14, 25] and also charge storage properties [32, 81] in silicon and germanium nanocrystals embedded in dielectric matrices such as SiO_2 and Al_2O_3, a lot of interest have been paid to this research area. Several methods such as ion beam synthesis, co-sputtering and PECVD have been used to synthesize silicon and germanium nanocrystals in these dielectric matrices. In this work we employed PECVD method as it has been shown in a work [82] that, PECVD synthesized samples have advantages over co-sputtered ones due to sharper interface with surrounding matrix which in turn can lead to easier observation of quantum confinement effect in nanocrystals. Also due to very few experimental reports on germanium nanocrystals embedded in silicon nitride matrix we focus our work on this non-oxidized matrix. In this chapter, first a systematic study on the influence of germanium content as well as annealing conditions on the growth of nanocrystals in silicon nitride matrix is carried out for samples containing different amount of germanium. The amount of Ge were determined to be 4, 9, 15 and 24 percent via RBS technique. Raman spectroscopy as well as HRTEM technique is carried out to examine crystallinity phase. Nanocrystals average size is obtained via TEM micrographs. Raman peak shift analysis is done to obtain stress state of nanocrystals. Raman shift of nanocrystals is result of a redshift compared to bulk germanium which is due to confinement of phonons in nanocrystals and a shift due to stress exerted by surrounding matrix which can be blue or red shift. In the case of compressive stress, this shift is a blue shift and for tensile stress a red shift occurs. to distinguish PCM induced shift from stress induced one,average size of nanocrystals is required which have been obtained from TEM micrographs. Our analysis shows nanocrystals with sizes between 3.8 to 7.0 nm experience almost the same value of stress. The stress is also measured via relaxation of Ge NCs from supporting matrix and comparing Raman spectra of embedded and free standing nanocrystals. Stress estimated with this method is in good agreement with the result obtained via applying a new phonon confinement model developed by [5]. After a detailed study on stress state of the nanocrystals in the silicon nitride matrix, we investigated tuning of stress state of Ge nanocrystals by some methods. First, role of annealing method on stress state of the nanocrystals is studied, then role of surrounding matrix is investigated by synthesis and stress analysis of Ge nanocrystals in SiO_2 and Ge_3N_4 matrices. Finally in this chapter, synthesis of superlattice structures containing Ge nanocrystals has been discussed. Ultrathin films consisting of Ge NCs embedded in Silicon nitride matrix with thickness between 3.0 to 9.0 nm and SiO_2 or Si_3N_4 buffer layers have been fabricated. SiO_2 and Si_3N_4 buffer layers have been used as barrier for Ge atoms diffusion during annealing. This method allows for controlling over size and density of nanocrystals simultaneously. Role of SiO_2 and Si_3N_4 buffer layers have been examined and observed that SiO_2 result in compressive stress while SiN_4 leads to tensile stress. Therefore we have managed to tune stress state of nanocrystals from compressive to tensile.

4.2 Synthesis and stress measurement of Ge nanocrystals

Ge:SiNy thin films with thicknesses around 200nm are deposited using PECVD approach (Model PLASMA lab 8510c) on quartz and silicon substrates. The amount of germanium in as-grown films is probably the most important step in the whole process of crystallization. Therefore we fabricated films with different elemental composition to investigate the role of germanium content on crystallization. Processing gases for growing Ge:SiNy are SiH_4 diluted in N_2, NH_3 and GeH_4 diluted in He gas. To obtain films with different amount of Ge, flow rate of GeH_4 are varied while taking flows of other gases constant. Recipes are represented in Table(4.1) Ge content found to be between 4 to 24 percent via RBS measurements. Ge content are determined using RBS technique. Fig.(4.1) shows RBS spectra for four series of samples. Arrows indicate the signals due to Si, Ge and N in the Ge:SiNy film (starting respectively at around 1600, 1150 and 630 keV of $He+$ backscattered energy for the used configuration). All samples exhibit a homogeneous depth distribution of Ge atoms and the spectra have been fitted through SIMNRA software simulation [83], Fig.(1.b), in order to estimate the atomic content of Si, Ge and N in the film. Table(4.1) summarizes the ratios of Ge/Si and Ge/N evaluated by RBS analysis for Ge:SiNy films. The Ge content in Ge:SiNy films increases with the GeH4 flux, from 4 to about 24 percent. Ge dose were found to be 45, 95, 190 and 275 $*1015at/cm2$, respectively. As expected Ge content increased by increasing GeH_4 flow rate.

After growing of films, all sets of samples were annealed in a conventional furnace in N2 ambient from 700C to 1000 C for 30 min or longer times to form Ge

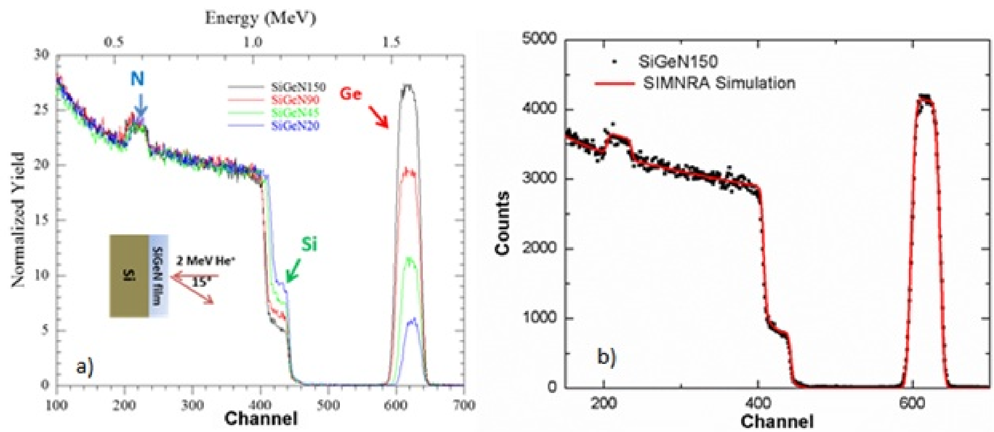

Figure 4.1: RBS spectra of four as grown samples containing different amount of germanium. Backscattered signal due to Ge is obvious with Si and N displaying significant shoulders. The inset image represents the schematic of experimental setup.b SIMNRA simulation of the RBS spectra to determine the composition.

Table 4.1: Sample description and properties of Ge:SiNy thin films with various concentration of Ge. Atomic doses are determined in terms of $atoms/cm^2$.

Sample ID	$GeH4Sccm$	Ge Dose	$Ge/Si/Nratio$	Ge percentage
$SiN : Ge20$	20	45	1/7.5/9.5	4
$SiN : Ge45$	45	95	1/3.5/5	9
$SiN : Ge90$	90	190	1/1.5/2.5	15
$SiN : Ge150$	150	275	1/1/1.5	24

NCs. Ge NCs of some samples were measured using high resolution transmission electron microscopy (HRTEM) technique. Raman spectroscopy was done for all samples using Ar ion laser at 514.5nm and a high resolution double monochromator with CCD detection to study the degree of Ge crystallization as well as the position and lineshape of the Raman phonon line as a function of size. Fig.(4.2a) shows Raman spectra of samples containing different amount of Ge atoms. The amount of Ge atoms in the silicon nitride matrix is critical in the formation of Ge nanocrystals. To investigate this effect, samples named as A, B, C and D which contain 4, 9, 15 and 24 percent of Ge atoms respectively are annealed at 900C for 30 minutes inside furnace. Under these annealing conditions, concentration threshold of Ge content for crystallization is found to be around 15 percent. Even at this Ge value, Raman spectra shows a broad band which is indication of non uniform NCs distribution and also low degree of crystallization that is still a considerable amount of amorphous Ge exist in the film, moreover relatively low intensity of Raman signal is due to smaller nanocrystals in the sample. Samples with 24 percent of Ge atoms, however, shows a narrow and intense peak illustrating larger nanocrystals with uniform size distribution and high degree of crystallization. We focus our work on the samples with 24 percent Ge for further study. The most direct approach to structural analysis of such samples is the use of high resolution transmission electron microscopy (HRTEM) that provides visual as well as analytical data such as size distribution, crystallinity, orientation, defects and interplanar distances on individual nanocrystals. High resolution transmission electron microscopy (HRTEM) micrographs and corresponding selected area electron diffraction patterns (SAD) of single Ge:SiNy with thickness of around 200 nm before and after annealing with conventional furnace annealing (CFA) method are shown in Fig.(4.3) The sample was annealed at 900C for 30 min. It can easily be seen that Ge nanocrystals with well-defined spherical are formed. The nanocrystals also exhibited clear lattice fringes. Smaller NCs are obtained for samples annealed for shorter times. Generally,the desirable sizes might be obtained by controlling the annealing duration, i.e. for a larger nanocrystal, the annealing duration could be increased. The sizes of NCs were determined from TEM micrographs. To get information on stress state of the nanocrystals Raman spectroscopy is done.

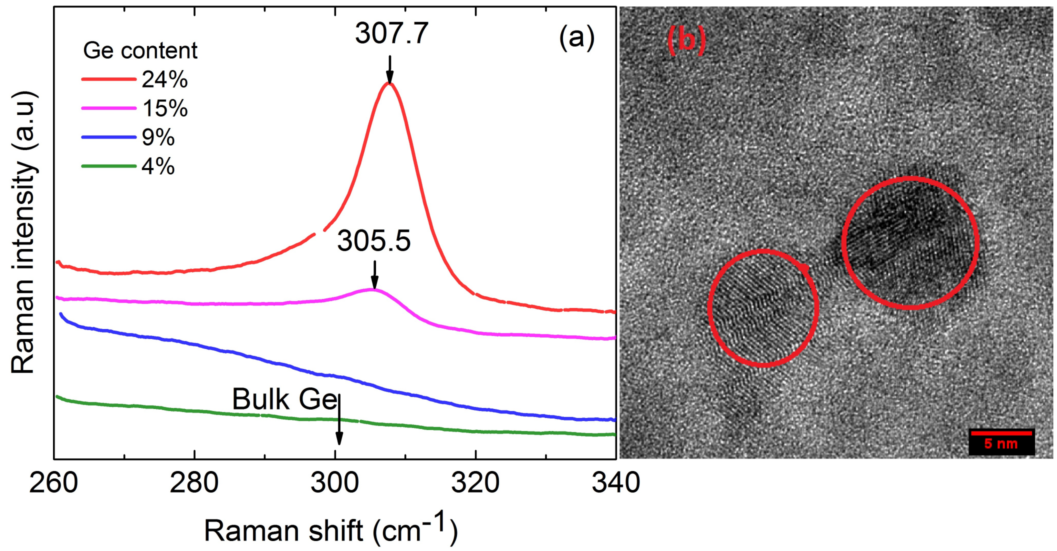

Figure 4.2: (a) Raman spectra for samples containing different amount of Ge atoms varied from 4 to 24 percent in Silicon nitride matrix. All samples are annealed at 900C for 30 minutes. (b). HRTEM micrograph for the sample with 24 percent of Ge. Crystallographic planes as well as associated line defects are well resolved.

Figure (4.4) Shows Raman spectra for samples with 24 percentage of Ge annealed under different conditions which show a blue shift as average naocrystal increase. Fig.(5a) and (5b) show HRTEM micrograph as well as Raman spectra of samples with 24 percent of Ge annealed at 900C for 30 min and 5 min respectively. Crystal planes are well formed in the samples. Sample (a) annealed for longer duration shows larger nanocrystals as well as more blue shift compared to sample (b) with smaller nanocrystals. This is due to stronger confinement of phonons in smaller nanocrystals which leads to more red shift compared to larger nanocrystals. Raman peak of nanocrystals are expected to show redshift compared to bulk crystal due to confinement of optical phonons in nanostructures [84] which leads to relaxation of momentum conservation rule and leads phonons with nonzero momentum to involve in Raman scattering. This redshift, exist always for free standing nanocrystals where other effects like stress are missing. When dealing with nanocrystals embedded in a matrix,however, there is a pressure on nanocrystals exerted from the matrix, which leads to a stress on nanocrystals

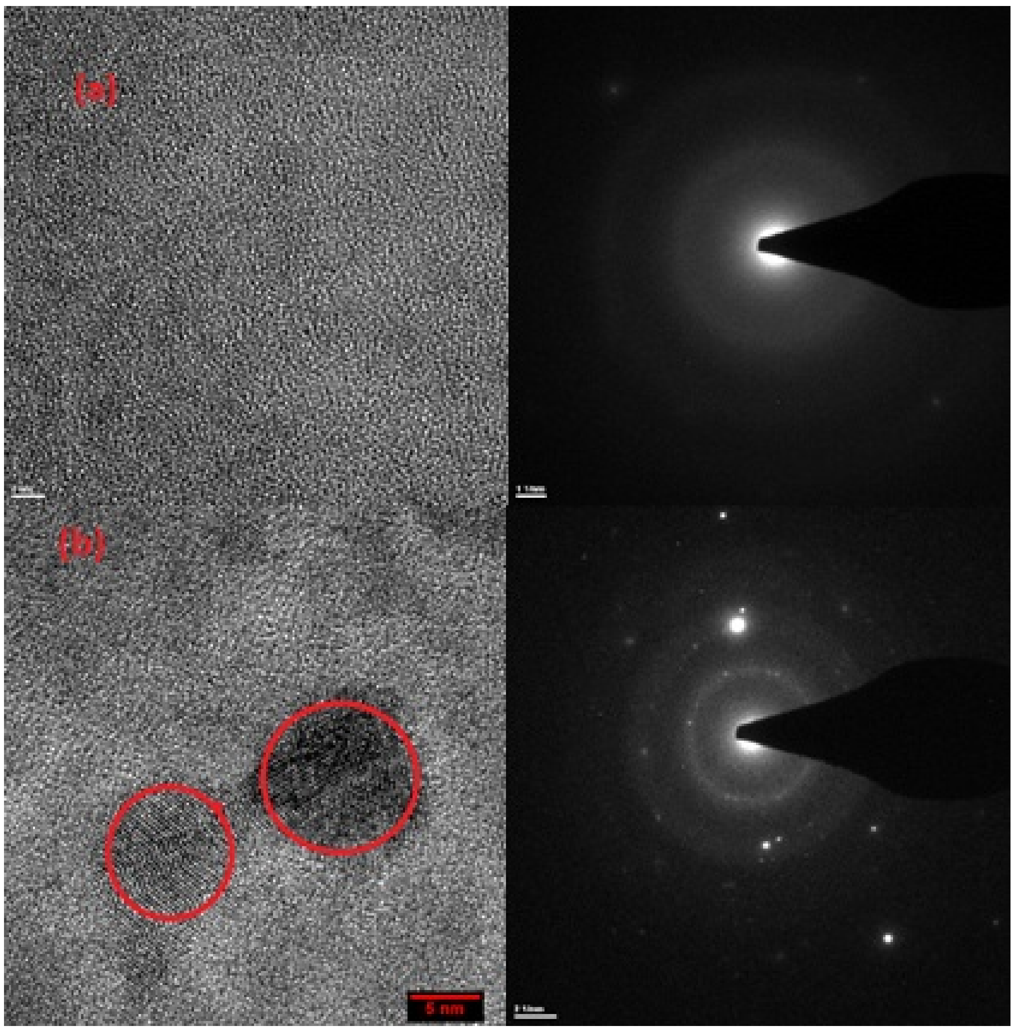

Figure 4.3: Typical HRTEM micrographs and SAD patterns of 200 nm thick single layer SiN:Ge sample a) before and b) after annealing at 900C for 30 min in a conventional furnace. No sign of crystallization is seen in the micrograph of as grown samples.Transformation from amorphous phase to nanocrystalline is obvious.

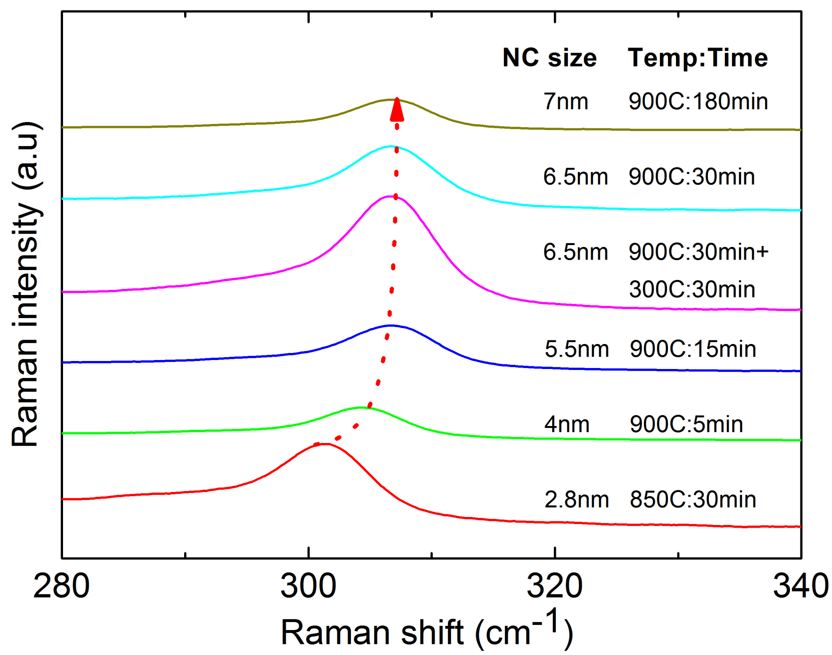

Figure 4.4: (**a**) Size dependent Raman shift. Stress induced shift can be calculated from the difference between these experimental data and phonon confinement induced shift predicted by equation(4.6).

which can be compressive or tensile and therefore modifies the frequency of vibrations. Compressive stress makes the phonons to oscillate faster and therefore a blueshift in Raman peak frequency would present [85], tensile stress on the other hand makes a red shift in Raman peak [85]. As a result, Raman spectra of embedded nanocrystals can be blue or red shifted which is a combination of stress induced shift and phonon confinement induced shift. Equation(4.1) is a simple representation of this total shift:

$$\Delta\omega_{Tot} = \Delta\omega_{PCM} + \Delta\omega_{Stress} \tag{4.1}$$

To measure the stress state of nanocrystals, one should distinguish the stress induced shift and phonon confinement induced shift. Here, Raman spectra of all samples show blueshift with respect to bulk Ge. Larger NCs also show larger blueshift. Total Raman shift with respect to bulk Ge can be understood in terms of combination of redshift due to phonon confinement effect and blueshift caused by compressive stress exerted by the dense silicon nitride matrix as represented in equation(4.1). Previously strain measurement on Ge NCs embedded in $SiO2$ matrix have been done by Paillard et al. [69]Using Raman spectroscopy and HRTEM micrographs. They observed strong compressive stress induced by surrounding matrix. For calculating strain, they measured Raman shift for NCs with sizes between $11.0 - 14.5$ nm, phonon confinement induced shift is negligible and all the observed Raman shift can be attributed to strain induced shift. They observed size-independent strain for NCs with sizes below 14.5 nm. They applied this constant strain induced shift to all samples for analyzing Raman spectra. They also suggest as the origin of this strain to be due to liquid-solid phase transition of Ge during cooling. Strain on large Ge NCs embedded in SiO2 and Si3N4 also is measured in [59]. In that work, a complementary metal oxide-semiconductor-compatible process (CMOS) with SiO2 and Si3N4 layers and produce Ge NCs with sizes between 23-110 nm. In this size regime, the phonon confinement effects are negligible and all of the observed Raman shift can be attributed to stress effect. Their analysis show a size dependent tensile stress of $0.5 - 1$ percent and compressive stress of $0.7 - 4.5$ percent for Ge NCs embedded within SiO2 and Si3N4, respectively.This stress is inversely size dependent in NCs [59, 69]. However, for sizes below a critical value, it can be assumed to be constant [59, 69].

Phonon confinement effect (PCE) is also inversely size dependent [69]. Assuming constant blue shift for all samples and inversely size dependent PCE, a total blue shift is predicted which was found to be in good agreement with average size of NCs obtained from TEM results. In conventional PCM, the phonon wave function has the form [5]:

$$\Psi(r) = Aq \exp(-\frac{\alpha r}{2L^2}) \exp(-iqr) \tag{4.2}$$

where "q" is the phonon wave vector, "L" is diameter of NCs and α is a dimensionless parameter indicating degree of confinement of phonons to the center of NCs. The relation between Raman peak shift and NC size provides the possibility of determining NC size via Raman spectroscopy. However, there are problems using Eq(4.2) for analyzing the size of NCs: Phonon wave function suggested by Eq.(4.2) is ambiguous and "α" value is arbitrary. Based on works by [84] and [86] the parameters were determined as : $\alpha = 8\pi^2$ or $\alpha = 9.67$. These values are frequently used by groups as default values, during the use of Eq.(4.2) in Raman analysis of NCs. However, as can be seen from Eq.(4.2), "L" is part of the combination $(\alpha/L2)$ in PCM and as a result NC size value inherently depends on the value of "α". Therefore, using PCM for "α". Independent determination of NC size is not possible. The relationship between Raman peak shift and NC size is obtained taking into account the discreteness of NCs lattice vibrations [5]. In NCs much smaller than the phonon mean free path, phonons experience several reflection and scattering on NCs surfaces during phonon life time. This leads to standing waves for vibrational eigenmodes of NCs instead of traveling waves. A simple model of N atoms in one dimension is proposed to take into account the discretness of NCs vibration. Eigenmodes of this simple system is simply given by:

$$\omega_s = 2(\frac{k}{2m} \sin(\frac{qsa}{2}) \tag{4.3}$$

where qs=$\pi s/aN$, S=1,2,...,N-1 The maximum wave vector of this system with infinite length is $q = \pi/a$. However, for finite sizes, the maximum possible wave vector will be smaller than infinite case and it will differ from reciprocal wave vector π/a by:

$$\Delta q = \frac{\pi}{L + a} \tag{4.4}$$

where "L" is the dimension of NCs. For small NCs this change is considerable. By generalizing this relation to three dimensions and Taylor expansion of ω with respect to "q" and using this simple dispersion relation for optical phonon mode:

$$\omega(q) = A + B\cos(qa) \tag{4.5}$$

We get:

$$\Delta\omega = -\frac{3\pi^2 a^2 B}{2(L+a)^2} \tag{4.6}$$

where "a" is the lattice constant, "L" is NC diameter and "B" is a parameter which is calculated for germanium to be 18.6 cm^{-1}.B is calculated by comparing the Ge NCs sizes obtained from methods like XRD, TEM. Eq.(4.6) gives a relationship between the displacement of Raman peak position and the size of nanocrystals for crystals with a cubic lattice (diamond, silicon, germanium). The proposed model does not include any adjustable parameters, unlike the conventionally used phonon confinement model (PCM) and can be employed for estimation of NCs sizes. Figure(4.5) shows HRTEM micrograph and Raman spectra of samples annealed at 900C for 30 and 5 minutes.

Average Ge NC size is determined using TEM micrographs and determined to be 6.5 nm for the sample annealed for 30 min. and 4.0 nm for the sample annealed for 5 min. Raman peak shift for sample (a) and (b) are 306.9 cm^-1 and 304.8 cm^-1 respectively. These values show 6.2 cm^-1 and 4.1 cm^-1 blueshift with respect to bulk Ge peak which is at 300.7 cm^-1 [87].These shifts are combinations of stress induced and phonon confinement induced shifts. In order to analyze the size of the NCs from Raman spectra, we need to distinguish the shifts caused by phonon confinement and stress. To deduce the shift induced by phonon confinement, we used equation(4.6) . For the determination of NC size, we use the values obtained from HRTEM micrographs. For sample (a) with NCs diameter of 6.5 nm, from eq.4.6, we obtain, $\Delta_{PCM} = -1.8$ cm^-1 where we used a=5.66A for Ge lattice constant, L=6.5nm for NC size and B=18.6 cm^-1. Thus, stress induced shift can easily be calculated using $\Delta\omega_{strain} = \Delta\omega_{Tot} - \Delta\omega_{PCM} = 6.2 + 1.8 = 8.0$ cm^-1. The same approach, for sample(b) with NCs size 4.0 nm, phonon confinement model gives: $\Delta\omega_{PCM} = -4.1$ cm^-1 and stress induced shift is calculated to be, $\Delta\omega_{strain} = \Delta\omega_{Tot} - \Delta\omega_{PCM} = 4.1 + 4.1 = 8.2cm - 1$.

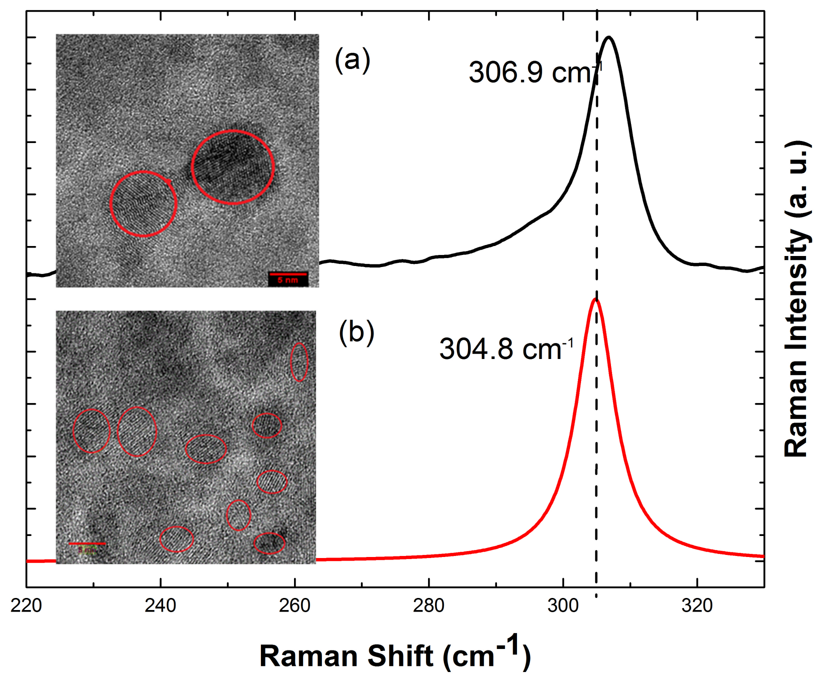

Figure 4.5: **H**RTEM and Raman spectra for samples annealed at 900C for a) 30min and b) 5 min. Sample annealed for longer time shows larger NCs.

Fig.(4.5) shows stress state of Ge NCs with different sizes embedded in silicon nitride matrix. We also measured stress of Ge NCs by obtaining free standing

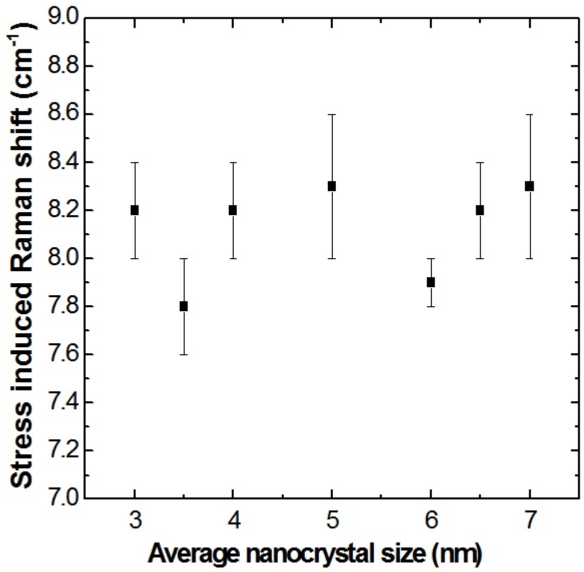

Figure 4.6: **Strain in Ge Nanocrystals vs average NC's size. In this size regime stress is independent of NC's size.**

nanoparticles. In this scenario a diluted HF is used for selective chemical etching of matrix and obtaining stress free Ge nanocrystals almost untouched. It was reported by Sharp et al. [88]that Ge NCs inside an oxide matrix remains almost same even after a long treatment with HF. HF also etches away silicon nitride matrix specially due to the fact that some amount of oxygen exist in matrix. After etching the surrounding matrix, Raman spectroscopy is done for free standing nanocrystals, the spectra shows a red shift compare to bulk germanium which can be considered to as shift induced totally by phonon confinement effect, Therefore comparing spectra of embedded and free standing nanocrystals we can obtain stress induced shift. As it can be seen from figure, these two approach provide same stress for nanocrystals and can be reliable. These results show that almost the same amount of stress induced shift exists for NCs with different sizes. Conversely, assuming the same stress induced shift one can unambiguously determine NC size from PCM using Raman spectroscopy. This results are in agreement with results of [59, 69] where, using CMOS lithographic processes to create nano-cylindrical pillars to size limit the multi-layer, sequential deposited

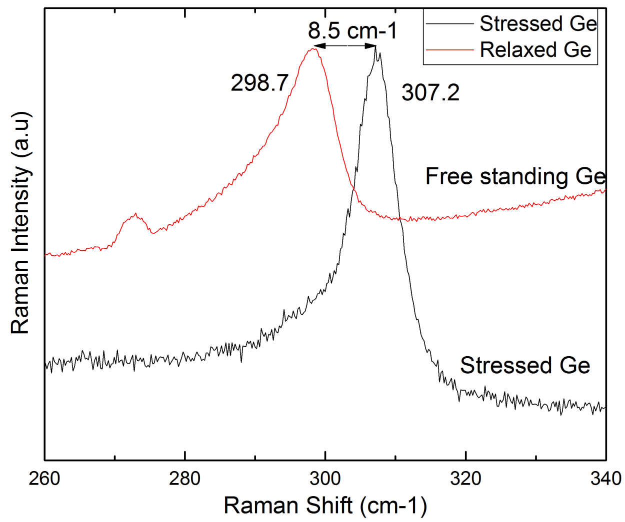

Figure 4.7: **Raman spectra of free standing Ge NCs. matrix is etched away via HF etching.**

SiGe films, proposed that in small Ge NC regime, stress induced shift can be considered constant for different sizes of Ge NCs embedded in SiO_2 or $Si3N4$. By considering this constant value for stress induced shift (around 8.0 cm^{-1} for our samples) and Eq.(4.6), it is possible to get NCs size from Raman spectra. We have done this for all samples and results are in good agreement with results obtained from HRTEM graphs. The sizes of samples annealed under different conditions are shown in Fig.(4.4) where sizes are determined via HRTEM, Stress state are shown in Fig.(4.6).

4.3 Stress evolution of Ge nanocrystals embedded in dielectric matrices

In the previous section of this chapter it was shown that fabrication of NCs in silicon nitride matrix result in big compressive stress. It was shown that magnitude of the stress is independent of size for the regime of our nanocrystals

(2.8-7.0nm). Origin of the stress was related to mismatch between Ge nanocrystal atoms and surrounding matrix. Furthermore due to volumetric difference between Ge nanocrystal an matrix. stress is generally compressive in nature. In a theoretical study Liu et al. [89] have shown that the distribution of stress has important role determining the physical and thermodynamic properties of NCs. Moreover it is shown [68] that stress induced band gap tuning in Si NCs which in turn leads to different optical properties of NCs. Wada et al. [45] also show band gap tuning of Ge films via tensile strain which result in a high performance photodetectors. Therefore it is potentially useful to tune stress state of Ge NCs embedded in dielectric matrices in the way that one can potentially tune the band gap of the NCs. In this part we study three different methods for tuning stress: First role of embedding matrix will be investigated by studying of stress state in three different matrices namely silicon nitride, silicon oxide, then effect of annealing method will be discussed by comparing stress of samples annealed using RTP and conventional furnace methods. Finally stress state will be studied in multilayer superlattice structures and effect of buffer layer on stress state of these structures will be discussed.

4.3.1 Formation and stress analysis of Ge NCs in silicon oxide matrix

In this section we study formation and stress state of Ge nanocrystals in silicon oxide matrix. Currently silicon oxide matrix is the most common host for germanium nanocrystals due to its compatibility and potential applications in optoelectronics, and memory devices. In a Ge:SiOx system, the direct decomposition of GeO2 is the simplest reaction for the reduction of GeO2 to Ge:

$$GeO_2 \rightarrow Ge + O_2 \tag{4.7}$$

Due to the limited solid solubility of Ge in SiO_2, Ge atoms in the silicon oxide matrix can precipitate and form nanocrystals by annealing. Formation of the nanocrystal can be separated into five steps: (I) $GeO2$ reduction leads to the formation of elemental Ge atoms (II) Diffusion of liberated germanium atoms in the silicon oxide matrix (III) nucleation due to $Ge-Ge$ collisions causes the formation of stable Ge nuclei. (IV) growth of Ge nanocrystals through the assimilation of diffusing Ge atoms. (V) Coarsening of the nanocrystalsin such that small nanocrystals shrink and large nanocrystals grow in size due to the Ostwald ripening. Fig.(4.8) represent HRTEM micrograph of Ge NCs in silicon oxide matrix annealed at conventional furnace at 900C for 30 minutes. We observe

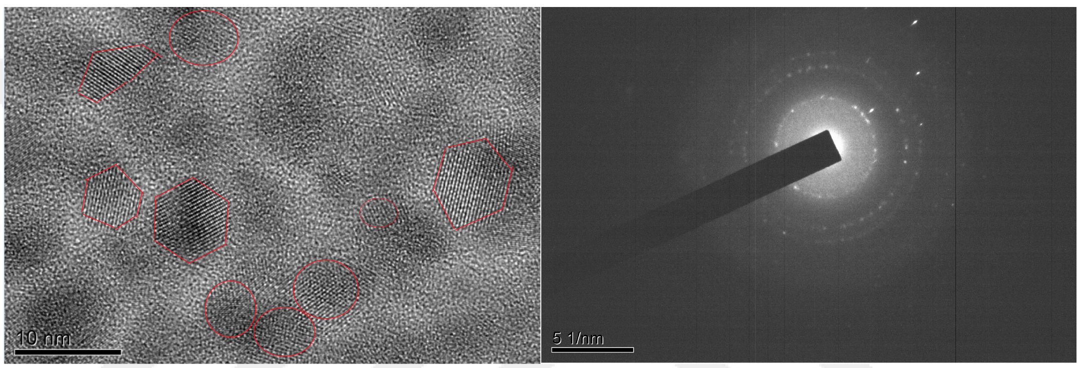

Figure 4.8: **HRTEM micrographs and associated selected area diffraction pattern for Ge:SiOx annealed at 900C for 30 minutes. The hexagonal shape nanocrystals are well-formed, showing facets that are bounded by crystal planes. This implies that it is possible to obtain the equilibrium interface energy minimizing configuration at 900C for NCs in silicon oxide.**

well-formed hexagonal and spherical shape nanocrystals, with hexagonal shaped ones showing facets of the nanocrystals that are bounded by crystal planes. This implies that it is possible to obtain nanocrystals where the equilibrium interface energy is a minimum at 900C for Ge NCs in the silicon oxide matrix. Growing nanocrystals in parallel to crystal planes might reduce pressure on nanocrystal and therefore lowering compressive stress. Fig.(4.9) shows Raman spectra of the Ge:SiOx samples. It is observed that crystallization starts at relatively lower temperature (825 C) for Ge NCs in silicon oxide matrix compared to ones embedded in silicon nitride which threshold crystallization is at 850C. This is suggested to be due to higher diffusivity of Ge atoms in silicon oxide matrix which leads to earlier crystallization. Stress analysis is done taking into account phonon confinement induced shift and stress induced shift. The same analysis as NCs embedded in silicon nitride shows a smaller compressive stress for NCs in silicon oxide matrix. Our stress analysis show compressive stress for the NCs to be $1.2 \pm 0.2\ cm^{-}1$.

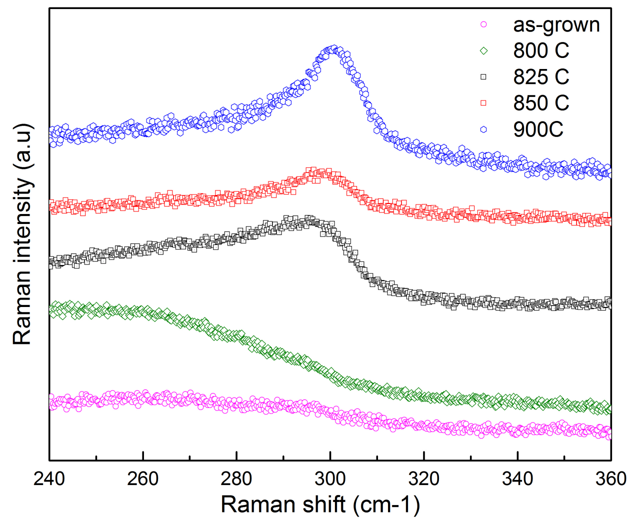

Figure 4.9: **Raman spectra of Ge:SiOx films.**

Fig.(4.10) compares stress state of Ge NCs embedded in silicon nitride and silcon oxide matrices.

Stress of NCs have different values in silicon oxide and silicon nitride matrices which is in the compressive stress form. Ge nanocrystals in silicon oxide matrix represent smaller compressive stress compared to those embedded in silicon nitride matrix. This could be due to different lattice constant in silicon oxide and silicon nitride matrices which leads to different state of mismatch between nanocrystals and surrounding matrix and therefore stress state. Nanocrystals in silicon oxide matrix also are formed at relatively lower annealing temperature which in turn leads to less thermal stress. Also due to more diffusivity of Ge nanocrystals in silicon oxide matrix and easier formation of nanocrystals in term of energy considerations, nanocrystals form in equilibrium state with planes parallel to crystal facets which in turn leads to decreasing of pressure on nanocrystal. However, for NCs in any matrix this stress is independent of NCs size in the range studied. This is in agreement with works of [90] who reported same stress value for small NCs. They argued that below a size, pressure is saturated and therefore a constant stress value exist for small enough particles.

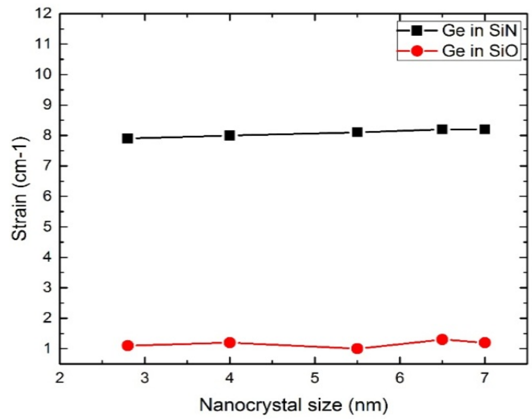

Figure 4.10: **Stress induced shift for Ge NCs embedded in silicon oxide and silicon nitride matrices. Nanocrystals embedded in nitride matrix experience larger compressive stress when compared to oxide matrix. Stress of the nanocrystals is independent of nanocrystal's size at this very small regime.**

4.3.2 Role of annealing method

To investigate the effects of rapid temperature rise in these samples we also used rapid thermal processing for crystallization of Ge in $N2$ ambient. Fig.(4.11) shows HRTEM images of sample RTP annealed at 900C for 90 sec. As it can be seen from TEM micrographs, conventional furnace annealed sample displays relatively larger NCs compared to RTP annealed ones at the same annealing temperature. This is due to much longer annealing duration of furnace annealing which assists the diffusion of Ge atoms and therefore the growth of the nanocrystals. Raman spectra of the RTP annealed samples are shown in Figure(4.12) In all samples, blue shift of the Raman peak relative to bulk Ge is observed

indicating presence of compressive stress. Relatively smaller blue shifts between samples reflect small variation in size with annealing temperature. Strong compressive stress observed in RTP annealed samples are similar to furnace annealed samples. We found the stress induced shift for RTP samples to be around $8.7cm-1$ which is slightly larger than CFA samples. This might be due to faster process of solidification in RTP samples. A few reports[3, 4] have discussed that

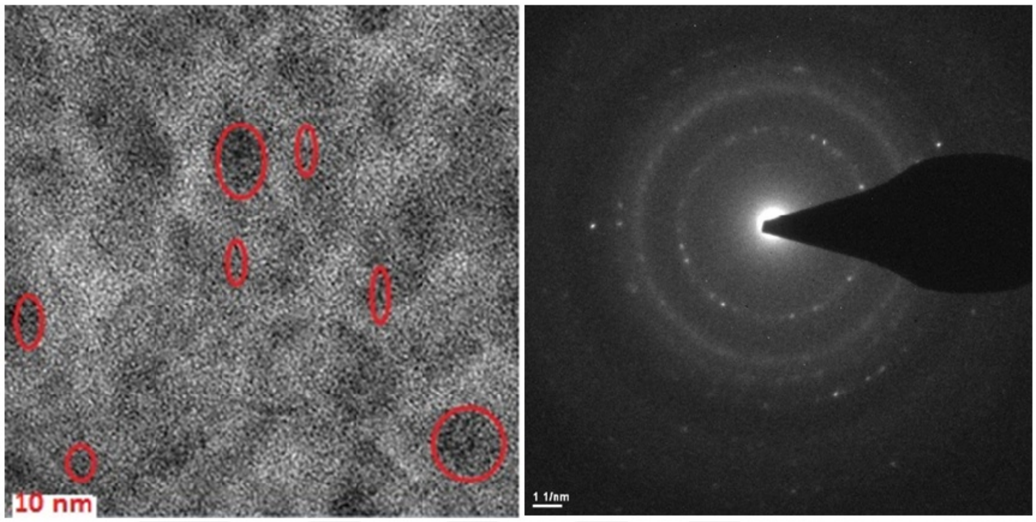

Figure 4.11: HRTEM micrograph (a) and electron diffraction (SAD) pattern of RTP annealed sample, b). Smaller NCs are formed during RTP annealing compared to samples annealed in a conventional furnace.

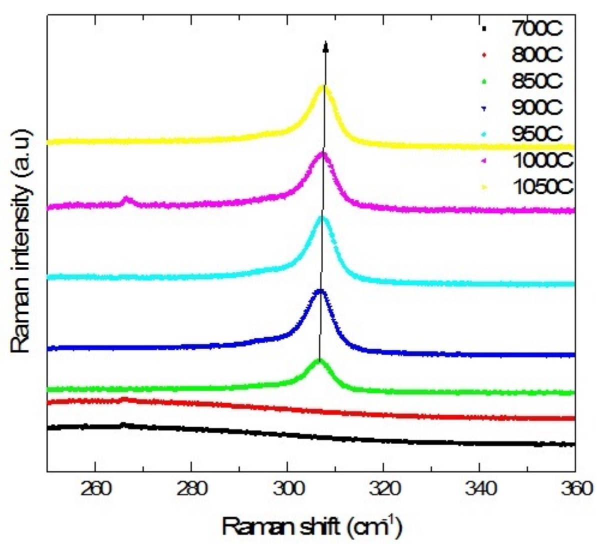

Figure 4.12: Raman spectra of Ge:SiNy samples annealed at different temperatures with RTP for 60 sec. In all samples, blue shift of the Raman peak compared to bulk Ge is observed indicating presence of compressive stress. Relatively smaller blue shifts between samples reflect small variation in size with annealing temperature.

conventional furnace annealing leads to higher activation energy for nucleation and therefore slower crystallization process, as compared to RTP . This, assist the Ge nanocrystals to form facets so as to minimize the interfacial energy. In the process of faceting, it is energetically favorable for the nanocrystals to grow along planes that exerted the least pressure on the matrix as it enables them to minimize their strain energy and thus minimize stress for the nanocrystals.

4.3.3 Stress tuning in superlattices

We also synthesized Ge NCs in superlattice samples. Here ultrathin Ge:SiNy films are separated with stoichiometric SiO2 or Si3N4 thin films. This closely spaced Ge NC structure would be potentially advantageous for third generation solar cells as this structure could improve electrical conductivity while confining the NCs growth. This approach also allows for controlling simultaneously size and density of NCs. Here, we fabricated two different sets of superlattices: Ge:SiNy/SiO2 and Ge:SiNy/Si3N4 and use HRTEM and Raman study to investigate the stress state in samples. In Fig.(4.13), we show HRTEM micrographs of multilayers consisting of ultrathin Ge:SiNy films and stoichiometric SiO2 buffer layers which are used as buffers for Ge diffusion and controlling the size of NCs. The thickness of Ge:SiNy and SiO2 buffer layers are the same in a given sample. However, thickness of Ge:SiNy layer is varied between 3.0 to 9.0 nm from sample to sample. The undulations in the Ge containing layer shows that there is some Ge diffusion into the buffer layers, as Ge diffuses in plane during crystallization. It is noteworthy that the undulation amplitude increases in the Ge containing layers away from the substrate. In the extreme case, we may expect that undulations lead to spherical droplets in the form of worry beads in order to minimize the total energy of formation. Fig 9b. indicates that annealing at 900 C leads to Ge diffusion to form a mixture of amorphous and nanocrystal clusters. We would expect that at longer anneal durations or higher temperatures all material would be crystalline in the form of undulated nanosheets.

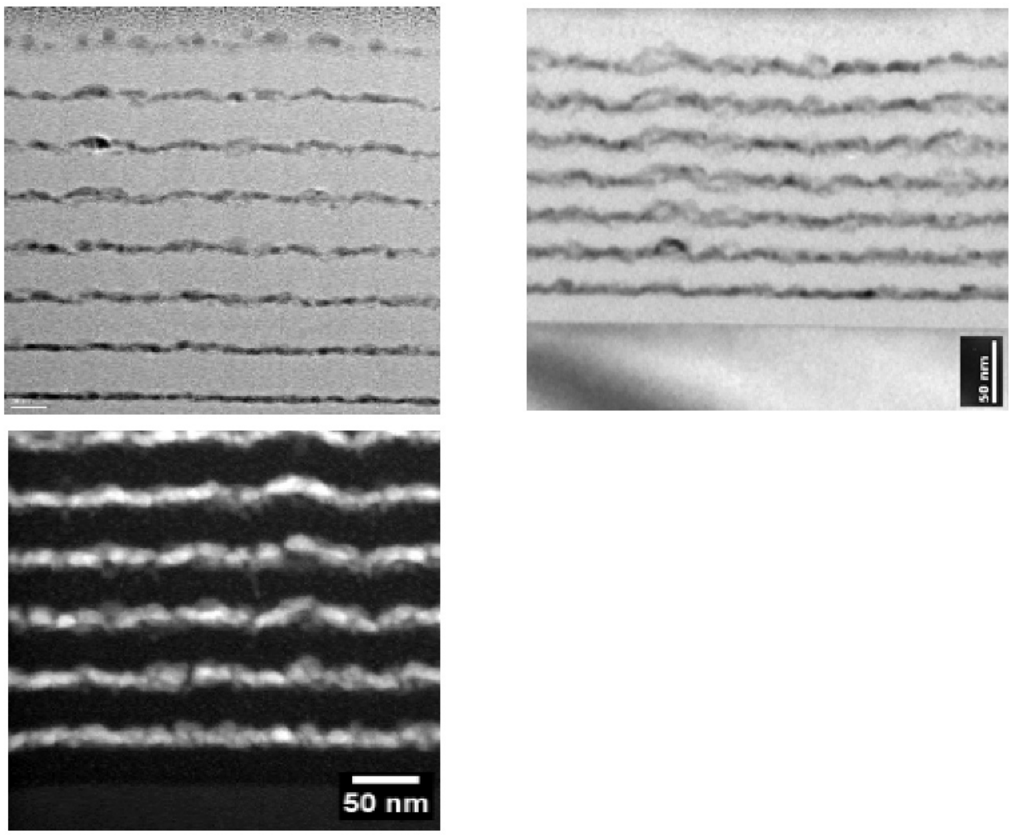

Figure 4.13: TEM micrograph of multilayer samples consisting of Ge:SiN film and SiO2 buffer layers. TEM micrographs of multilayer Ge:SiNy samples with SiO2 buffer layers. The thickness of Ge:SiNy and SiO2 buffer layers are the same in a given sample. However, thickness of Ge:SiNy layer is varied between 3.0 to 9.0 nm from sample to sample. The undulations in the Ge containing layer shows that there is some Ge diffusion into the buffer layers, as Ge diffuses in plane during crystallization.

Table 4.2: Stress induced frequency shift (strain) and correlation between stress and crystallization threshold for $Ge : SiNy/SiO_2$ multilayer superlattices

Sample ID	$Averagesize(nm)$	Raman shift	Strain	Crystallization threshold
$ML3$	3.0	2.4	9.4	775C
$ML6$	6.0	2.7	4.9	800C
$ML9$	8.5	1.0	2.1	850C

Figure(4.14), shows Raman spectrum of multilayer Ge:SiNy:SiO2 samples annealed at different temperatures. Compressive stress is observed for all samples. Stress induced Raman shift is calculated taking into account a simple phonon confinement model [31]. Table.2 summarizes the correlation between stress, size and crystallization threshold for Ge:SiNy/SiO2 samples.

As it can be seen smaller nanocrystals experience larger compressive stress. Temperature threshold for crystallization for samples with thicknesses 3, 6 and 9 nm are 775C, 800C and 850C, respectively. This can be discussed in terms of different values of stress for different samples. As we see there is a rather strong correlation between crystallization threshold and compressive stress in these multilayer samples. We observe that the more compressive stress there is, the lower is the temperature threshold for crystallization. The spectra for 3.0 nm thick Ge:SiNy layers are detailed and illustrative. Annealing at 775 C, a shoulder starts to develop at around 300 $cm - 1$. At higher temperatures this shoulder develops into a full fledged peak and shifts towards the red.

For sample with 3.0 nm Ge:SiNy, stress induced Raman shift is 9.4 $cm-1$ with the corresponding crystallization temperature threshold being 775C. For samples with Ge nanocrystal sizes of 6.0 nm and 8.4nm, stress induced Raman shift is 4.9 $cm - 1$ and 2.1 $cm - 1$ respectively. We note that in contrast with single layer samples, stress on nanocrystals is size dependent in multilayer samples with larger stress for smaller nanocrystals. Notice that in multilayer samples, the environment of the nanocrstal is more complicated where they are partially surrounded by silicon nitride and also by buffer layers and therefore stress relation on nanocrystals can be complex. Further work is needed to study the details of stress

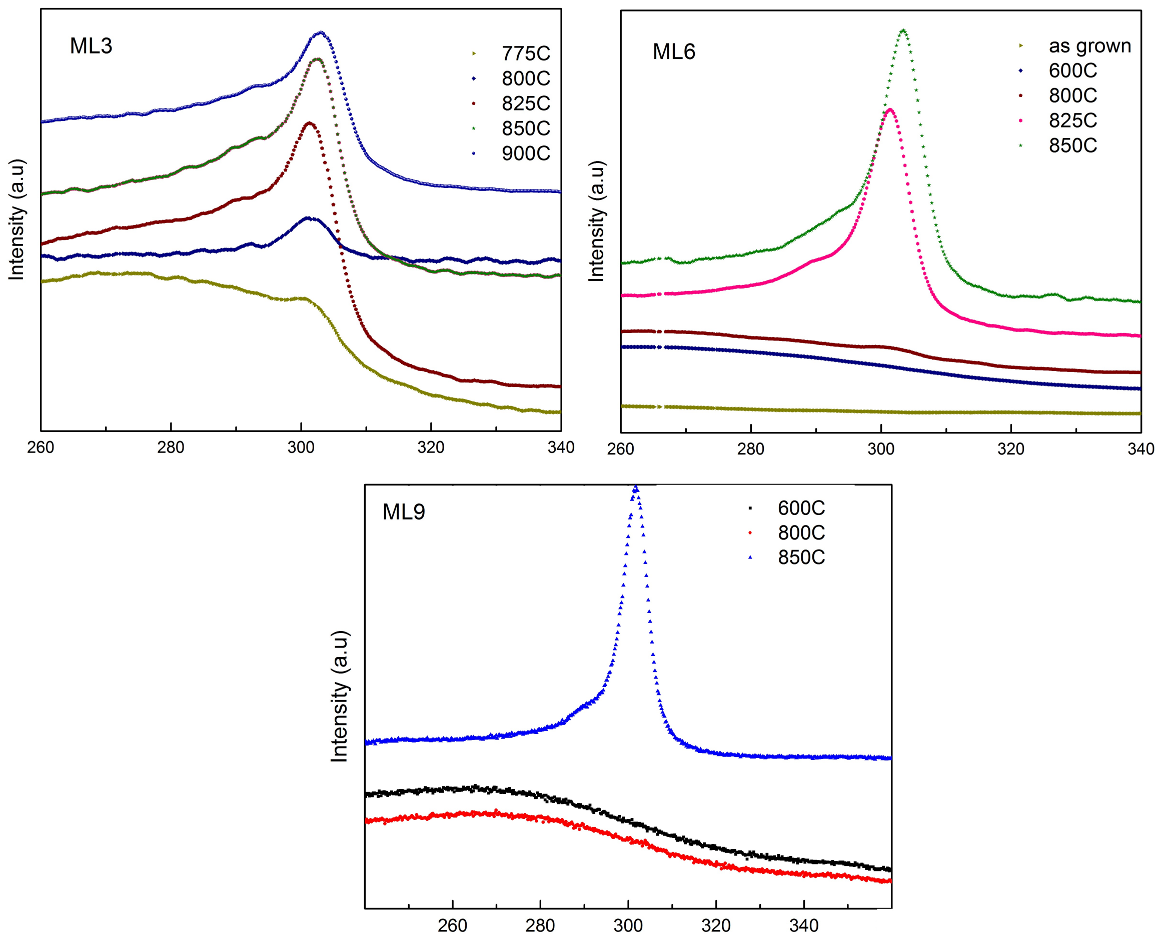

Figure 4.14: Raman scattering of multilayer samples. Crystallization threshold depends on stress state of NCs in samples. compressive stress supports the crystallization

accumulation in these type so samples. For these samples, crystallization temperature threshold is between 800 C and 850 C. This is in agreement with work in [34]. In that work, it was shown that application of an external mechanical compressive stress during annealing for copper-induced growth of polycrystalline Ge leads to enhancement of crystallization. We also fabricated multilayers with near stoichiometric Si3N4 as buffer layer. It has been reported that the annealed PECVD SiN films exhibit considerable tensile strain. This tensile strain increases with annealing temperature from 750 C and saturates at a value of 1.2 GPa at around 1100 C.1618 This is suggested to be linked to the release of hydrogen and reformation of Si-N bond network after the annealing. SiN is commonly used as a barrier material to prevent interdiffusion of metal and semiconductor. Therefore, it is reasonable to expect that, in the sample with the SiN cap, the relatively higher Ge supersaturation would lead to a reduction of barrier to nucleation and hence more nanocrystal formation. Figure(4.15) illustrates TEM micrographs of multilayer samples with Si3N4 buffer layers. Figure(4.16) illustrates TEM micrographs of multilayer samples with Si3N4 buffer layers annealed at 900C for 30 minutes. Crystallization starts at layer next to the substrate NCs is observed for other layers in sample annealed at 900 C. This is suggested due to existence of higher nucleation energy at layers closer to substrate. Consequently, Ge nanocrystals can nucleate and form earlier and faster. Figure 4.17 shows HRTEM of the sample after annealing at 1000C for 30 minutes. At this temperature NCs are formed in all layers due to higher activation energy at this temperature. Moreover size of NCs are larger compared to sample annealed at 900C. This is in good agreement with the Raman spectra shown in Figure (4.18) where, we, agnain, used Eq.(4.6) for PCE induced Raman shift:

In figure (4.18), Raman spectra of multilayer samples consisting Si3N4 ultrathin films as buffer layers. Sample annealed at 900 C shows no Raman peak which is in agreement with results obtained via HRTEM micrographs. Threshold for crystallization for these multilayer structures is around 950C. Moreover despite single layer samples and multilayer samples with SiO2 as buffer there is a large red shift in Raman peak which is because of tensile strain presents in the samples. Table 4.3 summarizes correlation between crystallization temperature threshold

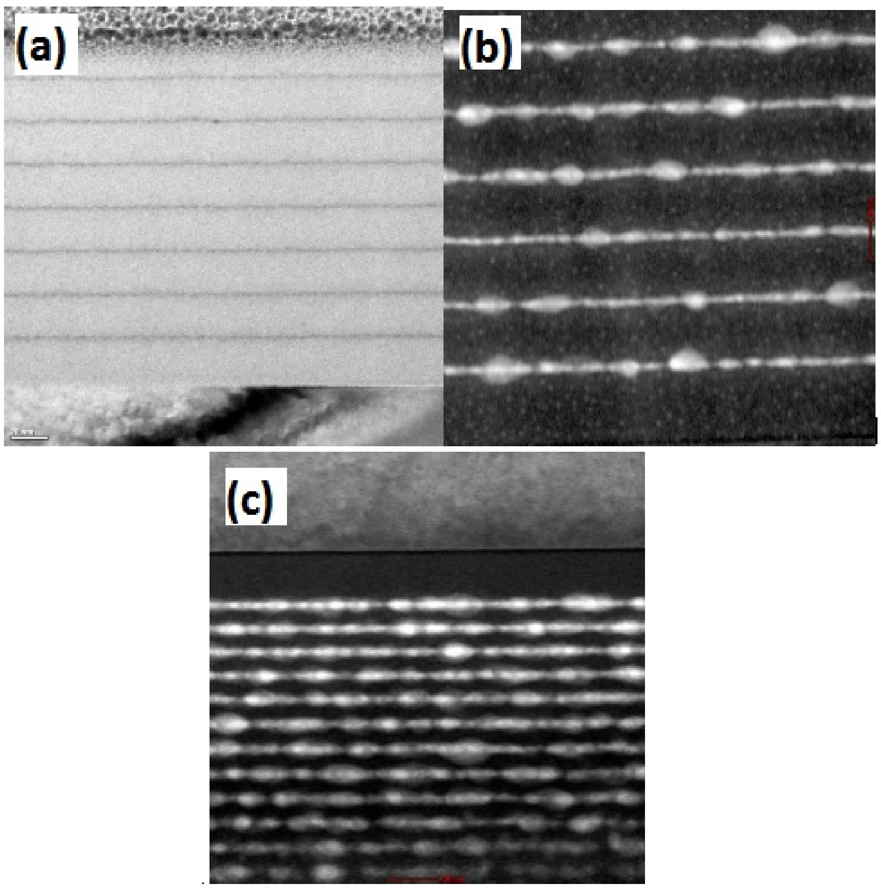

Figure 4.15: TEM micrograph of superlattices consist of Ge:SiNy thin films and Si3N4 buffer layers.

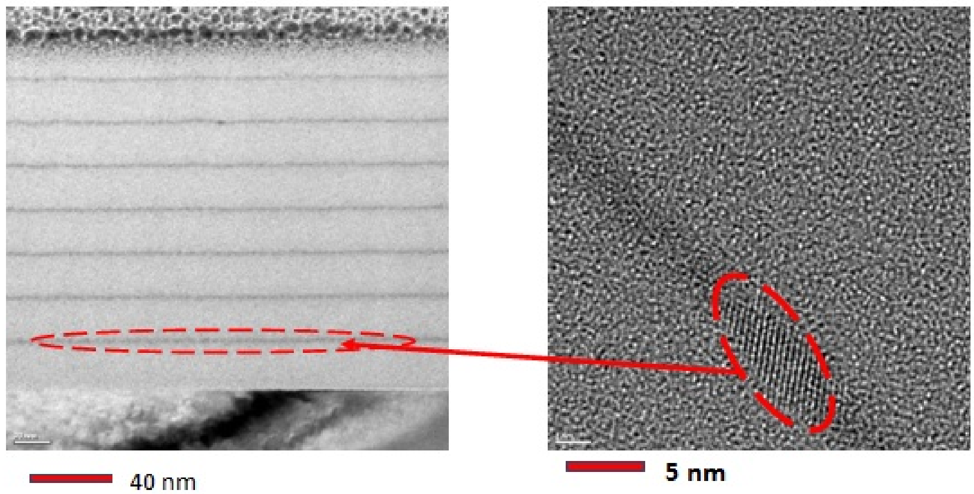

Figure 4.16: Cross sectional TEM micrograph of Ge:SiNy/Si3N4 multilayers annealed at 900 C for 30 min. The dark lines correspond to Ge:SiNy layers and the white bands to Si3N4 buffer layers. NCs are formed only in layer next to substrate.

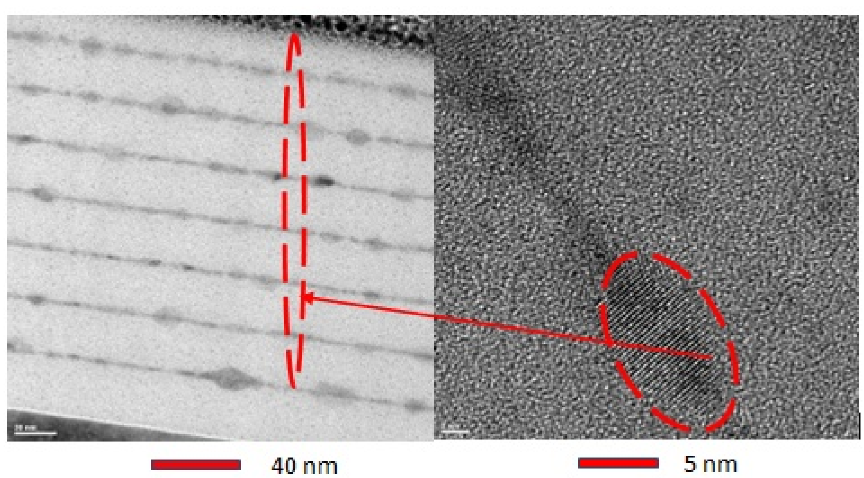

Figure 4.17: Cross sectional TEM micrograph of Ge:SiNy/Si3N4 multilayers annealed at 1000 C for 30 min. NCs are formed in all layers with larger sizes compare to sample annealed at 900C

Table 4.3: Stress induced frequency shift (strain) and correlation between stress and crystallization threshold for $Ge : SiNy/Si_3N_4$ multilayer superlattices

Sample ID	$Averagesize(nm)$	Raman shift	Strain	Crystallization threshold
$ML4$	4.4	-4.7	-1.2	950C
$ML6$	6.3	-16.2	-14.4	950C

and tensile strain.

The samples are labeled as $ML4$ and $ML6$ with the numbers showing approximate size of nanocrystals which are around 4 and 6 nm respectively. Sample ML4 is annealed at 950 C for 30 min while $ML6$ annealed at 1050 C for 60 minutes, which leads to formation of larger nanocrystals. Both samples represents considerable red shift . Sample $ML4$ shows a tensile strain of -1.2 $cm-1$, while increasing annealing time and temperature leads to more red shift reaching to a tensile strain of -14.4 $cm-1$ for sample ML6 annealed at 1050 C for 60 minutes. This corresponds to a tensile stress of 3.8 GPa obtained from equation (4.7). [59]:

$$\omega(p) = (300.6 \pm 0.5) + (3.85 \pm 0.05)p - (3.9 \pm 0.6) * 10^{-2}p^2 \tag{4.8}$$

Where "p" is the pressure exerted on the Ge NCs by the surrounding matrix. At temperature as high as 1050C, Ge become molten and its diffusivity increases drastically, therefore larger nanocrystals are formed. Note also that when annealed at 1050C, the viscosity of the silicon oxide decreases and this will also assist in the stress relief for the nanocrystals. This can lead to the reduction of intrinsic compressive stress presents in nanocrystals or in other words more redshift in Raman peak. Figure(4.19) shows correlation between crystallization threshold temperature and stress on germanium nanocrystals for multilayer samples. For sample experiencing largest compressive stress, crystallization starts at around 775C, however for sample with tensile stress this temperature is 1000 C. This is in agreement with works of several groups who reported relation between stress and crystallization [91] and [34,39 ,40]. As tensile strain increases, the strain energy at the Ge nanocrystal surface increase, and the $Ge-Ge$ bonds become more stretched at the surface of the Ge nancrystal. When the strain energy eventually becomes comparable to the bond energy of the Ge atoms, the Ge atoms will preferentially detach from the surface of the nanocrystal, which slows

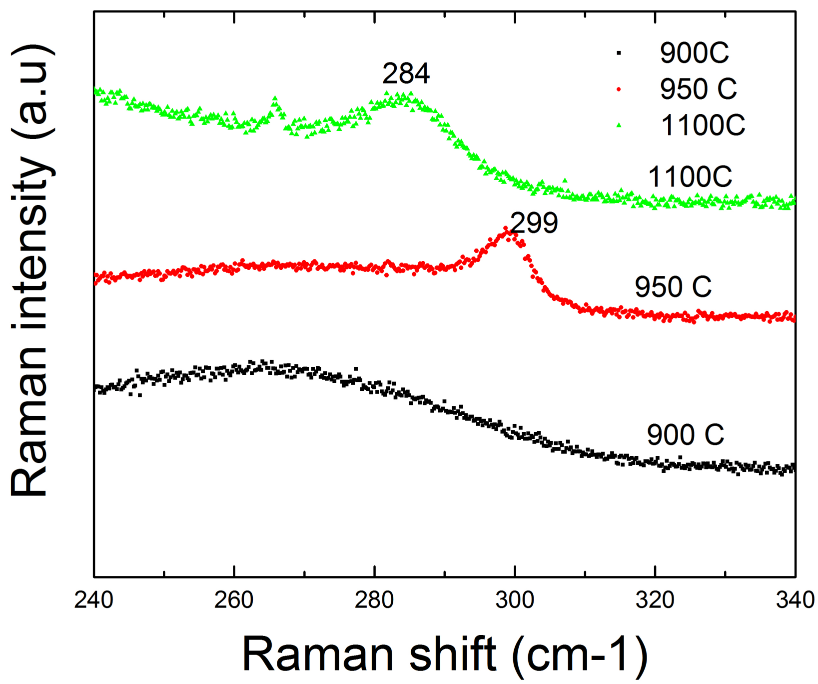

Figure 4.18: Raman spectra of superlattices consist of Ge:SiNy and Si3N4 buffer layers. Tensile stress and late annealing is seen for the samples.

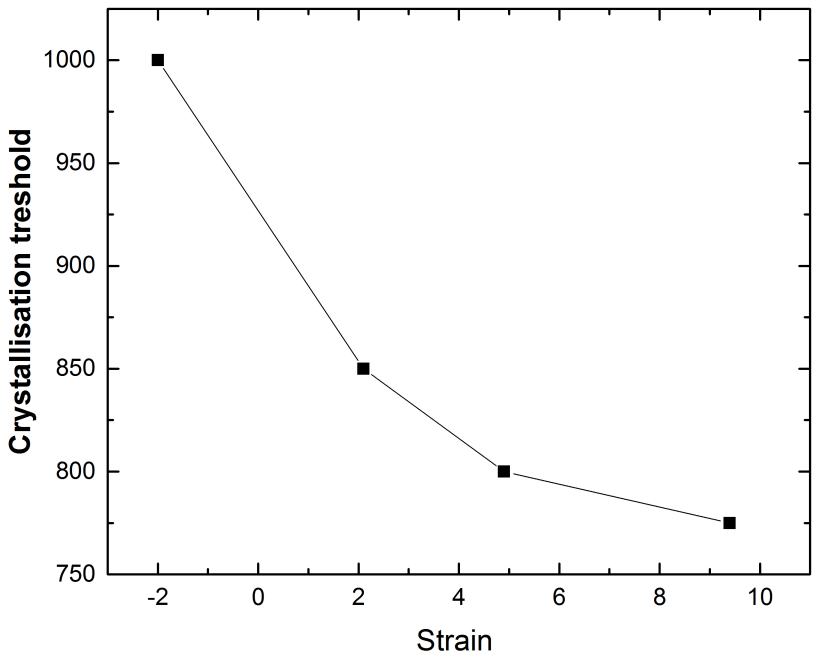

Figure 4.19: Correlation between stress satae and crystallization threshold. Compressive stress supports crystallization while tensile stress suppresses crystallization.

the growth of the nanocrystals . As a result for tensile strained samples more temperature is required to provide high kinetic energy for Ge atoms to involve in crystallization process. Crystallization at lower temperature is a desirable property in technological applications. lowering the crystallization temperature by controlling stress can be a good method. Kimura et.al [92] investigated the effect of stress on a-Si and observed suppression of crystallization by applying tensile strain. A compressive stress-assisted, Cu induced lateral-crystallization technique for the preparation of polycrystalline Ge at temperatures as low as 1500 C is also [34] reported. Huang et al [36] also reported positive effect of compressive stress on crystallization of a-Si. However some reports show tensile strain assists the crystallization. Recently, the effects of external mechanical stress on the crystallization of amorphous silicon have been reported by Hashemi et al.[42]. It was shown that tensile stress applied to silicon films during annealing enhanced the crystallization properties of silicon, while an applied compressive stress suppresses the crystallization process. However our results shows the enhancement of crystallization by using compressive stress and reduced crystallization in tensile strained samples. Kimura [92] used a model to discuss the effect of stress on crystallization of a-Si. Based on this model the driving energy of crystallization is difference of Helmholtz energy between c-Si and a-Si under stress. According to this analysis when the stress does not relax the driving energy decreases which leads to reduction in crystallization and therefore crystallization starts at higher temperatures. The effect of compressive and tensile strain on crystallization needs to be further investigated.

In this chapter fabrication of germanium nanocrystals in a dielectric matrix leads to a residual stress which is usually in the form of compressive stress. In the present work, we aim to change the stress state of the nanocrystals from the intrinsic compressive state to tensile stress by changing the annealing conditions, the dielectric matrix material or the buffer as a stressor. We fabricated germanium nanocrystals in silicon oxide and silicon nitride matrices via PECVD method and post annealing in N2 ambient. Crystallization were observed via TEM and Raman spectroscopy. Raman shift of nanocrystal compared to bulk material is mainly due to stress exerted on nanocrystals and confinement of phonons in nanostructure. We distinguished these two compartments by applying a phonon confinement model to obtain the stress state of the nanocrystals. We found that constant value of stress exist for nanocrystals in each dielectric matrix. However the nanocrystals experience different amount of stress in any matrix, that is changing the matrix does not tune the stress state from compressive to tensile stress but the value of compressive stress. We also examined effect of annealing method on stress state of the samples and found small change in stress amount of nanocrystals. Finally we synthesized germanium nanocrystals in superlattice multilayer structures. Two sets of multilayers are fabricated, first set consist of SiGeN ultrathin films sandwiched between stoichiometric SiO2 thin layers, in the second set SiO2 are replaced by stoichiometric Si3N4 thin films. For the first set of multilayers with $SiO2$ barriers, Ge nanocrystals experience compressive stress which is size dependent with larger stress for smaller nanocrystals. For second set of nanocrystals with Si3N4 barriers, tensile stress exist, therefore, we are able to tune stress state of nanocrystals from compressive to tensile via stressor barriers. This is very important as the stress state of Ge is intimately connected to the band gap of the material. We also observed dependence of crystallization threshold temperature with stress state of samples, our results show that compressive stress leads to earlier crystallization while tensile stress suppresses crystallization. These results are consistent with the claims of some studies [34-43] which claim the compressive stress and lattice shrinkage, as the driver for the reduction of crystallization temperature.

Chapter 5

Photoluminescence of Ge nanocrystals in single layer and superlattice samples

This chapter is based on publication "Ge nanocrystals embedded in ultrathin Si3N4 multilayers with SiO2 barriers "Rahim Bahariqushchi, Sinan Gundogdu, Atilla Aydinli *Superlattices and microstructures 2017.*

5.1 Introduction

Since observation of visible photoluminescence in Ge nanocrystals in silicon oxide matrix by Maeda in 1991 [25] there have been an intense study on optical properties of Ge nanocrystals in dielectrics. Despite several reports on observation of emission from Ge nanocrystals in different dielectric matrices there is lack of agreement of experimental results with those predicted by quantum confinement models which predict blue shift with decreasing nanocrystal's size. According to our knowledge there is only one report [4] on embedded Ge nanocrystal's emission in agreement with quantum confinement models. Other reports show a emission peaks independent of nanocrystals size which suggest that the observed photoluminescence have other origin than confinement of charge carriers in nanostructures. In this chapter we perform an optical study via photoluminescence spectroscopy using a HeCd laser operating at 325nm at room temperature. Our study is focused on Ge nanocrystals embedded in silicon nitride matrix with different Ge concentration. For studying of single layer samples, 6 set of samples are prepared all with thickness around 200 nanometers and Ge concentration varied between 4 to 40 percent. Effect of annealing temperature and Ge concentration on photoluminescence spectra is discussed.Then we turn on photoluminescence of multilayer samples namely Ge nanocrystals embedded in silicon nitride matrix separated by SiO2 buffer layers. Samples consist of 8 Ge:SiN/SiO2 bilayers. thickness of GeSiN films varied between 3.0 to 40.0 nm and therefore size of NCs is controlled at least in growth direction. SiO2 which perform as buffer layer is around 25nm for all samples. PL measurements show size dependent intensity of nanocrystals with higher intensity for smaller nanocrystals. this suggests that origin of this emission is defects located at the surface of nanocrystals. Also there is an enhancement of photoluminescence of multilayer samples compare to single layer samples with same effective thickness. Origin of this enhancement is also discussed.

5.2 Single layer samples

Ge:SiN films with thickness around 200 nm are grown on Si substrate. Ge concentration are estimated to be 4, 9, 15, 24,30 and 40 percent by RBS method as discussed in previous sections and are named as A, B, C, D, E, F, G respectively. The samples are processed by conventional furnace annealing in temperatures from 500 C up to 1100 C. The Structural analysis of these samples are performed in the previous sections. Figure(5.1) illustrate TEM micrograph as well as selected area diffrcation (SAD) of an as-prepared sample. Thickness of the film is around 200nm. Amorphous structure of sample is obviousfrom both TEM and SAD patterns. Fig.(5.2) shows photoluminescence of these 5 sets of samples annealed at different temperatures. Fig(5.3) represents PL intensity vs Ge

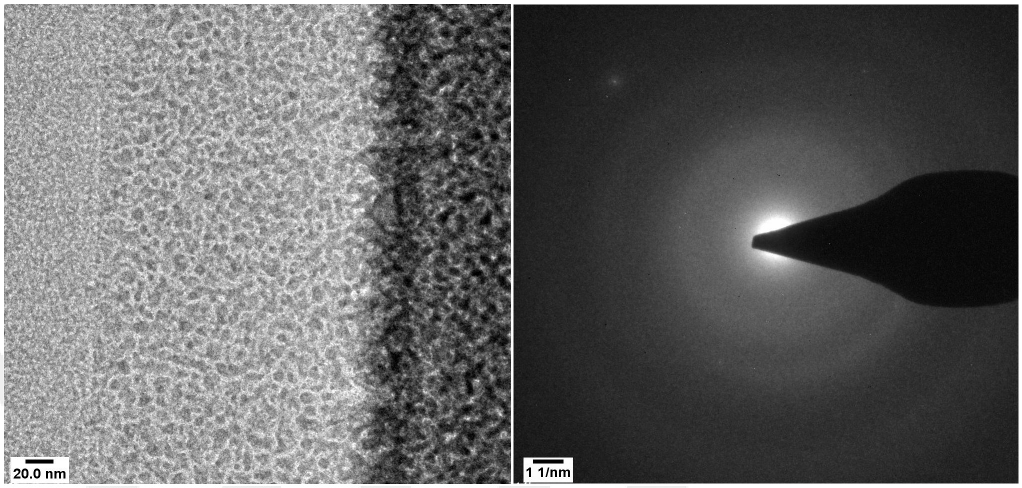

Figure 5.1: (a).HRTEM micrograph of an as prepared Ge:SiN film with thickness around 200nm. Film is in amorphous state.(b). Selected area diffraction (SAD) of the sample confirms amorphous state of the sample

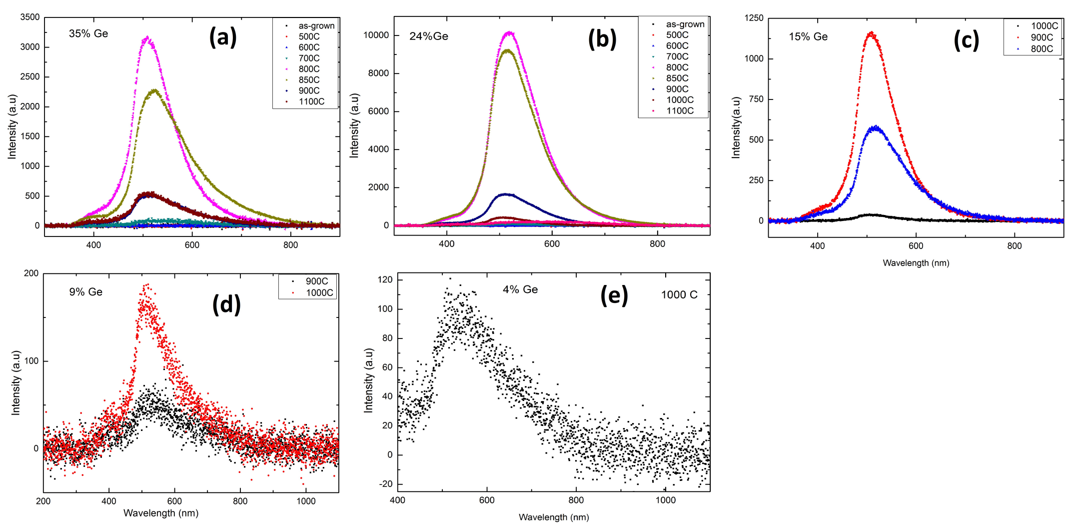

Figure 5.2: PL spectra of single layer samples containing 4 to 35 percent of Ge. Emission starts at the threshold temperatures for crystallization confirming that origin of emission is related to nanocrystals. All Samples show emission at a constant wavelength with no peak shift suggesting that origin of PL can not be ascribed to QCE. Intensity of PL depend strongly on temperature (and therefore size of NCs) with higher intensities for samples with smaller NCs suggesting the origin of emission to be defect states at the surface of NCs.

concentration for five samples. Highest PL intensity for any sample is taken to have a comparative study on effect of Ge concentration on PL intensity. Fig(5.4) shows PL intensity for any samples vs annealing temperature. Now we discuss

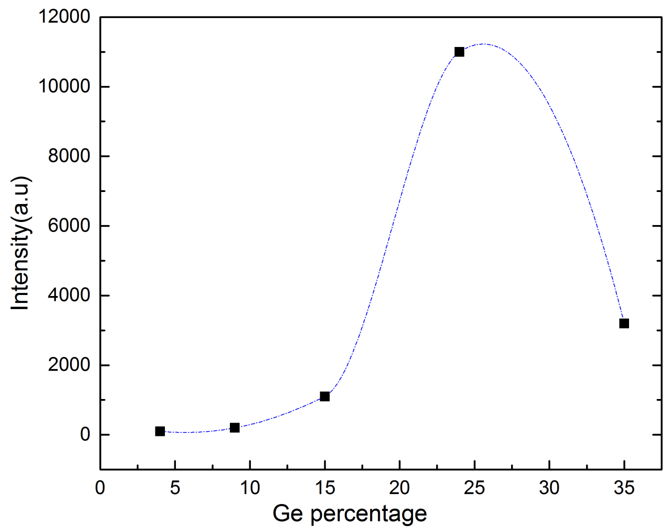

Figure 5.3: PL intensity vs germanium content. Intensity enhances with increasing germanium content from 4 to 24 percent. further increasing of germanium to 35 percent result in a decrease in PL intensity. Maximum intensity is observed for samples containing 24 percent of germanium

the origin of this visible emission from films. All samples show a peak position at around 2.4 ev with no blue shift with decreasing size of nanocrystals. However there is a correlation between crystallization and luminescence. Intensity of luminescence is also strongly size-dependent with higher intensities for smaller nanocrystals which can be seen from Figers(5.2),(5.3) and (5.4). For amorphous films there is no emission, luminescence for samples containing 24 and 35 percent Ge starts at 800C which corresponds to crystallization threshold for these two samples. For sample with 15 percent of Ge ,however, emission starts at 900C where crystallization occurs at higher temperature due to lower Ge content. For samples containing 4 and 9 percent of Ge, very weak emission is seen at temperatures around 1000C where crystallization starts. Moreover there is a decrease in intensity of PL after annealing above threshold temperatures which leads to Ostwald ripening and larger NCs. So it is obvious from spectra of all samples

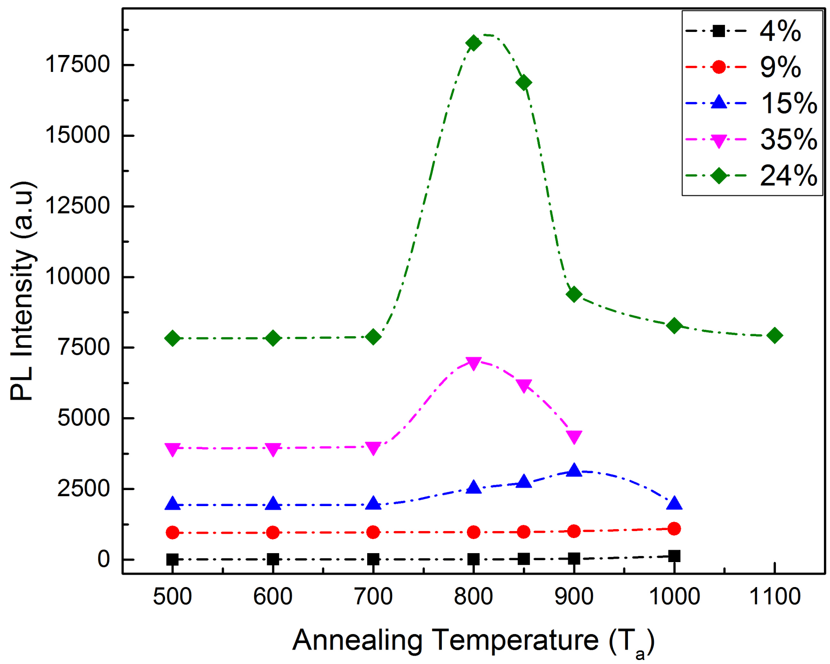

Figure 5.4: PL intensity vs annealing temperature for samples containing 4 to 35 percent germanium. Maximum emission intensity for all samples, is around 800C where crystallization starts. At higher temperatures and therefore larger nanocrystals, intensity decreases suggesting origin of emission to be defects located at the surface of nanocrystals

that smaller nanocrystals emit higher intensities. Despite all works [31, 66, 93–95] on Ge NCs in different matrices and different NC preparation methods, there is no agreement on the origin of PL in Ge NCs. Up to our knowledge the report by Takeoka [4] is the only PL observation of embedded Ge in consistent with QCE. Theses inconsistencies arise from ill-defined surface chemistry and complex-defective interfaces between Ge NCs and the surrounding matrix [4]. These surface related effects makes the observation of QCE more challenging in Ge NCs compare to Si NCs. Generally the PL from films containing Ge NCs is attributed to three effects: First, it can originate from quantum confinement of electrons and holes inside NCs. This inevitably leads to the expectation that a size dependent shift of the luminescence wavelength [25, 31, 95, 96] should be observed. This is not the case for our samples. Since the PL spectra shows no peak shift with NCs size in our samples, this possibility is ruled out. Second, photoluminescence may also be observed in samples with matrix defects [59, 97] which are created during film growth or diffusion of Ge during annealing. This is not also the case for our samples. We do not observe PL in as-grown samples, so that defect originated during sample growth, does not seem to be a possibility. Also, the defects due to diffusion of Ge during annealing is expected to be present in all samples including samples with lower Ge contents. However these samples also show no PL. We, therefore, conclude that matrix defects is not considered to be the origin of PL in our samples. The third possibility is PL due to states related to the interface of NC-dielectric matrix. Besides QCE, decreasing the size of NCs, cause a notable increase of surface to volume ratio of Ge NCs, which in turn, increases surface related effects. We believe this is the most likely origin of PL in our samples. This is supported by the fact that PL intensity is correlated with crystallization of Ge and with the size of Ge NCs. Raman and PL data for samples with 15,24 and 35 percent of Ge show that PL emission threshold is associated with beginning of crystallization of Ge. PL emission is observed when crystallization becomes apparent in the Raman spectra. Even though there is no peak shift as the NCs size changes, there is a strong dependence of PL intensity on NCs size. This can be due to larger number of surface effects at smaller Ge NCs since they have larger surface to volume ratio. Fig 5.5 illustrates HRTEM micrograph of three samples with different Ge NC size and corresponding PL spectra. Sample(a) with smallest NCs has highest intensity, sample(c) with very large NCs shows no emission, this also confirm s the origin of PL is defects located at the surface of nanocrystals. This is in agreement with results of Maeda et al. [25] and Barbagiovanni [30] who observed strong visible PL originating from interface states

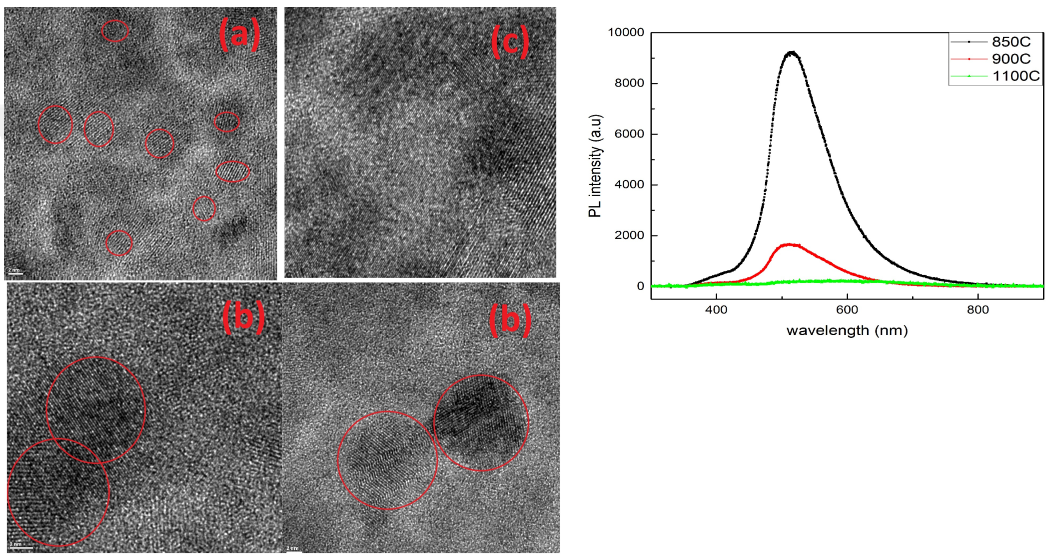

Figure 5.5: HRTEM micrograph of sample with 24 percent of Ge annealed at (a).850C (b).900C and (c)1000C. In fig(a) small NCs are distributed throughout the film. in Sample (b) larger NCs are formed and in sample(c) very large NCs exist. PL spectra for these three samples shows size dependent intensity with higher intensity for smaller nanocrystals suggesting that origin of luminescence is defects located at the surface of nanocrystals

5.3 Multilayer Samples

In this section, we study optical properties of Ge NCs embedded in thin Si3N4 layers with SiO2 barriers in Ge:SiN/SiO2 multilayer structures using photoluminescence (PL) spectroscopy. Multilayer structures have several advantages over single layer samples, where Ge content in as-grown samples is central in the determination of nanocrystal sizes. Typically, NC size is controlled by annealing temperature and duration or the content of the relevant material in the dielectric matrix [22] when annealed at fixed temperatures. In single layers, size of small Ge NCs are limited by the amount of Ge in SiN which leads to low density of nanocrystals that reduces photoluminescence efficiency. Multilayer approach can overcome this problem by controlling the size of NCs by confining them in thin layers and by increasing the number of Ge containing layers. Here, we separate adjacent layers of Ge containing nitride layers with dielectric barriers such as SiO2 which is expected to prevent Ge cross diffusion during annealing and therefore, can lead to small NCs with high concentration. This allows the controlling of the size and density of NCs, simultaneously. Moreover this approach, provides the local control of NCs and NC-NC distance in the growth direction. The structure of samples with different Ge:SiNy thickness were observed using high resolution transmission electron microscopy (HRTEM) after annealing them up to 900 C for 30 minutes. Fig.(5.6) shows overall TEM micrographs for all three samples with differing thicknesses of Ge:SiN layer annealed at 850-900 C. Samples with 3, 6 and 9 nm thick $Ge : SiN$ layers show similar behaviors, albeit some differences, Fig.5.6 a, b and c, respectively. The periodicity of the SiO2 barrier is the same in all samples and we clearly see the clustering and crystallization of Ge in the Ge:SiN layers in all three samples. It is also clear that while there is no diffusion of Ge atoms from layer to layer, lateral diffusion of Ge in the Ge:SiN plane is accompanied in thicker Ge:SiN layers with vertical growth of the nanocrystals leading to ellipsoidal shapes in an effort to minimize the surface free energy which is minimum for spheres[23]. Lateral diffusion of Ge and subsequent ellipsoidal growth leads to bead like formations modulating the NC sizes. We note that the sizes of the Ge NCs along the growth direction are larger as the thickness of SiGeN layer increases. This would lead to variations in the effective band gap of the NCs as well as creating bottlenecks in carrier transport. On the other hand, it may present opportunities to create controlled three dimensional growth of nano-Ge lattices. It is clear from the TEM micrographs that the driving force for the ultimate spherical shape is large enough that some diffusion into SiO2 barriers takes place. The extend of the diffusion increases with the thickness of the Ge containing SiGeN layer due to available Ge atoms. Thinner layers do not contain enough Ge atoms to support the drive to spherical

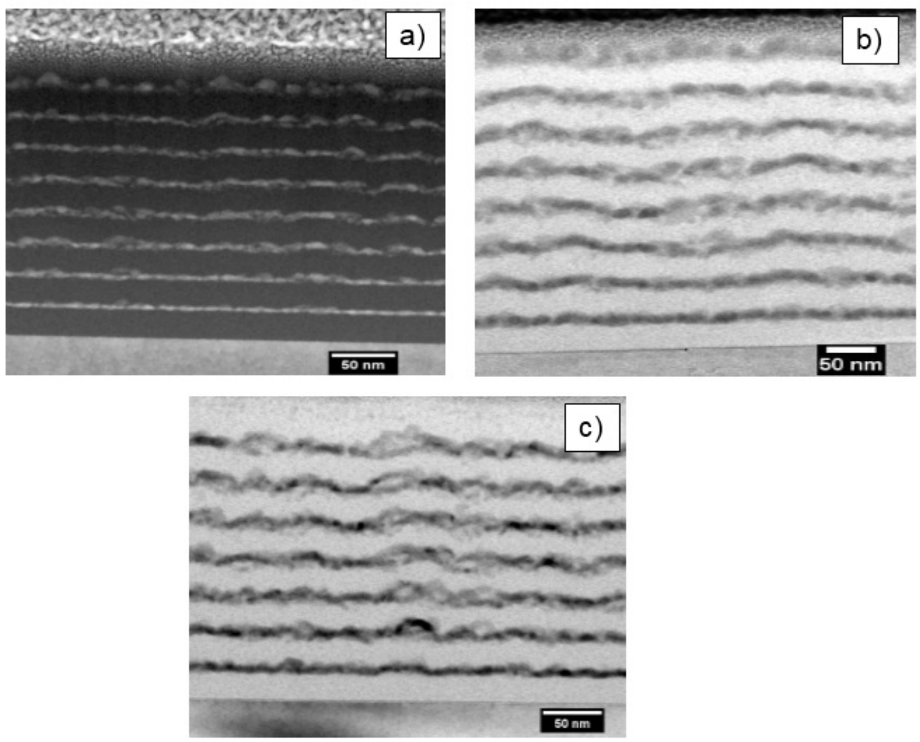

Figure 5.6: TEM micrographs of samples with Ge:SiNy thicknesses and annealing temperatures of samples with a) 3 nm (900 C), b) 6 nm (850 C) and c) 9 nm (900 C). The barriers are SiO2 with thickness of 25 nm.

shapes. As the amount of Ge in SiGeN layers increase, while not observed here, vertical diffusion accompanying the lateral crystallization may be expected to increase, reaching to a point that Ge NC layers touch each other. Close up TEM micrographs are shown in Fig.5.7 starting with a) sample ML3 (multilayer with nominal 3 nm SiGeN) Sample with the thinnest Ge:SiNy layer. The SiO2 barrier

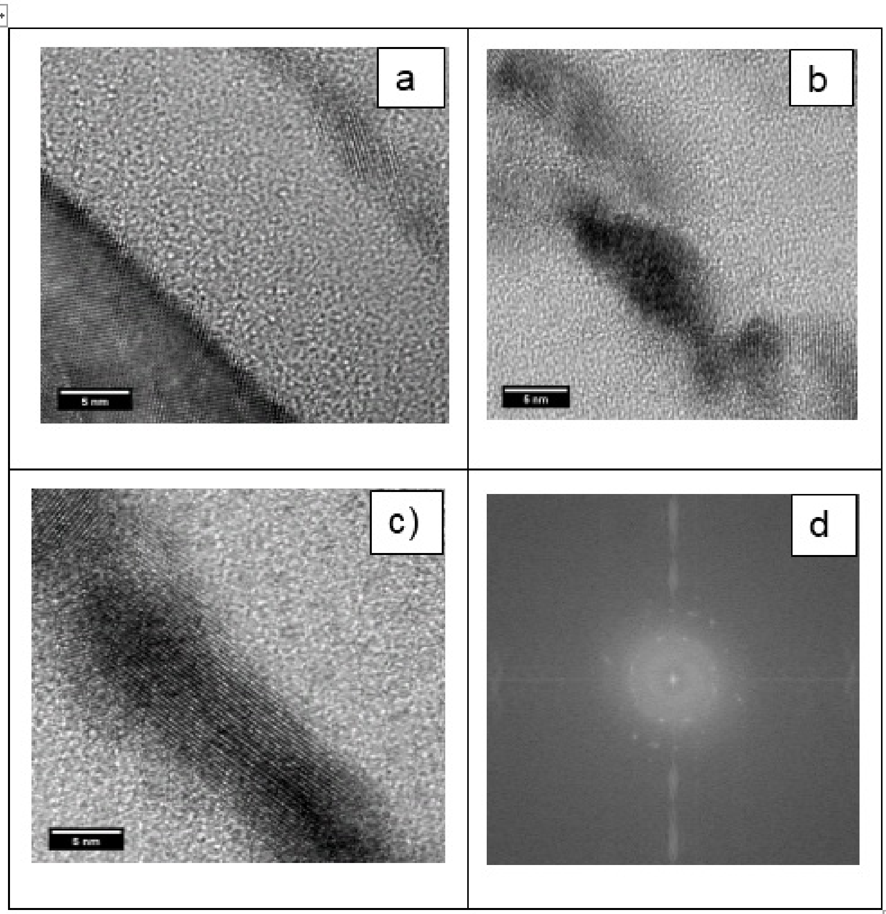

Figure 5.7: Cross-section TEM and typical FFT micrograph of multilayer samples: (a),(b),(c) HRTEM graphs of samples with 3, 6 and 9 nm of SiGeN layers, respectively.(d) FFT micrograph of sample (c) The graphs show good crystalinity as well as control over size by multilayer approach.

thickness of 25 nm is observed along with the diffused Ge in layers between the barriers. The in-plane diffusion of Ge atoms leads to thicknening of the Ge layer and buckling of the Ge NCs where some parts of the Ge NCs is thicker with periodicity of around 25 nm. We note that, Ge diffusion perpendicular to the

Ge NCs is limited by the lateral in plane diffusion of Ge atoms such that the size of NCs is expected to be restricted by the thickness of Ge:SiNy films [96]. In single bulk-like layers, NCs are typically spherical in shape [98]since minimum surface to volume ratio for spherical geometry leads to minimization of interface energy for spherical NCs. Spherical NCs are, therefore, expected. However, these HRTEM micrographs show confinement of Ge along the growth direction and in plane growth of small Ge NCs in thin Ge:SiNy layers and lateral growth of elongated Ge NCs for thicker samples. As shown in these images, in all samples, our Ge:SiNy layers have wavy shape with smoother interfaces at layers closer to substrate. This behavior is reported in several works [99–101]. Theoretical calculations also have been done [102] and predicted flatter and sharper interfaces at layers closer to substrate. In [99] also much smoother interfaces are observed in the as-grown samples compared to annealed samples. This has been attributed to interlayer diffusion of Ge confirmed by RBS study of Ge content. However, in our case, the as-grown samples show the same wavy structure as annealed samples. It seems that the effect of Ge diffusion during annealing plays a limited role in the formation of the wavy structure. We have not observed a Ge diffusion channel between Ge rich layers under the conditions of our experiments. Our as-grown samples are similar to samples in [101] where the origin of wavy structure in as-grown samples is attributed to insufficient energy of arriving atoms to make atomic rearrangement upon surface adsorption. The arriving atoms stick where they land. The exact shape of the interface depends on deposition conditions. Then the small intrinsic waviness in initial layers of a multilayer system leads to a large cumulative waviness towards top of the system. We also suggest this is the possible responsible mechanism of waviness in our samples. Fig.(5.8) shows size distribution for these three samples with different thicknesses. The NC size is referred to here is the NC diameter in the growth direction which is controlled via Ge:SiN thickness. Fig.(5.9) shows the photoluminescence spectra of samples ML3, ML6 and ML9. at room temperature.

The photoluminescence peak position does not show observable shift with annealing temperature. However, we observe a size-dependent photoluminescence intensity. We note that, the highest photoluminescence intensity of NCs of 3.1

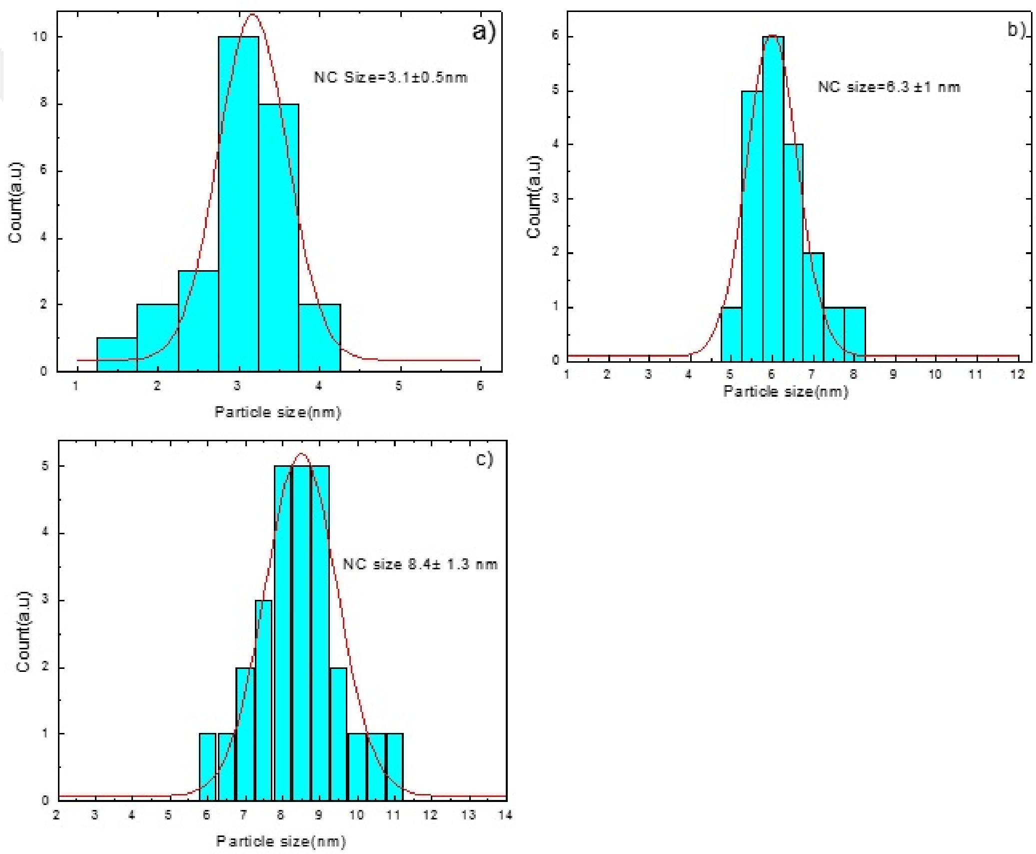

Figure 5.8: Size distributon for multilayer structures with different thicknesses and related Gaussian fit. It is clear that size of NCs is mostly determined by the thickness of the SiGeN layer thickness. The size distribution is narrow in all three samples.

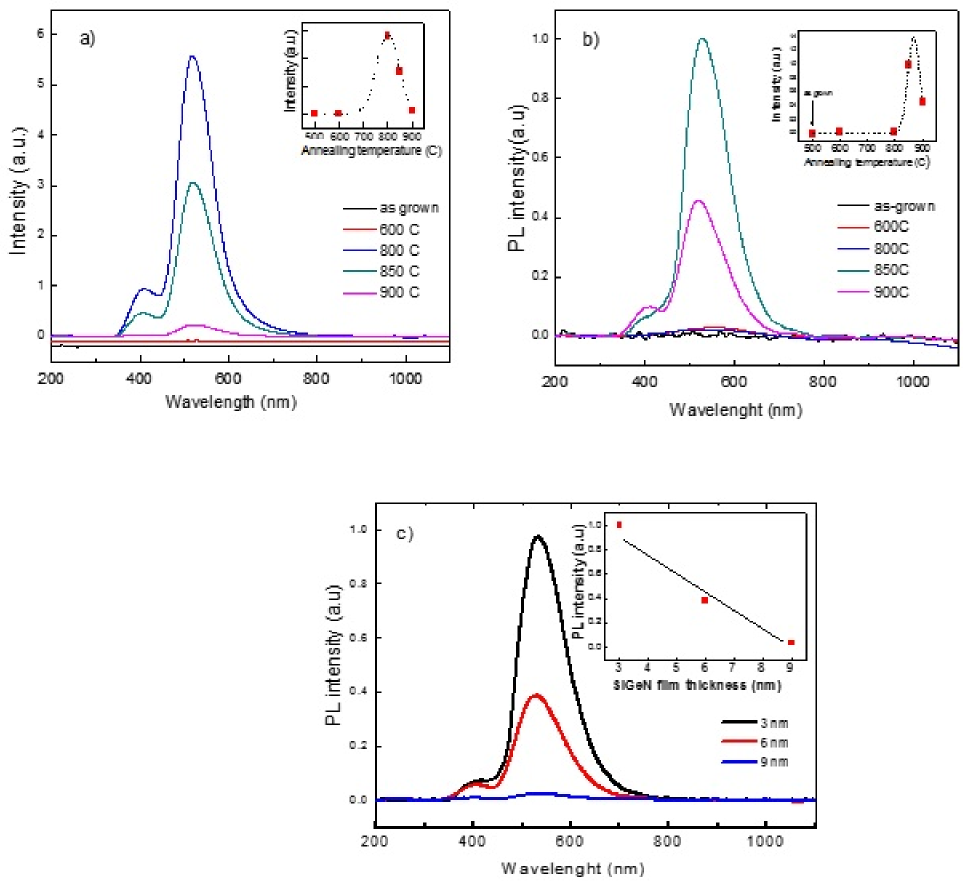

Figure 5.9: PL spectra of samples a) ML3 and b) ML6 annealed at different temperatures. c) Comparison of PL intensity of samples ML3, ML6 and ML9 annealed at 900 C. The inset shows a plot of PL intensity versus NC size. We note that PL spectra intensity is enhanced with reduction of NCs size. Insets in a) and b) show the variation of PL intensity as a function of annealing temperature while c) shows variation of Pl intensity with NC size.

nm decreases as the NC size increases to 6.4 nm finally decreasing to zero when the quantum size is 9.0 nm. We observed a size dependent PL intensity at 2.3 and 3.1eV. The samples with NCs below or equal to 6 nm show visible PL. We observed the enhancement of the PL intensity with reduction of the NCs size. The reduction of NC size is accompanied with increasing surface to volume ratio and therefore increasing surface related states. The origin of PL is suggested to be due to recombination through states at the NC/matrix interface.

5.4 Conclusions

In this chapter we performed an optical study on Ge nanocrystals in silicon nitride matrix in single layer and multilayer samples. HeCd laser operating at 325 nm is used as exciting source. First single layers with thickness around 200nm and Ge content from 4 to 35 percent are studied. Our study shows a constant peak position at 2.4ev for all samples suggesting that origin of emission can not be quantum confinement effect. Emission also is related to crystallization of samples and starts at crystallization threshold for any concerned sample. moreover, Intensity of emission depends on concentration of Ge in as prepared samples, a fairly value of Ge is needed for efficient light emission from NCs. Our analysis also shows higher emission intensity for samples containing smaller NCs which we believe is due to higher defects at surface of smaller NCs, we attributed this emission to surface states of NCs. In the second part of this chapter, multilayer samples are studied using same HeCd laser, size controlled NCs with narrower size distribution were studied and PL emission at the same position as single layers observed , these samples also show stronger emission for smaller NCs suggesting same origin of PL as single layer samples. Finally we observed an enhancement of emission for multilayer sample compared to that of single layer samples with the same thickness. This might be due to higher Ge density of NCs in multi layers, in multilayer samples SiO2 layer which perform as buffer layer, block the out diffusion of Ge during annealing and therefore an increased concentration of Ge in multilayer samples is expected. This effect can be responsible for enhancement of PL in multilayer samples compare to single layer samples.

Chapter 6

Conclusions and future work

In this chapter, we review a summary of the work. Main scope of the thesis is to investigate formation of Ge nanocrystals embedded in dielectric matrices, their structural and optical properties. In the first part, we focused on fabrication of Ge NCs in dielectric matrices. Ge NCs are synthesized in two different matrices namely silicon oxide and silicon nitride. Formation of NCs were confirmed by Raman spectroscopy and high resolution transmission electron microscopy. Raman spectroscopy and HRTEM micrographs are used for extraction of stress state of the nanocrystals. Raman spectra of NCs is different from bulk crystals. First difference is broader spectra of NCs compare to that of bulk Ge, this can give information about size distribution of NCs within matrix. Second difference of Raman spectra of NCs compare to bulk Ge is a blue or red shift of Raman peak of NCs compare to bulk Ge, There are two main physical reason behind this shift: First origin of this shift is confinement of phonons inside the Ge NCs, due to spatial enclosure of phonons, relaxation of phonon's momentum conservation rule takes place which is due to Heisenberg uncertainty principle. As a result, phonons with nonzero momentum (that is phonons out of center of first Brilouin zone) can involve in Raman scattering, frequency of these phonons are lower than those centered at first Brilouin zone, therefore Raman spectra of these phonons will represent a red shift compare to bulk crystal. Furthermore a broadening of Raman spectra is expected due to a distribution of phonons with varied values of momentum in Raman scattering process. There is also another reason for Raman shift, compressive or tensile stress affect the vibrational frequency in NCs, theoretical models predict that compressive stress increases the vibrational frequency and therefore leads to a blueshift in Raman spectra, tensile stress on the other hand results in a red shift in Raman peak. Therefore observed Raman shift in NCs is a combination of PCE induced red shift and stress induced shift which can be red or blue. Since PCE shift can be calculated knowing the size of NCs, it is possible to extract stress induced shift by obtaining average size of NCs from TEM micrographs. In this work we estimated stress state of NCs in different dielectric matrices by measuring Raman shift of NCs and extracting the PCE induced shift. Our study show a compressive stress for ge NCs embedded in all three matrices. Value of this stress is different in three matrices, however it turns out that for any given matrix the amount of stress is independent of NC's size. We also measured the stress of NCs by obtaining free standing NCs by a careful HF etching of matrix and getting only free standing NCs, these NCs are free of stress and therefore observed Raman spectra is only due to phonon confinement effect, comparing Raman shift of free standing and embedded NCs gives the stress state of NCs. We compared the stress state obtained by two methods and good agreement observed in the results. After investigating role of matrix on stress state of nanocrystals, we studied on the role of annealing method on stress state of NCs. Two processing methods namely conventional furnace annealing (CFA) and rapid thermal processing (RTP) are compared. RTP samples show smaller NCs compare to CFA samples still same stress for the samples observed, therefore stress of NCs is independent of annealing approach which suggest that origin of stress to be largely due to mismatch of NCs and matrix and thermal stress is negligible. After estimating and tuning of stress state of nanocrystals in single layer films we focused on fabrication and stress analysis of NCs in multilayer samples. Two sets of multilayers are studied, first set consist of Ge:SiNy/SiO2 bilayers. Second set has Ge:SiNy/Si3N4 bilayer structures. Number of bilayers were 8 or 16. Synthesis of NCs in these samples were performed via conventional furnace annealing and Raman and TEM micrographs are used for stress analysis, our study show possibility of tuning stress state of samples from compressive to tensile stress with changing buffer layer of samples. Stress state of nanocrystals can adjust the microstructure of the nanocrystals which in turn leads to change in the band gap of material, therefore controlling stress in NCs can be important in band structure engineering of nanocrystals, in the first part of the thesis we show possibility of tuning stress state of nanocrystals from compressive to tensile stress, three different methods are used for performing that namely matrix, processing approach and using buffer layer as stressor in multilayer samples. In the next part of this work we focused on optical properties of Ge NCs embedded in silicon nitride matrix. Optical study was performed using HeCd laser operating at 325 nm as exiting source. Role of Ge content on luminescence efficiency of Ge NCs is investigated and it was observed that a fairly high concentration of Ge atoms in as prepared samples is required for efficient emission, several sets of single layer and multilayer samples are studied, our analysis show size independent peak for samples which suggest that origin of PL can not be attributed to quantum confinement effect, however samples exhibit a size dependent PL intensity with higher intensity for smaller nanocrystals which suggest that origin of luminescence should be defects located at the surface of nanocrystals. An enhancement of PL in multilayer samples compare to single layers also observed and attributed to lack of out diffusion of Ge atoms in multilayer samples which leads to increasing density on NCs.

Bibliography

[1] P. Y. Yu and M. Cardona, *Fundamentals of semiconductors: physics and materials properties*. Springer, 2010.

[2] A. Saar, "Photoluminescence from silicon nanostructures: the mutual role of quantum confinement and surface chemistry," *Journal of Nanophotonics*, vol. 3, no. 1, pp. 032501–032501, 2009.

[3] C. Bulutay, "Interband, intraband, and excited-state direct photon absorption of silicon and germanium nanocrystals embedded in a wide band-gap lattice," *Physical Review B*, vol. 76, no. 20, p. 205321, 2007.

[4] S. Takeoka, M. Fujii, S. Hayashi, and K. Yamamoto, "Size-dependent near-infrared photoluminescence from ge nanocrystals embedded in sio 2 matrices," *Physical Review B*, vol. 58, no. 12, p. 7921, 1998.

[5] A. Meilakhs and S. Koniakhin, "New explanation of raman peak redshift in nanoparticles," *Superlattices and Microstructures*, 2017.

[6] C.-Y. Tsao, J. W. Weber, P. Campbell, G. Conibeer, D. Song, and M. A. Green, "In situ low temperature growth of poly-crystalline germanium thin film on glass by rf magnetron sputtering," *Solar Energy Materials and Solar Cells*, vol. 94, no. 9, pp. 1501–1505, 2010.

[7] A. L. Efros and A. L. Efros, "Interband absorption of light in a semiconductor sphere," *Soviet Physics Semiconductors-Ussr*, vol. 16, no. 7, pp. 772–775, 1982.

[8] A. M. Green and M. J. Keevers, "Optical properties of intrinsic silicon at 300 k," *Progress in Photovoltaics: Research and Applications*, vol. 3, no. 3, pp. 189–192, 1995.

[9] G. Conibeer, M. Green, R. Corkish, Y. Cho, E.-C. Cho, C.-W. Jiang, T. Fangsuwannarak, E. Pink, Y. Huang, T. Puzzer, *et al.*, "Silicon nanostructures for third generation photovoltaic solar cells," *Thin solid films*, vol. 511, pp. 654–662, 2006.

[10] D. C. Oertel, M. G. Bawendi, A. C. Arango, and V. Bulović, "Photodetectors based on treated cdse quantum-dot films," *Applied Physics Letters*, vol. 87, no. 21, p. 213505, 2005.

[11] Y. Shirasaki, G. J. Supran, M. G. Bawendi, and V. Bulović, "Emergence of colloidal quantum-dot light-emitting technologies," *Nature Photonics*, vol. 7, no. 1, pp. 13–23, 2013.

[12] A. Dâna, I. Akca, A. Aydinli, R. Turan, and T. G. Finstad, "A figure of merit for optimization of nanocrystal flash memory design," *Journal of nanoscience and nanotechnology*, vol. 8, no. 2, pp. 510–517, 2008.

[13] X. Michalet, F. Pinaud, L. Bentolila, J. Tsay, S. Doose, J. Li, G. Sundaresan, A. Wu, S. Gambhir, and S. Weiss, "Quantum dots for live cells, in vivo imaging, and diagnostics," *science*, vol. 307, no. 5709, pp. 538–544, 2005.

[14] L. T. Canham, "Silicon quantum wire array fabrication by electrochemical and chemical dissolution of wafers," *Applied Physics Letters*, vol. 57, no. 10, pp. 1046–1048, 1990.

[15] S. Ray and K. Das, "Luminescence characteristics of ge nanocrystals embedded in sio 2 matrix," *Optical Materials*, vol. 27, no. 5, pp. 948–952, 2005.

[16] B. Averboukh, R. Huber, K. Cheah, Y. Shen, G. Qin, Z. Ma, and W. Zong, "Luminescence studies of a si/sio 2 superlattice," *Journal of applied physics*, vol. 92, no. 7, pp. 3564–3568, 2002.

[17] A. Puzder, A. Williamson, J. C. Grossman, and G. Galli, “Surface chemistry of silicon nanoclusters,” *Physical review letters*, vol. 88, no. 9, p. 097401, 2002.

[18] G. Hadjisavvas and P. Kelires, “Structure and energetics of si nanocrystals embedded in a- s i o 2,” *Physical review letters*, vol. 93, no. 22, p. 226104, 2004.

[19] X. Wang, J. Zhang, L. Ding, B. Cheng, W. Ge, J. Yu, and Q. Wang, “Origin and evolution of photoluminescence from si nanocrystals embedded in a sio 2 matrix,” *Physical Review B*, vol. 72, no. 19, p. 195313, 2005.

[20] C. Delerue, G. Allan, and M. Lannoo, “Theoretical aspects of the luminescence of porous silicon,” *Physical Review B*, vol. 48, no. 15, p. 11024, 1993.

[21] S. Öğüt, J. R. Chelikowsky, and S. G. Louie, “Quantum confinement and optical gaps in si nanocrystals,” *Physical Review Letters*, vol. 79, no. 9, p. 1770, 1997.

[22] S. Godefroo, M. Hayne, M. Jivanescu, A. Stesmans, M. Zacharias, O. Lebedev, G. Van Tendeloo, and V. V. Moshchalkov, “Classification and control of the origin of photoluminescence from si nanocrystals,” *Nature nanotechnology*, vol. 3, no. 3, pp. 174–178, 2008.

[23] L. Pavesi and R. Turan, *Silicon nanocrystals: fundamentals, synthesis and applications*. John Wiley & Sons, 2010.

[24] M. Zacharias, J. Heitmann, R. Scholz, U. Kahler, M. Schmidt, and J. Bläsing, “Size-controlled highly luminescent silicon nanocrystals: A sio/sio 2 superlattice approach,” *Applied Physics Letters*, vol. 80, no. 4, pp. 661–663, 2002.

[25] Y. Maeda, N. Tsukamoto, Y. Yazawa, Y. Kanemitsu, and Y. Masumoto, “Visible photoluminescence of ge microcrystals embedded in sio2 glassy matrices,” *Applied physics letters*, vol. 59, no. 24, pp. 3168–3170, 1991.

[26] H. Chew, F. Zheng, W. Choi, W. Chim, Y. Foo, and E. Fitzgerald, "Influence of reductant and germanium concentration on the growth and stress development of germanium nanocrystals in silicon oxide matrix," *Nanotechnology*, vol. 18, no. 6, p. 065302, 2007.

[27] C.-W. Jiang and M. A. Green, "Silicon quantum dot superlattices: Modeling of energy bands, densities of states, and mobilities for silicon tandem solar cell applications," *Journal of applied physics*, vol. 99, no. 11, p. 114902, 2006.

[28] F. Gao, M. A. Green, G. Conibeer, E.-C. Cho, Y. Huang, I. Pere-Wurfl, and C. Flynn, "Fabrication of multilayered ge nanocrystals by magnetron sputtering and annealing," *Nanotechnology*, vol. 19, no. 45, p. 455611, 2008.

[29] K. Teo, S. Kwok, P. Yu, and S. Guha, "Quantum confinement of quasi-two-dimensional e 1 excitons in ge nanocrystals studied by resonant raman scattering," *Physical Review B*, vol. 62, no. 3, p. 1584, 2000.

[30] E. Barbagiovanni, D. Lockwood, N. Rowell, R. Costa Filho, I. Berbezier, G. Amiard, L. Favre, A. Ronda, M. Faustini, and D. Grosso, "Role of quantum confinement in luminescence efficiency of group iv nanostructures," *Journal of Applied Physics*, vol. 115, no. 4, p. 044311, 2014.

[31] M. Zacharias and P. Fauchet, "Blue luminescence in films containing ge and geo 2 nanocrystals: the role of defects," *Applied Physics Letters*, vol. 71, no. 3, pp. 380–382, 1997.

[32] S. Tiwari, F. Rana, H. Hanafi, A. Hartstein, E. F. Crabbé, and K. Chan, "A silicon nanocrystals based memory," *Applied Physics Letters*, vol. 68, no. 10, pp. 1377–1379, 1996.

[33] Y.-C. King, T.-J. King, and C. Hu, "Charge-trap memory device fabricated by oxidation of $si/sub\ 1-x/ge/subx$," *IEEE Transactions on Electron Devices*, vol. 48, no. 4, pp. 696–700, 2001.

[34] Y.-C. King, T.-J. King, and C. Hu, "Mos memory using germanium nanocrystals formed by thermal oxidation of si/sub 1-x/ge/sub x," in *Electron Devices Meeting, 1998. IEDM'98. Technical Digest., International*, pp. 115–118, IEEE, 1998.

[35] C. Claeys and E. Simoen, *Germanium-based technologies: from materials to devices*. Elsevier, 2011.

[36] J. Michel, J. Liu, and L. C. Kimerling, "High-performance ge-on-si photodetectors," *Nature Photonics*, vol. 4, no. 8, pp. 527–534, 2010.

[37] D. Ahn, C.-y. Hong, J. Liu, W. Giziewicz, M. Beals, L. C. Kimerling, J. Michel, J. Chen, and F. X. Kärtner, "High performance, waveguide integrated ge photodetectors," *Optics express*, vol. 15, no. 7, pp. 3916–3921, 2007.

[38] W. Guter, J. Schöne, S. P. Philipps, M. Steiner, G. Siefer, A. Wekkeli, E. Welser, E. Oliva, A. W. Bett, and F. Dimroth, "Current-matched triple-junction solar cell reaching 41.1% conversion efficiency under concentrated sunlight," *Applied Physics Letters*, vol. 94, no. 22, p. 223504, 2009.

[39] J. Liu, X. Sun, R. Camacho-Aguilera, L. C. Kimerling, and J. Michel, "Ge-on-si laser operating at room temperature," *Optics letters*, vol. 35, no. 5, pp. 679–681, 2010.

[40] J. Liu, X. Sun, D. Pan, X. Wang, L. C. Kimerling, T. L. Koch, and J. Michel, "Tensile-strained, n-type ge as a gain medium for monolithic laser integration on si," *Optics express*, vol. 15, no. 18, pp. 11272–11277, 2007.

[41] S.-W. Chang and S. L. Chuang, "Theory of optical gain of $ge - -si_x ge_y Sn_{1-x-y}$ quantum-well lasers," *IEEE Journal of Quantum Electronics*, vol. 43, no. 3, pp. 249–256, 2007.

[42] P. H. Lim, S. Park, Y. Ishikawa, and K. Wada, "Enhanced direct bandgap emission in germanium by micromechanical strain engineering," *Optics express*, vol. 17, no. 18, pp. 16358–16365, 2009.

[43] G. Pizzi, M. Virgilio, and G. Grosso, "Tight-binding calculation of optical gain in tensile strained [001]-ge/sige quantum wells," *Nanotechnology*, vol. 21, no. 5, p. 055202, 2009.

[44] M. El Kurdi, G. Fishman, S. Sauvage, and P. Boucaud, "Band structure and optical gain of tensile-strained germanium based on a 30 band k p formalism," *Journal of Applied Physics*, vol. 107, no. 1, p. 013710, 2010.

[45] Y. Ishikawa, K. Wada, D. D. Cannon, J. Liu, H.-C. Luan, and L. C. Kimerling, "Strain-induced band gap shrinkage in ge grown on si substrate," *Applied Physics Letters*, vol. 82, no. 13, pp. 2044–2046, 2003.

[46] Y. Bai, K. E. Lee, C. Cheng, M. L. Lee, and E. A. Fitzgerald, "Growth of highly tensile-strained ge on relaxed in x ga 1- x as by metal-organic chemical vapor deposition," *Journal of Applied Physics*, vol. 104, no. 8, p. 084518, 2008.

[47] Y.-Y. Fang, J. Tolle, R. Roucka, A. Chizmeshya, J. Kouvetakis, V. DCosta, and J. Menéndez, "Perfectly tetragonal, tensile-strained ge on ge 1- y sn y buffered si (100)," *Applied physics letters*, vol. 90, no. 6, p. 061915, 2007.

[48] M. De Kersauson, M. El Kurdi, S. David, X. Checoury, G. Fishman, S. Sauvage, R. Jakomin, G. Beaudoin, I. Sagnes, and P. Boucaud, "Optical gain in single tensile-strained germanium photonic wire," *Optics express*, vol. 19, no. 19, pp. 17925–17934, 2011.

[49] L. Pavesi, "Will silicon be the photonic material of the third millenium?," *Journal of Physics: Condensed Matter*, vol. 15, no. 26, p. R1169, 2003.

[50] A. Nassiopoulou, "Silicon nanocrystals in sio2 thin layers," *Encyclopedia of Nanoscience and Nanotechnology. Edited by: Nalwa HS. Valencia: American Scientific*, vol. 9, pp. 793–813, 2004.

[51] E. G. Barbagiovanni, D. J. Lockwood, P. J. Simpson, and L. V. Goncharova, "Quantum confinement in si and ge nanostructures," *Journal of Applied Physics*, vol. 111, no. 3, p. 034307, 2012.

[52] F. Reboredo, A. Franceschetti, and A. Zunger, "Dark excitons due to direct coulomb interactions in silicon quantum dots," *Physical Review B*, vol. 61, no. 19, p. 13073, 2000.

[53] E. G. Barbagiovanni, D. J. Lockwood, P. J. Simpson, and L. V. Goncharova, "Quantum confinement in si and ge nanostructures: theory and experiment," *Applied Physics Reviews*, vol. 1, no. 1, p. 011302, 2014.

[54] M. S. Hybertsen, "Absorption and emission of light in nanoscale silicon structures," *Physical Review Letters*, vol. 72, no. 10, p. 1514, 1994.

[55] D. Kovalev, H. Heckler, M. Ben-Chorin, G. Polisski, M. Schwartzkopff, and F. Koch, "Breakdown of the k-conservation rule in si nanocrystals," *Physical review letters*, vol. 81, no. 13, p. 2803, 1998.

[56] B. Garrido, M. Lopez, A. Pérez-Rodrı, C. Garcı, P. Pellegrino, R. Ferré, J. Moreno, J. Morante, C. Bonafos, M. Carrada, *et al.*, "Optical and electrical properties of si-nanocrystals ion beam synthesized in sio 2," *Nuclear Instruments and Methods in Physics Research Section B: Beam Interactions with Materials and Atoms*, vol. 216, pp. 213–221, 2004.

[57] H. Takagi, H. Ogawa, Y. Yamazaki, A. Ishizaki, and T. Nakagiri, "Quantum size effects on photoluminescence in ultrafine si particles," *Applied Physics Letters*, vol. 56, no. 24, pp. 2379–2380, 1990.

[58] Z. Lu and D. Grozea, "Crystalline si/sio 2 quantum wells," *Applied physics letters*, vol. 80, no. 2, pp. 255–257, 2002.

[59] P.-H. Liao, T.-C. Hsu, K.-H. Chen, T.-H. Cheng, T.-M. Hsu, C.-C. Wang, T. George, and P. Li, "Size-tunable strain engineering in ge nanocrystals embedded within sio2 and si3n4," *Applied Physics Letters*, vol. 105, no. 17, p. 172106, 2014.

[60] L.-W. Wang, A. Franceschetti, and A. Zunger, "Million-atom pseudopotential calculation of γ-x mixing in gaas/alas superlattices and quantum dots," *Physical review letters*, vol. 78, no. 14, p. 2819, 1997.

[61] P. Friedel, M. Hybertsen, and M. Schlüter, "Local empirical pseudopotential approach to the optical properties of si/ge superlattices," *Physical Review B*, vol. 39, no. 11, p. 7974, 1989.

[62] Z. Zhou, L. Brus, and R. Friesner, "Electronic structure and luminescence of 1.1-and 1.4-nm silicon nanocrystals: oxide shell versus hydrogen passivation," *Nano Letters*, vol. 3, no. 2, pp. 163–167, 2003.

[63] A. Tsolakidis and R. M. Martin, "Comparison of the optical response of hydrogen-passivated germanium and silicon clusters," *Physical Review B*, vol. 71, no. 12, p. 125319, 2005.

[64] F. Trani, G. Cantele, D. Ninno, and G. Iadonisi, "Tight-binding calculation of the optical absorption cross section of spherical and ellipsoidal silicon nanocrystals," *Physical Review B*, vol. 72, no. 7, p. 075423, 2005.

[65] L. W. Wang and A. Zunger, "Electronic structure pseudopotential calculations of large (. apprx. 1000 atoms) si quantum dots," *The Journal of Physical Chemistry*, vol. 98, no. 8, pp. 2158–2165, 1994.

[66] Y. Kanemitsu, H. Uto, Y. Masumoto, and Y. Maeda, "On the origin of visible photoluminescence in nanometer-size ge crystallites," *Applied physics letters*, vol. 61, no. 18, pp. 2187–2189, 1992.

[67] J. Wilcoxon, G. Samara, and P. Provencio, "Optical and electronic properties of si nanoclusters synthesized in inverse micelles," *Physical Review B*, vol. 60, no. 4, p. 2704, 1999.

[68] C. Yuan, Q. Liu, and B. Xu, "Strain-induced structural phase transition of si nanoparticles," *The Journal of Physical Chemistry C*, vol. 115, no. 33, pp. 16374–16377, 2011.

[69] A. Wellner, V. Paillard, C. Bonafos, H. Coffin, A. Claverie, B. Schmidt, and K. Heinig, "Stress measurements of germanium nanocrystals embedded in silicon oxide," *Journal of applied physics*, vol. 94, no. 9, pp. 5639–5642, 2003.

[70] F. Ay and A. Aydinli, "Comparative investigation of hydrogen bonding in silicon based pecvd grown dielectrics for optical waveguides," *Optical materials*, vol. 26, no. 1, pp. 33–46, 2004.

[71] P. B. Griffin, J. D. Plummer, and M. D. Deal, "Silicon vlsi technology: fundamentals, practice, and modeling," *1a edição, Prentice Hall Inc*, 2000.

[72] J. D. Plummer, *Silicon VLSI technology: fundamentals, practice and modeling*. Pearson Education India, 2009.

[73] J. Guzman, *Structural characterization of germanium and gold-germanium nanoclusters embedded in silica*. University of California, Berkeley, 2011.

[74] C. R. Brundle and C. A. Evans, *Encyclopedia of materials characterization: surfaces, interfaces, thin films*. Gulf Professional Publishing, 1992.

[75] M. Mayer, "Simnra user's guide," 1997.

[76] D. Briggs, "Handbook of x-ray photoelectron spectroscopy cd wanger, wm riggs, le davis, jf moulder and ge muilenberg perkin-elmer corp., physical electronics division, eden prairie, minnesota, usa, 1979. 190 pp. 195," *Surface and Interface Analysis*, vol. 3, no. 4, 1981.

[77] N. Colthup, *Introduction to infrared and Raman spectroscopy*. Elsevier, 2012.

[78] E. Smith and G. Dent, *Modern Raman spectroscopy: a practical approach*. John Wiley & Sons, 2013.

[79] S. Wei, C. Li, and M. Chou, "Ab initio calculation of thermodynamic properties of silicon," *Physical Review B*, vol. 50, no. 19, p. 14587, 1994.

[80] S. Horiuchi, *Fundamentals of high-resolution transmission electron microscopy*. North Holland, 1994.

[81] W. Choi, W. Chim, C. Heng, L. Teo, V. Ho, V. Ng, D. Antoniadis, and E. Fitzgerald, "Observation of memory effect in germanium nanocrystals

embedded in an amorphous silicon oxide matrix of a metal–insulator–semiconductor structure,” *Applied Physics Letters*, vol. 80, no. 11, pp. 2014–2016, 2002.

[82] S. Cosentino, A. Mio, E. Barbagiovanni, R. Raciti, R. Bahariqushchi, M. Miritello, G. Nicotra, A. Aydinli, C. Spinella, A. Terrasi, *et al.*, “The role of the interface in germanium quantum dots: when not only size matters for quantum confinement effects,” *Nanoscale*, vol. 7, no. 26, pp. 11401–11408, 2015.

[83] M. Mayer, “Simnra, a simulation program for the analysis of nra, rbs and erda,” in *AIP Conference Proceedings*, vol. 475, pp. 541–544, AIP, 1999.

[84] I. Campbell and P. M. Fauchet, “The effects of microcrystal size and shape on the one phonon raman spectra of crystalline semiconductors,” *Solid State Communications*, vol. 58, no. 10, pp. 739–741, 1986.

[85] F. Cerdeira, C. Buchenauer, F. H. Pollak, and M. Cardona, “Stress-induced shifts of first-order raman frequencies of diamond-and zinc-blende-type semiconductors,” *Physical Review B*, vol. 5, no. 2, p. 580, 1972.

[86] J. Zi, K. Zhang, and X. Xie, “Comparison of models for raman spectra of si nanocrystals,” *Physical Review B*, vol. 55, no. 15, p. 9263, 1997.

[87] J. Parker Jr, D. Feldman, and M. Ashkin, “Raman scattering by silicon and germanium,” *Physical Review*, vol. 155, no. 3, p. 712, 1967.

[88] I. Sharp, D. Yi, Q. Xu, C. Liao, J. Beeman, Z. Liliental-Weber, K. Yu, D. Zakharov, J. Ager III, D. Chrzan, *et al.*, “Mechanism of stress relaxation in ge nanocrystals embedded in si o 2,” *Applied Physics Letters*, vol. 86, no. 6, p. 063107, 2005.

[89] L. Liu, K. Teo, Z. Shen, J. Sun, E. Ong, A. Kolobov, and Y. Maeda, “Raman scattering investigation of a g e/s i o 2/si nanocrystal system under hydrostatic pressure,” *Physical Review B*, vol. 69, no. 12, p. 125333, 2004.

[90] M. Fujii, S. Hayashi, and K. Yamamoto, "Growth of ge microcrystals in sio2 thin film matrices: a raman and electron microscopic study," *Japanese Journal of Applied Physics*, vol. 30, no. 4R, p. 687, 1991.

[91] D. Shahrjerdi, B. Hekmatshoar, L. Rezaee, and S. Mohajerzadeh, "Low temperature stress-induced crystallization of germanium on plastic," *Thin Solid Films*, vol. 427, no. 1, pp. 330–334, 2003.

[92] Y. Kimura, M. Kishi, and T. Katoda, "The model of solid phase crystallization of amorphous silicon under elastic stress," *Journal of Applied Physics*, vol. 87, no. 8, pp. 4017–4021, 2000.

[93] S. Okamoto and Y. Kanemitsu, "Photoluminescence properties of surface-oxidized ge nanocrystals: Surface localization of excitons," *Physical Review B*, vol. 54, no. 23, p. 16421, 1996.

[94] D. Paine, C. Caragianis, T. Kim, Y. Shigesato, and T. Ishahara, "Visible photoluminescence from nanocrystalline ge formed by h2 reduction of si0. 6ge0. 4o2," *Applied Physics Letters*, vol. 62, no. 22, pp. 2842–2844, 1993.

[95] T. K. Purkait, A. K. Swarnakar, B. Glenda, F. A. Hegmann, E. Rivard, and J. G. Veinot, "One-pot synthesis of functionalized germanium nanocrystals from a single source precursor," *Nanoscale*, vol. 7, no. 6, pp. 2241–2244, 2015.

[96] J. Shen, X. Wu, R. Yuan, N. Tang, J. Zou, Y. Mei, C. Tan, X. Bao, and G. Siu, "Enhanced ultraviolet photoluminescence from sio 2/ge: Sio 2/sio 2 sandwiched structure," *Applied Physics Letters*, vol. 77, no. 20, pp. 3134–3136, 2000.

[97] A. Dana, S. Tokay, and A. Aydinli, "Formation of ge nanocrystals and sige in pecvd grown sinx: Ge thin films," *Materials science in semiconductor processing*, vol. 9, no. 4, pp. 848–852, 2006.

[98] D. Sagar, J. M. Atkin, P. K. Palomaki, N. R. Neale, J. L. Blackburn, J. C. Johnson, A. J. Nozik, M. B. Raschke, and M. C. Beard, "Quantum confined electron–phonon interaction in silicon nanocrystals," *Nano letters*, vol. 15, no. 3, pp. 1511–1516, 2015.

[99] E. Vieira, J. Martín-Sánchez, A. G. Rolo, A. Parisini, M. Buljan, I. Capan, E. Alves, N. P. Barradas, O. Conde, S. Bernstorff, *et al.*, "Structural and electrical studies of ultrathin layers with si0. 7ge0. 3 nanocrystals confined in a sige/sio2 superlattice," *Journal of Applied Physics*, vol. 111, no. 10, p. 104323, 2012.

[100] S. P. Vernon, D. G. Stearns, and R. S. Rosen, "Ion-assisted sputter deposition of molybdenum-silicon multilayers," *Applied optics*, vol. 32, no. 34, pp. 6969–6974, 1993.

[101] A. Kling, A. Rodriguez, J. Sangrador, M. Ortiz, T. Rodriguez, C. Ballesteros, and J. Soares, "Combined grazing incidence rbs and tem analysis of luminescent nano-sige/sio 2 multilayers," *Nuclear Instruments and Methods in Physics Research Section B: Beam Interactions with Materials and Atoms*, vol. 266, no. 8, pp. 1397–1401, 2008.

[102] A. Payne and B. Clemens, "Influence of roughness distributions and correlations on x-ray diffraction from superlattices," *Physical Review B*, vol. 47, no. 4, p. 2289, 1993.